Improving *In Vitro* Myogenesis and Force Production in Engineered Skeletal Muscle Tissues

by

Brian Chen Syverud

A dissertation submitted in partial fulfillment
of the requirements for the degree of
Doctor of Philosophy
(Biomedical Engineering)
in the University of Michigan
2017

Doctoral Committee:

Professor Lisa M. Larkin, Co-Chair
Professor Ellen M. Arruda, Co-Chair
Professor Mary-Ann Mycek
Associate Professor Sunitha Nagrath
Professor Shuichi Takayama

Brian Chen Syverud

bsyverud@umich.edu

ORCID iD: 0000-0001-7781-1635

DEDICATION

This dissertation is dedicated to my wife, Kathleen, and my daughter, Clara, for all of their patience and support throughout.

ACKNOWLEDGEMENTS

The research in this dissertation was supported by funding from the National Institute of Arthritis and Musculoskeletal and Skin Diseases, the National Institute of Biomedical Imaging and Bioengineering, the Microfluidics in Biomedical Sciences Training Program at the University of Michigan, the Honor Society of Phi Kappa Phi, and the Rackham Graduate School.

Extensive contributions to the experiments in this dissertation were made by the members, past and present, of the Skeletal Tissue Engineering Laboratory at the University of Michigan, under the mentorship of Dr. Ellen Arruda and Dr. Lisa Larkin. I would also like to thank my collaborators in the laboratories of Dr. Mary-Ann Mycek, Dr. Sunitha Nagrath, and Dr. Christopher Mendias. Finally, this dissertation was written with contributions from the members of my dissertation committee, especially Dr. Lisa Larkin.

TABLE OF CONTENTS

DEDICATION ii

ACKNOWLEDGEMENTS iii

LIST OF TABLES vi

LIST OF FIGURES vii

ABSTRACT ix

CHAPTER I - Introduction 1

Skeletal Muscle Physiology 1

Skeletal Muscle Stem Cells 4

Growth Factors and Skeletal Muscle Tissue Engineering 20

Summary 31

CHAPTER II - Microfluidic Sorting of Isolated Skeletal Muscle Satellite Cells 34

Introduction 34

Methods 38

Results 46

Discussion 52

Conclusions 54

CHAPTER III - Dexamethasone Supplementation to Enhance Myogenic Differentiation in Engineered SMUs **55**

Introduction 55

Methods 58

Results 63

Discussion 72

Conclusions 74

CHAPTER IV - Quantitative, Label-Free Evaluation of Tissue-Engineered Skeletal Muscle through Multiphoton Microscopy **75**

Introduction 75

Methods 79

Results 86

Discussion 93

Conclusions 95

CHAPTER V - Conclusions **96**

BIBLIOGRAPHY **100**

LIST OF TABLES

1. Comparison of adhesion proteins for isolated satellite cells 11

2. Prospective surface markers for isolation of satellite cells 15

3. Purity of separated cell populations following sorting 47

LIST OF FIGURES

1. Hierarchical structural organization of skeletal muscle 2

2. Single fiber explant culture for isolation of satellite cells 8

3. Enzymatic dissociation for isolation of satellite cells 10

4. Example methodology for FACS purification of satellite cells 17

5. Initial skeletal muscle formation during embryogenesis 22

6. Growth factor signaling in skeletal muscle regeneration 24

7. Central pathways to regulation of skeletal muscle hypertrophy and atrophy 26

8. Microfluidic inertial separation in the labyrinth device 37

9. Fabrication of a Skeletal Muscle Unit (SMU) 42

10. Myogenic and fibrogenic proliferation of sorted cells 48

11. Structural maturation following microfluidic sorting 50

12. Effects of microfluidic sorting on myotube growth 51

13. SMU functional development with microfluidic sorting 52

14. Experimental timeline with dexamethasone timings and dosages 60

15. Myogenic and fibroblast cell proliferation following dexamethasone addition 64

16. DEX effects on myogenic differentiation 65

17. DEX effects on myotube growth 67

18. SMU structural maturation with DEX addition 69

19. SMU functional maturation with DEX addition 70

20. OMI processing schematic 83

21. OMI signal validation 87

22. Endogenous NADH and FAD fluorescence as indicators of metabolic activity 88

23. Myosin SHG in native and engineered skeletal muscle 89

24. Myosin and collagen SHG as indicators of structural organization 90

25. Comparison of SMU contractile properties and OMI measures 92

ABSTRACT

The growing deficit in suitable tissues for patients awaiting organ transplants demonstrates the clinical need for engineered tissues as alternative graft sources. In skeletal muscle, volumetric muscle loss is any injury exceeding the normal muscle repair mechanism and resulting in permanent functional impairment. Because available treatments seeking to fill the damaged site with healthy graft tissue are limited by a lack of suitable graft sources, tissue engineering of skeletal muscle has been identified as a promising alternative. To date, however, engineered muscles across the field have generated a fraction of the specific force present in native muscle, and this limitation may present a barrier to clinical applicability. This study addressed this force disparity by promoting *in vitro* muscle development through the following specific aims: 1) Improving myogenic purity of isolated muscle stem cells with microfluidic inertial separation, 2) Increasing myogenic differentiation in developing cells and engineered muscles with dexamethasone steroid supplementation, and 3) Evaluating engineered tissue structure and function in a non-invasive, label-free manner using multiphoton microscopy. All three experiments demonstrated significant improvements in engineered skeletal muscle force production as compared to previous fabrication methods. Especially as tissue-engineered skeletal muscle moves towards translation as a strategy for repairing volumetric muscle loss, consistently improving *in vitro* force production of engineered skeletal muscle using methods established in this dissertation is essential for advancing both our tissue engineering model and the tissue engineering and regenerative medicine field as a whole.

CHAPTER I

Introduction

Skeletal Muscle Physiology

Skeletal muscle is a soft tissue composing approximately 40% of the total mass of the human body[1]. Skeletal muscle creates voluntary motion of the human body, acting in response to electrical signals from the nervous system to generate force that is transmitted through tendons to the skeleton. Generation of contractile force is the primary function of skeletal muscle[2], and this functional behavior is closely related to its complex structure.

On the cellular level, muscle fibers or myofibers are the motors responsible for force generation. During development, myofibers are formed by fusion of mononucleated myoblasts into multinucleated myotubes (See Figure 1)[2]. Cylindrical in shape, myofibers can extend the full length of a given muscle. Each myofiber is composed of myofibrils arranged in parallel along its length. Division of myofibrils into a repeating pattern of sarcomeres gives skeletal muscle a striated appearance under high magnification and ultimately enables contractile behavior of the entire skeletal muscle system. Sarcomeres contain overlapping bands of the proteins, actin and myosin, that slide over each other during a contraction to generate force[2]. Overall force production by a given muscle fiber depends on the number of sarcomeres acting in parallel, a number that is directly related to the overall muscle cross-sectional area due to the uniform sarcomeric architecture. Figure 1 shows how sarcomeres in series form muscle fibers and how

muscle fibers are bundled into fascicles. In turn, several fascicles are bundled together to form an entire muscle, surrounded by an outer sheath termed the epimysium. Thus, it is clear how the structure of skeletal muscle is organized to maximize function, with each contractile unit, or sarcomere, repeated in a modular manner in progressively larger tissue subcomponents from myofibrils to myofibers to fascicles to whole muscles.

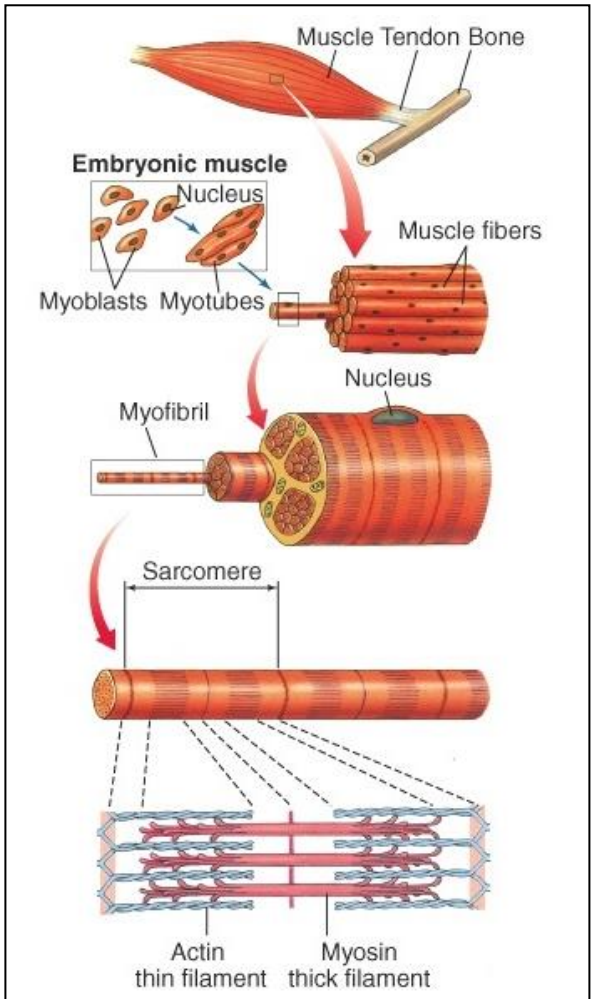

Figure 1. Hierarchical structural organization of skeletal muscle. Sarcomeres, formed by overlapping bands of myosin and actin, act as molecular motors to generate contractile force. These basic structural units are repeated in successively larger subcomponents, from myofibrils to muscle fibers to fiber bundles to the whole muscle. Adapted from Widmaier et al.[2]

On a tissue level, skeletal muscle is organized to provide access for the required stimuli and nutrients and the necessary matrix to transmit generated force. To support myofiber contraction, connective tissue, blood vessels, and nerves are thus present in the complex skeletal muscle architecture[1,2]. Nerve cells, specifically motor neurons, provide nervous control of muscle cells. As a highly metabolic tissue, skeletal muscle also requires vascularization via blood vessels and capillaries. As a result, each myofiber has a source of blood and nervous control in the endomysium, a layer of surrounding connective tissue. One of the key functions of connective tissue in skeletal muscle, especially the endomysium, is maintaining the complex architecture needed to provide both metabolites and nerve stimuli to each myofiber.

As one would expect based on the highly-organized structure of skeletal muscle, disruption due to trauma or disease severely affects the ability to produce force. The human body naturally repairs basic skeletal muscle injuries such as strains or tears, but traumatic damage often requires medical intervention[3]. The most prevalent such injury is volumetric muscle loss (VML), trauma overwhelming the normal muscle repair mechanism and resulting in permanent functional impairment and physical deformity[4]. Currently, clinical VML treatments have limitations including donor site morbidity and graft tissue scarcity[3]. Therefore, tissue engineers seek to fabricate skeletal muscle as an alternative graft tissue. Skeletal muscle tissue engineering approaches typically utilize muscle satellite cells to mature into a functional muscle construct. One of the primary challenges for tissue engineers, however, is obtaining the appropriate cellular component necessary for engineering skeletal muscle. The following section presents several techniques for addressing this issue, paying particular attention to: 1) cell isolation methods, 2) purification of isolated cells, and 3) optimization of *in vitro* culture conditions.

Skeletal Muscle Stem Cells

The text and figures in this sub-chapter were originally published with the following citation: Syverud BC, Lee JD, VanDusen KW, and Larkin LM. "Isolation and purification of satellite cells for skeletal muscle tissue engineering." *J Regen Med* 3(2): 117 (2014)[5]. Excerpts from this article have been included with permission from the publisher, SciTechnol.

Due to its tissue-specific regenerative potential, the satellite cell has been identified as the ideal progenitor cell for skeletal muscle tissue engineering[6,7]. In the early 1960's Mauro originally described the resident skeletal muscle stem cell, the satellite cell, by its cellular location beneath the basal lamina of a skeletal muscle fiber[8]. Since then, a great deal of research has attempted to elucidate the specific roles satellite cells play in skeletal muscle, particularly in muscle maturation, adaptation, and repair. During post-skeletal development, the satellite cell normally remains quiescent; however, satellite cell activity can be induced in response to muscle injury. In fact, recent studies demonstrate that satellite cells are indeed necessary for skeletal muscle to undergo regeneration[9-12]. These studies and others that evaluate satellite cell function utilize an important marker of satellite cells: paired box protein-7 or Pax7, encoded by the PAX-7 gene. Pax7 itself is a transcription factor that plays an integral role in myogenesis and regulation of muscle precursor cell proliferation. It is considered the requisite marker for satellite cell identification, and Pax7 genetic manipulation is utilized to assess specific myogenic function. Pax7 satellite cells, however, are not the only cell type that displays myogenic potential[6,13,14]. For example, mesoangioblasts, pericytes, Pax3, SK-34, CD45+/Sca1+, muscle side population, and PW1+/Pax7 interstitial cells have all been implicated in contributing to the myogenic cell pool.

However, formation of functional skeletal muscle *in vivo* utilizing most of these progenitors appears to require some level of Pax7 expression[15-17]. Ultimately, the complexity of the myogenic pool allows for diversity in tissue engineering strategies. Isolating Pax7-positive satellite cells for tissue engineering applications, however, is complicated by the heterogeneity and diversity of cells in this larger myogenic population.

Skeletal muscle tissue engineers choose to focus on isolating Pax7 satellite cells because of the proven regenerative potential of this specific population. While the variety of cell types detailed above display some degree of myogenic potential, the satellite cell has been identified as the primary source of regeneration in damaged skeletal muscle[6,18]. Quiescent satellite cells are activated in response to injury and progress toward a committed myogenic lineage, with a sub-population returning to quiescence to maintain the progenitor pool. Those satellite cells induced to a myogenic lineage are often referred to as myogenic precursor cells or myoblasts, characterized by their expression of the transcription factors myogenic differentiation 1 (MyoD) and myogenic regulatory factor 5 (Myf5)[19]. Following myoblast proliferation and differentiation, the myoblasts fuse with damaged fibers and promote regeneration.

In addition to extensive research into the satellite cell itself, a great deal of emphasis has focused on the microenvironment or "stem cell niche" which has been shown to be highly specific to and influential for satellite cell behavior and myogenic function[20,21]. The niche constituents include the satellite cell itself along with the surrounding extracellular matrix, vascular and neural networks, surrounding cells, and various diffusible molecules. This dynamic environment presents a unique challenge for engineered tissues *in vitro* because of the constant communication between the satellite cell and its niche *in vivo*. The growth factors and signaling

pathways dictating cellular regeneration are in constant flux, increasing the complexity of emulating myogenesis *in vitro*. Therefore, understanding the intrinsic and extrinsic signaling factors that influence the niche has been a priority for developing therapeutics in regenerative medicine[22], and similarly, strategies for muscle tissue engineering must aim to replicate the ideal conditions for skeletal muscle tissue repair.

Since the first skeletal muscle tissue engineering experiments by Vandenburgh and colleagues in 1988[23], the field has rapidly advanced to include a variety of techniques to enhance myogenesis and tissue regeneration. Although technologies include either scaffold materials ranging from acellularized tissues[24,25] to collagen and fibrin hydrogels[26,27] or a scaffold-free approach[28,29], the vast majority of these techniques utilize satellite cells as the cell source for muscle engineering. The complex satellite cell biology shows that isolating and culturing satellite cells presents a unique challenge. In particular, engineered skeletal muscle tissue requires a large quantity of isolated satellite cells with high purity. Engineered tissues to date have produced minimal force in comparison to healthy muscle, and the suspected cause of this disparity is decreased muscle fiber content and maturity[28,30,31]. As such, it is essential to maximize the myogenesis in engineered skeletal muscle tissue by isolating a pure satellite cell population. This process should result in both increased fiber content and improved functionality. Unfortunately, current methods for isolating satellite cells cannot yield both the population size and myogenic purity required by tissue engineers. It is instead necessary to combine these isolation techniques with additional purification methods, followed by controlled proliferation and induction conditions, and these approaches are described in detail in this sub-chapter.

Single Fiber Explant Culture

First described in 1986 by Bischoff and colleagues, techniques to explant and isolate individual muscle fibers have since been modified to isolate rat satellite cells[32]. In the original work, digestion of a dissected muscle and tendon in crude collagenase type I allowed liberation of individual myofibers. This procedure was found to be most successful after the fractionation of the collagenase, which enhanced the ability to remove the basal lamina from fibers and exposed the satellite cells. Because the separated fibers did not adhere to a standard polystyrene tissue culture substrate, a coating of either collagen or clotted chicken plasma was applied. This discovery opened an entire field of study on the use of similar substrates to promote adhesion of the satellite cells during the tissue engineering of skeletal muscle. Separation of individual fibers in this manner induced cellular signals of muscle injury, prompting satellite cell proliferation up to 4 days *in vitro*. Satellite cells remained attached to their respective fibers, however, so further study was needed to isolate the satellite cells from their basal lamina niche.

A modification of the Bischoff system by Rosenblatt and colleagues yields a pure population of both rat and mouse satellite cells from single fiber explants[33]. Following enzymatic digestion and separation, each fiber is plated individually with the aid of a dissecting microscope. A schematic of this protocol is shown in Figure 2. Central to this approach, satellite cells dissociate from their fibers and adhere to the tissue culture plate. Matrigel, an extract of basement membrane proteins derived from Engelbreth-Holm-Swarm mouse sarcoma cells, was used as a substrate coating in this case because it allowed both satellite cell attachment and subsequent removal of the fiber. As a result, when the fibers are removed from the plate after 3-4 days *in vitro*, a highly myogenic adherent cell population remains for further expansion and study. Using

this method, up to 300 satellite cells can be obtained per fiber, with potential for approximately 300-fold expansion to 100,000 myogenic cells[33].

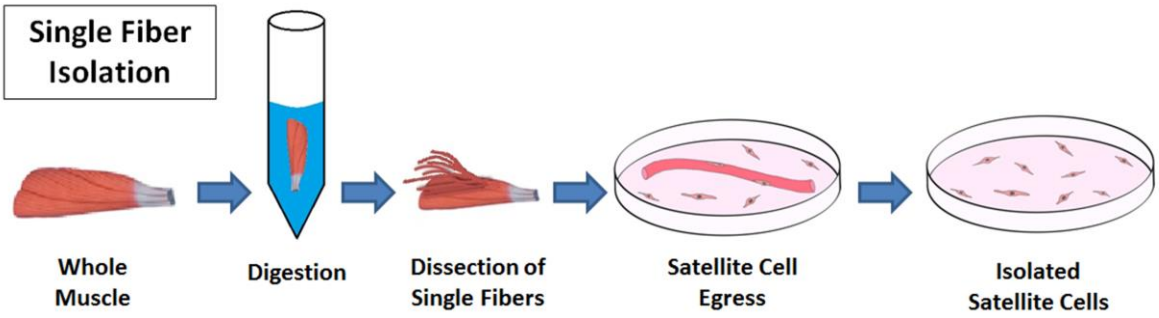

Figure 2. Single fiber explant culture for isolation of satellite cells. This technically challenging and labor-intensive isolation method yields a highly pure, but relatively small satellite cell population. The desired muscle is dissected and enzymatically dissociated until individual myofibers can be removed under a microscope. These fibers are then cultured for several days, allowing for egress of satellite cells onto the culture substrate. When the myofiber is removed, the isolated satellite cell population remains.

Since its introduction and subsequent modification, the single fiber method for isolating satellite cells has remained relatively unchanged. A much more detailed procedure was published in 2010 by Conboy and colleagues, but the basic steps are consistent with previously published papers[34]. This approach is generally accepted to yield the purest satellite cell populations, approximately 95% or higher[33] but has serious limitations in that dissecting individual muscle fibers is a highly precise and time-consuming task. Furthermore, although only individual fibers are needed for the final explant culture step, this protocol dictates removal of the entire muscle to avoid fiber damage. Because of its ability to yield satellite cells *in vitro* with high purity, single fiber isolations serve as powerful tool for the study of satellite cell biology, but the relatively low overall cell yield from such a large muscle volume make this technique sub-optimal for tissue engineering applications.

Enzymatic Dissociation

To increase overall yield, many researchers use an enzymatic digestion of whole muscles to isolate satellite cells (Figure 3)[35,36]. This technique was also pioneered in the rat by Bischoff and colleagues[37], with significant modifications by Rando and Blau in the mouse[36]. Using this approach, muscle tissue is dissected and dissociated into a single cell suspension. Initially, all visible tendon and connective tissue is removed from the harvested muscle to maximize final myogenic purity. It is common for researchers to use a combination of enzymes to specifically digest the various skeletal muscle extracellular matrix components and "release" cells of interest. However, a rigorous enzymatic digestion process will also liberate a population of fibroblasts, leading to a diluted satellite cell suspension. Current methods have identified various combinations of trypsin, pronase, dispase, and several collagenases as optimal mixtures[37-39], and a study by Tebbets and colleagues highlights this variety in proteolytic enzymes used across the field[40]. Several studies have compared the relative efficacy of these enzymes[41-43]. It is believed that a mixture of collagenase and dispase minimally affects cell surface antigens, allowing for easier future enrichment of isolated cells[41]. On the other hand, pronase may inhibit survival and proliferation of non-myogenic cells and yield a purer isolated satellite cell population[42]. Ultimately, direct comparison suggests that these enzymes are all suitable for liberation of satellite cells, assuming one uses the correct duration of enzymatic digestion[43]. Following digestion, debris is removed from the suspension by filtration, and isolated cells are seeded for proliferation and differentiation.

Selection of the proper substrate adhesion protein is important at this stage in promoting satellite cell attachment. Collagen, polylysine, fibronectin, Matrigel, and laminin are commonly

used as adhesion proteins[31,38]. Several studies have compared the efficacy of different adhesion proteins in preferentially promoting satellite cell adhesion, proliferation, and differentiation[44-49] (Table 1). As these compiled results show, no specific adhesion protein has been identified as ideal for culturing satellite cells, but it is clear that the adhesion proteins described in Table 1 (fibronectin, Matrigel, gelatin, and laminin) promote increased attachment and proliferation relative to uncoated polystyrene tissue culture plastic or alternative proteins (polylysine and collagen types 3 or 4)[38,44].

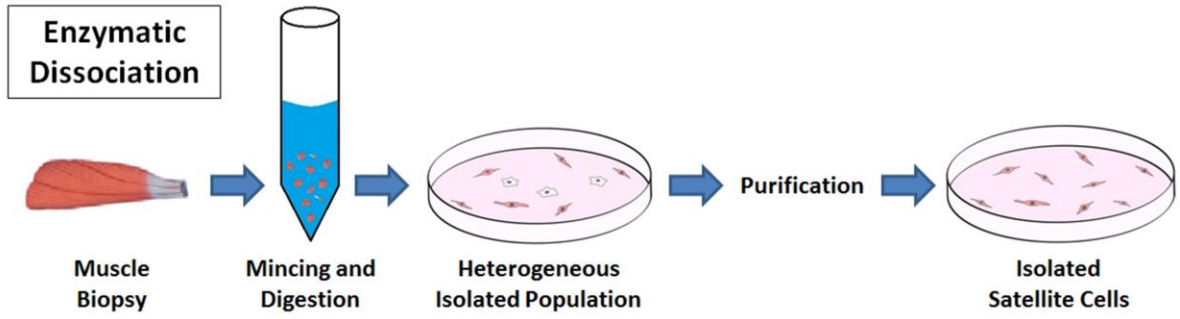

Figure 3. Enzymatic dissociation for isolation of satellite cells. This isolation method can yield a large satellite cell population suitable for tissue engineering purposes, but requires additional purification to remove non-myogenic cells. A muscle biopsy is mechanically and enzymatically digested to yield a single cell suspension. The resulting heterogeneous population contains a mixture of satellite cells, fibroblasts, hematopoietic cells, and several other types. As a result, it is often necessary to enrich the myogenic satellite cell population through the purification methods described in this sub-chapter.

Following isolation, characterizing the purity of the final cell population is essential when engineering skeletal muscle. While flow cytometry, described in detail below, certainly presents a high-throughput technique for identifying the various cells in a heterogeneous population, the use of cytochemistry for identifying myogenic and non-myogenic cells is a more traditional approach. Using markers of satellite cell activation, it is possible to stain isolated cells for canonical proteins that identify not only their myogenicity but also their state in the regenerative process. It is known that quiescent and activated satellite cells express Pax7[20,50]. Following

activation, identified by Myf5 upregulation and MyoD expression, the satellite cell becomes a myogenic progenitor or myoblast. By examining cultured satellite cells for Pax7, Myf5 and MyoD, it has been determined that removal of satellite cells from their niche during isolation immediately leads to their activation, and that a minimal quiescent population remains *in vitro*[38]. MyoD staining can therefore be used to identify proliferating satellite cells as soon as 24 hours post-isolation[38].

Publication	Adhesion Proteins	Optimal Attachment	Optimal Proliferation	Optimal Differentiation
Wilschut et al. 2010[49]	Matrigel, Gelatin, Collagen-1, Fibronectin, Laminin	Fibronectin, Laminin	Matrigel, Laminin	Matrigel, Laminin
Boonen et al. 2009[48]	Matrigel, Collagen-4, Laminin, Poly-D-lysine	-	Matrigel	Laminin, Poly-D-Lysine
Maley et al. 1995[46]	Gelatin, Collagen-4, Fibronectin, Laminin	-	-	Matrigel
Doumit et al.1992[44]	Gelatin, Collagen-3, Fibronectin	-	Gelatin	Gelatin
Dodson et al. 1990[47]	Gelatin, Collagen-1, Collagen-4, Fibronectin, Laminin, Poly-L-lysine, Poly-D-lysine	Fibronectin	Gelatin	Gelatin

Table 1. Comparison of adhesion proteins for isolated satellite cells. Overall, fibronectin, Matrigel, gelatin, and laminin seem ideal for culturing satellite cells, and these four adhesion proteins are most commonly used. From a tissue engineering perspective, Matrigel has limited clinical relevance because it is derived from a cancer cell line.

As regeneration continues, fusion of myoblasts and terminal differentiation occurs, accompanied by expression of myogenin, desmin, and c-met. Desmin, in particular, has often been utilized as an indicator of proliferating myogenic cells at time points ranging from 30 hours to several days post-isolation[36,38]. After myotube formation, typically occurring around 7 days post-isolation but varying with seeding density and onset of differentiation, neonatal or

embryonic myosin heavy chain isoforms can be used to identify nascent muscle. By following these previously established markers to identify myogenic cells within the overall isolated population, it is possible to evaluate the overall success and purity of the isolation process.

Using such characterization methods, it has been determined that the final cell suspension isolated via the enzymatic dissociation method is significantly less myogenically pure than the single fiber isolation method. The isolates are contaminated by a small population of hematopoietic and neural cells, and connective tissue fibroblasts form the majority of the non-myogenic population. This fibroblast fraction plays an essential role in myogenesis through a reciprocal interaction with the proliferating satellite cells, but in large numbers can inhibit regeneration[11,51]. On the other hand, fibroblasts proliferate more rapidly than satellite cells[7,38], and this non-myogenic population can potentially overwhelm proliferating myogenic cells if too numerous initially. As a result, knowing the starting cell populations and monitoring the interaction between isolated satellite cells and fibroblasts is essential to understanding growth of muscle tissue during skeletal muscle tissue engineering. For reference, yields of approximately 10,000 satellite cells per 100mg of digested muscle have been reported, with potential proliferation to 10 million cells[35]. Due to the ease at which significant volumes of muscle can be harvested, the potential for obtaining relevant numbers of satellite cells for tissue engineering is much larger with this method than through the single fiber isolation method. As a result, tissue engineers utilize this enzymatic dissociation method preferentially for high cell volume requirements. However, because of the lower myogenic purity, supplemental purification steps are often necessary to increase regenerative potential of the isolated satellite cells, and such purification methods are discussed in the following section.

Pre-Plating

One of the most common methods for rapidly purifying satellite cells from a muscle homogenate is a selective pre-plating method published by Richler and Yaffe[52]. Following enzymatic dissociation, this serial pre-plating technique has been used to enrich the isolated myogenic cell population. Instead of seeding isolated cells directly onto a substrate coated with adhesion protein, the cell suspension is distributed onto uncoated tissue culture plastic for a period ranging from 15 minutes to 24 hours[36,40]. Fibroblasts and epithelial cells present in the muscle homogenate rapidly adhere to the tissue culture plastic, and the satellite cells remaining in suspension can be collected in the non-adherent cell population[35,52]. Using multiple iterations of pre-plating to enrich the non-adherent cells, a purified myogenic cell population can be obtained prior to the final seeding. Previous work has demonstrated increased purification with each subsequent step finding a 94% myogenic purity following six pre-plate steps over the course of 6 days[53].

The technical simplicity of using pre-plating as a purification step following enzymatic dissociation is certainly an advantage. However, during the pre-plating process, some myogenic cells inevitably attach either to the tissue culture plastic or to the adherent fibroblasts and are lost. Careful control of the pre-plate time is thus necessary to balance retention and purification. The major drawback of this technique is its time-consuming nature. Satellite cells and myoblasts have a limited potential for proliferation, because isolation typically leads to their activation, terminal differentiation, and loss of the potential for self-renewal[38]. As a result, maximizing the *in vitro* proliferative capacity of these myogenic cells is essential. Any time spent purifying through pre-plating, however, decreases this limited capacity for proliferation. Additionally, pre-

plating is limited by the potential for myogenic and non-myogenic cell populations to vary significantly in the final cell suspension. Although the purity of isolated cells has certainly been increased, the degree of improvement is inconsistent, and final purity remains unknown without additional analysis of cellular content. For tissue engineers, knowing the final myogenic purity is essential for consistent tissue fabrication. Fluorescence activated cell sorting (FACS) and magnetic activated cell sorting (MACS) have been used to evaluate the success of the pre-plating process, leading researchers to consider whether they can be used to skip pre-plating and immediately sort instead[54,55].

FACS - Fluorescence Activated Cell Sorting

Among the sorting techniques that may be applied to the isolation of satellite cells, FACS shows promise due to its efficiency in sorting large populations of cells. This technique has been used extensively as both a diagnostic and research tool to obtain information rapidly about heterogeneous cell populations including cell number, relative cell size, and cell viability. FACS operates through laser-based identification of fluorophore-conjugated cell markers and applied electrical charges to physically separate individual cells. The use of FACS in satellite cell purification, however, is complicated by the absence of a definitive surface marker. Early work on myoblast isolations by the Blau laboratory demonstrated that semi-pure primary mouse myoblasts could be isolated using FACS and antibodies to α7 Integrin alone[24]. Recent work has focused on improving the purity of isolated satellite cells by using a combination of markers to identify and isolate satellite cells from other muscle-derived cells, as described in Table 2[42].

Recently, Pasut et al. demonstrated successful FACS isolation of satellite cells using a combination of positive markers α7 Integrin and CD34 with negative markers CD45, CD31, CD11b,

and Sca-1[56]. Likewise, Sherwood et al. demonstrated similar FACS isolation of myogenic cells using positive markers CXCR4 and β1-integrin and negative markers CD45, Sca-1, and Mac-1, and cell purity was confirmed by growing the sorted cells into myotubes in cell culture[57]. Because of the heterogeneity of the satellite cell population, with certain sub-populations displaying unique surface marker profiles, various additional marker combinations specific to satellite cells have been identified[58,59].

Publication	Sorted Population	Positive Markers	Negative Markers	Heterogeneous Markers
Pasut et al. 2012[56]	Satellite Cells	α7-Integrin, CD34	CD45, CD31, CD11b, Sca-1	-
Bosnakovski et al. 2008[60]	Pax7-ZsGreen Satellite Cells	CD29, CD34	CD45, CD105, PDGFRα, c-Kit	CXCR4
Montarras et al. 2005[146]	$Pax3^{GFP/+}$ Satellite Cells	CD34	CD45, Sca-1	-
Sherwood et al. 2004[57]	Myogenic Progenitors	β1-Integrin, CXCR4	CD45, Sca-1, Mac-1	-
Asakura et al. 2002[59]	Satellite Cells	CD34	CD45, Sca-1	-
	Muscle Side Population Cells	-	-	CD45, Sca-1
Jankowski et al. 2001[61]	Proliferating Muscle-Derived Stem Cells	-	CD45, c-Kit	CD34, Sca-1

Table 2. Prospective surface markers for isolation of satellite cells. Due to the heterogeneity of the myogenic pool, FACS targeting different cell populations has identified various surface marker combinations. The most consistent trend is the use of CD34 as a positive marker, with CD45 and Sca-1 as negative markers. In several cases, these and other markers were identified on a unique subset of the isolated population, and they are labelled as heterogeneous markers as a result.

Consistent with the work described above, Bosnakovski et al. identified CD34 as a positive marker and CD45 as a negative marker for satellite cells sorted from a Pax7-ZsGreen^{+} mouse[60]. Bosnakovski's work also found that only half of the sorted satellite cells expressed CXCR4, in

partial disagreement with Sherwood's work. This finding again suggests the presence of unique sub-populations within the larger satellite cell pool, potentially complicating the sorting process. A similar heterogeneity within the satellite cell pool also occurs with injury to the muscle prior to isolation, evident when sorting yields Sca-1 positive, rather than negative, satellite cells. Similar variation in satellite cell surface markers has been demonstrated when examining CD34 and Sca-1 expression in myogenic cells *in vitro*[61]. In particular, distinct sub-populations, both positive and negative for CD34 and Sca-1, were found within the heterogeneous myogenic cell population over a period of 6 days *in vitro*. When examined together, these studies illustrate the difficulties in purifying satellite cells presented by the heterogeneous surface marker profiles across the overall isolated population. Ultimately, FACS has proven successful in purifying myogenic cells from a heterogeneous cell population isolated in a mouse model, illustrated in Figure 4. Such plots also demonstrate the considerable technical expertise required to differentiate the sub-populations typically overlapping each other. Although researchers have utilized a wide variety of surface markers, the common trend across these strategies is the use of CD34 as a positive marker and CD45 and Sca-1 as negative markers. However, as tissue engineers seek to use larger animal models, study of these heterogeneous surface markers present in the myogenic pool will be required for each new species. Again, while satellite cell sorting with FACS has proven effective, potential damage to cells or alteration of their proliferation during the sorting process remain significant drawbacks to the use of FACS in muscle tissue engineering. The electrical charge applied to separate cells requires a substantial voltage, and though the satellite cells typically survive this perturbation, it is thought that gene expression may be altered[62].

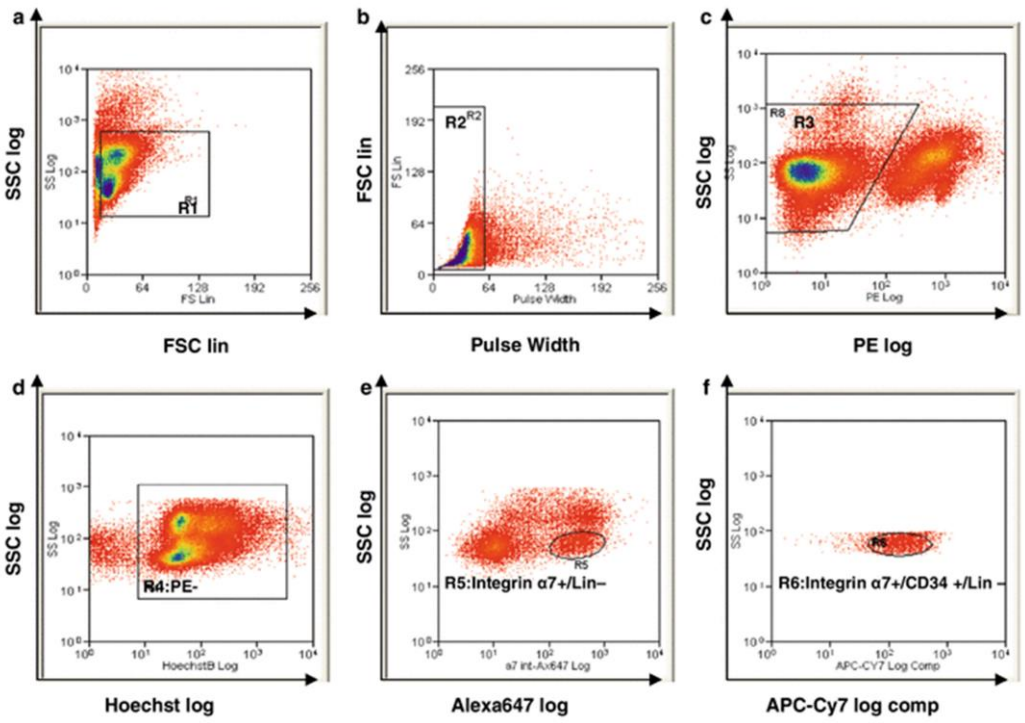

Figure 4. Example methodology for FACS purification of satellite cells. Dot plots representing the sequential gating strategy used to identify satellite cells from a heterogonous muscle sample based on: **(a)** Side Scatter (SSC) and Forward Scatter (FSC), **(b)** Doublets discrimination, **(c)** PE- gating to remove CD45 and CD11b blood lineage cells, Sca-1 mesenchymal progenitors, and CD31 endothelial cells, **(d)** Hoechst staining for live (Hoechst+) and dead (Hoechst−) cells, **(e)** Integrin α7+ and Sca-1- (Lin−) gating, and finally **(f)** Integrin α7+ and CD34+ gating to sort the population defined as satellite cells. As the plots above illustrate, unique populations are rarely completely distinct, and substantial technical expertise is necessary to design such gating strategies properly. Adapted from Pasut et al.[56]

Specific studies to examine the effects of FACS on satellite cell viability and subsequent proliferation *in vitro* have not been conducted, so it remains to be seen if sorted cells are still suitable for tissue engineering purposes. The use of FACS in isolating human embryonic stem cells, however, led to decreased viability[63], and destabilization of the membrane was observed in sorted spermatozoa[64]. Unless such damaging effects can be avoided in the case of satellite cells, skeletal muscle tissue engineers may choose not to use FACS to purify isolated cells and instead use it only for characterization.

MACS - Magnetic-Activated Cell Sorting

Magnetic-activated cell sorting (MACS) offers an alternative method for satellite cell sorting. Commonly utilized in immunology, neuroscience, and cancer research, MACS operates by incubating cells with antibodies for specific markers of interest conjugated to magnetic microbeads. Because it similarly relies on sorting by antigen expression, MACS suffers from the same primary limitation as FACS—the lack of a definitive surface marker prevents direct sorting of satellite cells, and some combination of markers must instead be used. Research by the Blau laboratory demonstrated that semi-pure mouse myoblast populations may be isolated using MACS technology to select for α7 Integrin$^+$ cells, with similar purification levels as found with FACS[55]. Although MACS has been used in some cases to purify CD56 positive satellite cells[65], direct comparison of pre-plating and MACS indicated much greater purification using the pre-plating technique[54]. From these studies, it is clear that multiple markers are likely needed to isolate a highly pure population.

An additional complication associated with MACS sorting is the magnetic labelling. While the antibody-marker conjugation used in FACS is certainly a modification of the target cells, with antibody binding potentially activating or blocking signaling pathways associated with the target surface receptor[62], the attachment of magnetic microbeads is a far more significant alteration[66]. From a tissue engineering standpoint, concerns arise regarding implantation of cells that may retain attached or internalized microbeads. As a result, MACS may be limited for application in tissue engineering to negative sorting, the removal of cell types other than that of interest, resulting in a semi-pure cell population. This technique has been demonstrated by using MACS to remove CD45$^+$ cells from a cell isolate[67]. Until methods for magnetically sorting satellite cells

has been improved and concerns about magnetic microbead retention have been resolved, MACS may not provide a realistic cell sorting approach for tissue engineering.

Summary

Considerable effort has been dedicated to isolating and purifying satellite cells. Because of these advances, several powerful tools are available to tissue engineers. Single fiber explant culture isolations yield small populations with high purity, whereas enzymatic dissociation isolates a mixture of myogenic and non-myogenic cells with a need for additional purification. Pre-plating is the most common method for purification and has proven effective, but it ultimately lacks a quantitative measure of the final myogenic cell population. FACS and MACS have also been considered, with FACS potentially providing the ability to both sort and characterize isolated cells. Further understanding of satellite cell surface markers may make FACS an increasingly viable alternative; however, the need for labelling and the potential for alteration during the sorting process ultimately limit FACS and MACS.

As researchers seek to translate engineered skeletal muscle technologies from small animal models to larger animals and eventually humans, more efficient and reliable isolation methods will become essential. Techniques for increasing myogenic cell proliferation and inducing differentiation in vitro by controlling culture conditions and seeking to recapitulate the satellite cell niche are being developed to utilize isolated satellite cells maximally, but the scaling up process could exceed these capabilities. It is expected that rapid development will continue in the areas covered in this sub-chapter since they will help translate tissue engineering of skeletal muscle into a viable clinical treatment.

Growth Factors and Skeletal Muscle Tissue Engineering

The text and figures in this sub-chapter were originally published with the following citation: Syverud BC, VanDusen KW, and Larkin LM. "Growth factors for skeletal muscle tissue engineering." Cells Tissues Organs 202: 169 (2016)[68]. Excerpts from this article have been included with permission from the publisher, S Karger AG.

Proposed applications for tissue-engineered skeletal muscle include implantation as a graft material for repair of traumatic damage[30,69], recapitulation *in vitro* of native development and regeneration for detailed physiological study or pharmaceutical testing[27], and use as biomechanical actuators[70,71]. In all cases, mimicking the complex structure and function of skeletal muscle *in vivo* is an essential consideration. To date, however, engineered tissues have been characterized by a neonatal phenotype in terms of vascularity, force production, and structural maturity[26,29]. Without major advances, especially in vascularization, use of engineered muscle as a graft material will be severely limited. Implantation of engineered skeletal muscle into an *in vivo* regenerative environment, however, has promoted development towards the adult phenotype[24,72], and several recent studies have attempted to utilize key chemical and mechanical stimuli to improve the maturity of these engineered muscles *in vitro* [65,73]. This review focuses on important *in vitro* biochemical stimuli, summarizing the current state of the art in growth factors utilized for skeletal muscle tissue engineering.

Skeletal Muscle Development During Embryogenesis

Before attempting to describe the ideal *in vitro* biochemical environment for engineered skeletal muscle, it is necessary to understand the *in vivo* environment tissue engineers seek to emulate. During embryogenesis, morphogen gradients control patterning of the developing

tissues. Following germ layer formation in the pre-patterned embryo, localized variations in gene expression and signaling gradients prompt condensations of the paraxial mesoderm into somites (Figure 5)[74]. Genes in the Notch and Wnt pathways prompt somitogenesis in concert with spatiotemporal gradients of fibroblast growth factor (FGF) and Wnt proteins. The most dorsal section of the somite becomes the dermomyotome, from which the majority of skeletal muscles are derived. Myogenesis is initiated as the $Pax3^{+}$ progenitor cell pool present in the somite delaminates and progressively establishes the primary myotome[75]. Members of the Wnt family of proteins again play a central role in this process. Through binding to Frizzled receptors, Wnt signaling activates the β-catenin/TCF complex and induces somite patterning and expression of the myogenic transcription factors Pax3 and Myf5[74]. A small subset of the progenitor cell pool migrates into the myotome, proliferates, and then terminally differentiates into myoblasts. In turn, the terminally differentiated myoblasts fuse with each other to form the first multinucleated myotubes and primary myofibers[76]. This stage of myogenesis is primarily regulated by the canonical myogenic regulatory factors: Myf5, MyoD, and myogenin. Sonic hedgehog (Shh), released from the notochord and floor plate of the neural tube, promotes Myf5 expression and commitment to the myogenic lineage[74,76]. With the establishment of innervation, the remaining cells from the progenitor pool differentiate into myoblasts and fuse to form secondary myofibers. In addition, a subset of skeletal muscle progenitor cells start to co-express Pax3 and Pax7, becoming post-natal progenitor cells often referred to as satellite cells[8,77]. These satellite cells are not activated during embryonic myogenesis and remain as a reserve pool for post-natal muscle growth and regeneration. Bone morphogenic proteins (BMPs), a sub-class of

the transforming growth factor-beta (TGFβ) superfamily, serve to preserve this progenitor pool by inhibiting Myf5 and MyoD expression while upregulating Pax3.

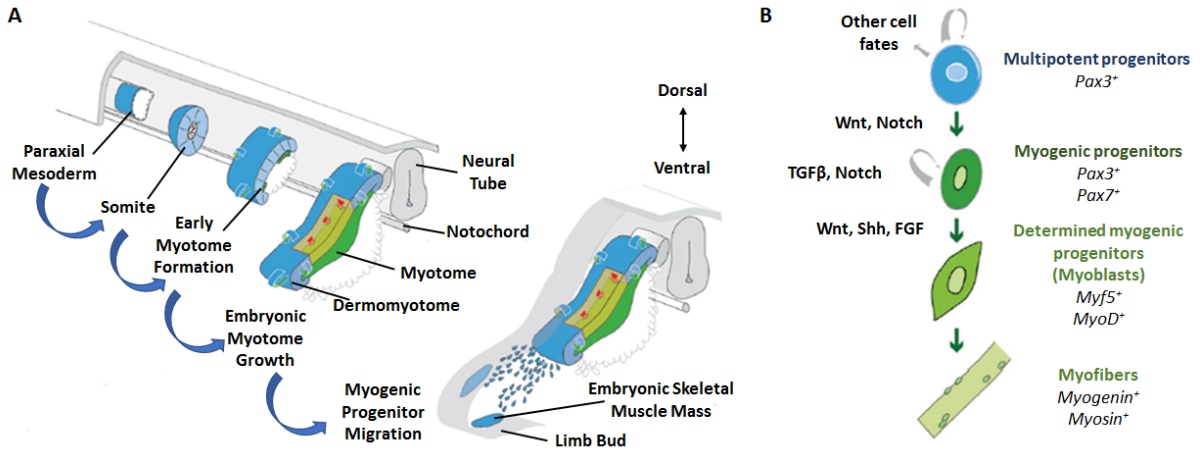

Figure 5. Initial skeletal muscle formation during embryogenesis. **(A)** Development of the somite and subsequent establishment of the myotome. **(B)** Regulation of progenitor cell renewal and differentiation by myogenic regulator factors and external signaling. Adapted from Buckingham and Mayeuf 2012[76].

In summary, myogenesis during embryonic development is primarily regulated by Myf5, MyoD, and myogenin[76], but several molecular signals and growth factors interact with these myogenic regulatory factors. Wnt and FGF gradients direct initial somitogenesis. Subsequently, Shh and Wnt signaling lead to specification and expression of Myf5. Additionally, TGFβ is known to act through serine-threonine kinase receptors, activating SMAD proteins inhibiting Myf5 and MyoD induction. As a result, the onset of skeletal muscle formation is delayed and the myogenic progenitor pool is preserved. Finally, FGF acts as an antagonist to TGFβ in regulating the equilibrium between renewal and differentiation of progenitor pool. Specifically, FGF upregulates Myf5 and MyoD, promotes activation of progenitors in the myogenic lineage[78], and begins the transition to post-natal skeletal muscle development.

Post-natal Skeletal Muscle Development

Post-natal skeletal maturation and lengthening of skeletal muscle relies on the contribution of nuclei and contractile proteins by satellite cells to keep pace with the growing skeleton and to mature in structure. This process is characterized by addition of new sarcomeres along the length of each fiber, establishment of myotendinous junctions, and the transition in myosin heavy chain (MHC) expression from embryonic to adult fast and slow isoforms[75,79]. Satellite cells provide the nuclei required to regulate this continued growth. Until activated, satellite cells remain quiescent under the basal lamina of skeletal muscle fibers and are characterized by the expression of Pax7[8]. The surrounding stem cell microenvironment or niche, composed of extracellular matrix, vascular and neural networks, neighboring cells, and growth factors, is highly influential on myogenic function (Figure 6)[20,80]. In response to a complex series of signals, satellite cells are activated and progress toward a committed myogenic lineage, with a sub-population returning to quiescence to maintain the progenitor pool. As in embryonic development, Notch signaling and Wnt proteins act as essential regulators of post-natal maturation of the satellite cell. In particular, Wnt3a signaling promotes satellite cell activation and differentiation, whereas Wnt7a induces self-renewal and maintenance of the satellite cell pool[74]. Mammalian (or mechanistic) target of rapamycin (mTOR) also plays a key role in mediating post-natal satellite cell activation, proliferation, and differentiation. Although more commonly associated with skeletal muscle hypertrophy and homeostasis, mTOR has recently been shown to regulate satellite cell activity and myogenesis by upregulating expression of Pax7, Myf5, MyoD, and myogenin[81].

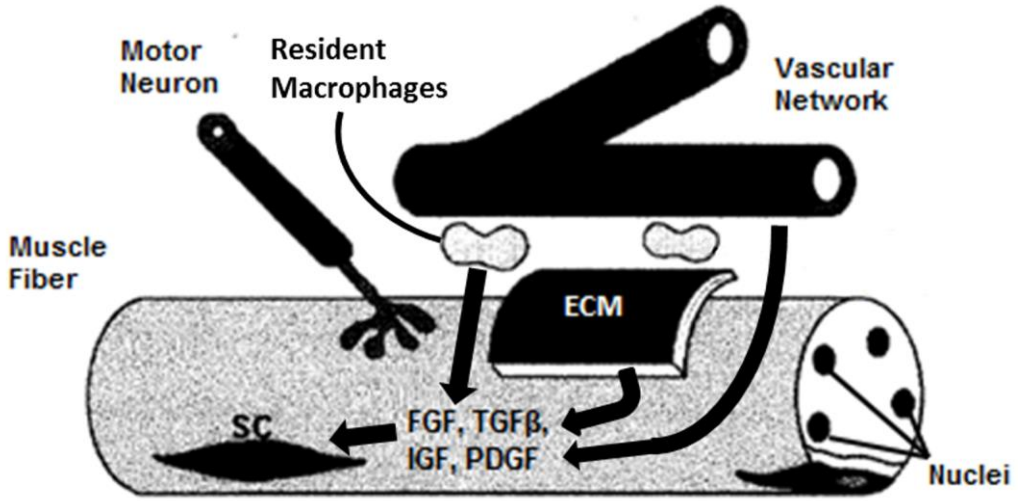

Figure 6. Growth factor signaling in skeletal muscle regeneration. The microenvironment surrounding the satellite cell (SC) niche regulates repair of skeletal muscle damage. Resident immune cells, extracellular matrix (ECM), and capillary and neural networks compose this niche. This schematic describes a simplified process by which essential growth factors (FGF, TGFβ, IGF, and PDGF) are supplied to stimulate and regulate SCs.

Additionally, several growth factors stimulate quiescent satellite cells. Hepatocyte growth factor (HGF) is present in inactive form in the extracellular matrix adjacent to satellite cells[79]. When released due to injury or length damage, HGF is thought to bind c-met receptors present on quiescent satellite cells, leading to their activation. Similarly, members of the FGF family are present in the satellite cell niche and bind to quiescent satellite cell receptors following FGF release[76,79]. After activation via growth factors such as HGF or FGF, those satellite cells induced to a myogenic lineage are often referred to as myogenic precursor cells or myoblasts, characterized by their expression of canonical myogenic transcription factors MyoD and Myf5. Following their proliferation and differentiation, the myoblasts fuse with maturing muscle fibers and promote protein synthesis and muscle growth. Connective tissue fibroblasts in the extracellular matrix have been shown to interact with satellite cells throughout this stage, with reciprocal signaling between the two cell types prompting increased proliferation of both[82].

Furthermore, expression of the transcription factor Tcf4 by connective tissue fibroblasts intrinsically regulates the maturation of MHC isoforms through β-catenin activation[51,76]. In conclusion, post-natal skeletal muscle development depends on activation and myogenic differentiation of satellite cells. Although the satellite cell pool is considered heterogeneous, several common signaling pathways play essential roles in this myogenic lineage, with HGF and FGF as the primary growth factors involved.

Skeletal Muscle Homeostasis

Once skeletal maturation is complete, skeletal muscle homeostasis is maintained through hypertrophy and atrophy. Hypertrophy and regeneration are primarily regulated by a signaling pathway initiated by insulin-like growth factor 1 (IGF1)[78]. Whether expressed by muscle cells in response to injury and exercise, secreted by macrophages and endothelial cells with inflammation, or supplied by the circulatory system in the blood, IGF levels increase rapidly in preparation for protein synthesis[83]. Following IGF1 binding, an intracellular cascade mediates its effects (Figure 7)[84,85]. Among these intracellular signals, Akt, or protein kinase B (PKB), plays an essential role[86]. To promote protein synthesis and hypertrophy, Akt indirectly activates mTOR while simultaneously inhibiting glycogen synthase kinase 3b (GSK3b). At the same time, Akt prevents protein degradation and muscle atrophy by blocking the FoxO family of transcription factors[87]. Myostatin, a member of the TGFβ family predominantly expressed in skeletal muscle, conversely functions as a potent cytokine for the inhibition of muscle growth and induction of muscle atrophy. Following activation and release from the extracellular matrix, myostatin activates Smad2/3 and TAK1/P38 MAPK signaling cascades, leading to upregulation of Atrogin-1 and muscle RING-finger protein-1 (MuRF-1) and subsequent proteolysis[88]. Both IGF1 and

myostatin, along with their downstream effectors, have been targeted for therapeutic use *in vivo*[83,87], and it is expected that similar benefits will translate to engineered skeletal muscle.

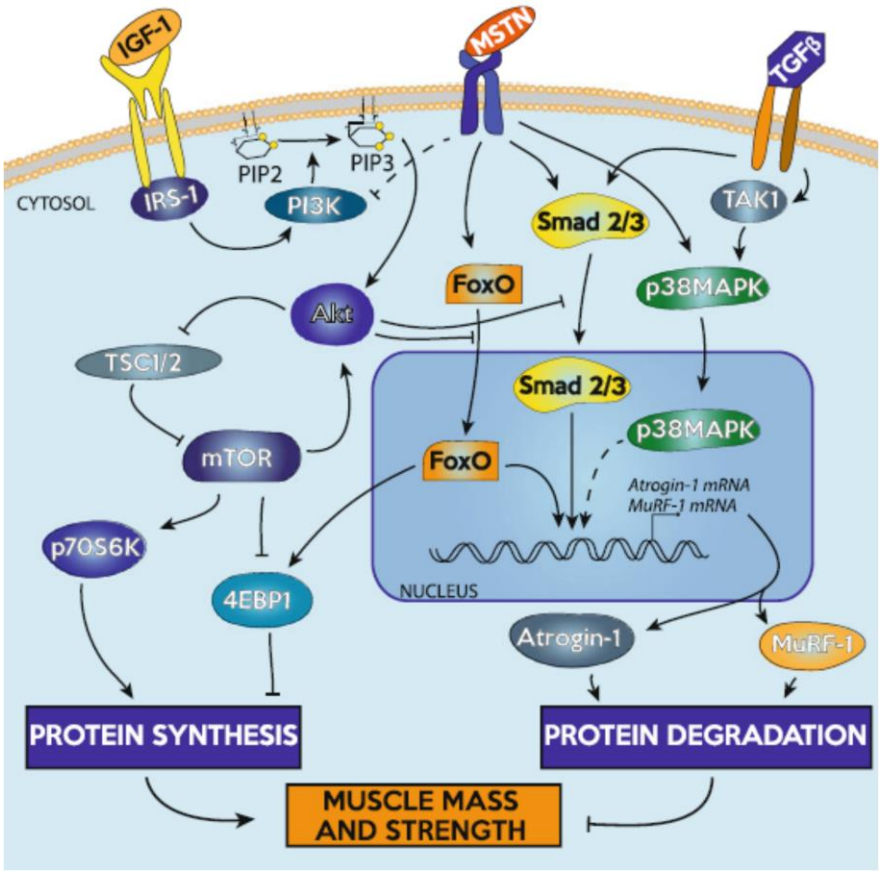

Figure 7. Central pathways to regulation of skeletal muscle hypertrophy and atrophy. The hypertrophic effects of IGF-1 have been widely documented. Binding of IGF-1 to its receptor leads to release of Akt to the cytosol and activation of mTOR and protein synthesis. Myostatin (MSTN) and TGF-β control skeletal muscle atrophy. When activated, these cytokines trigger a signaling cascade leading to upregulation of Atrogin-1 and MuRF-1 and protein degradation. Adapted from Gumucio and Mendias 2013[88].

External to the IGF/Akt/mTOR signaling pathway, several growth factors have been examined due to their effects on myogenic progenitor cells implicated in skeletal muscle growth and development. As in embryonic development, TGFβ inhibits progression of muscle precursor cells[87,89]. In contrast, HGF, FGF, and platelet derived growth factor (PDGF) have all been associated with muscle repair and hypertrophy[90,91]. As in post-natal development, HGF is

released from the extracellular matrix with injury to prompt satellite cell activation and proliferation via p38 MAPK and PI3K[83]. FGF serves a similar purpose, mainly stimulating proliferation of satellite cells. After release from activated platelets and macrophages, PDGF again promotes myogenic proliferation, in addition to angiogenesis. Interestingly, these three growth factors (HGF, FGF, and PDGF) all have an inhibitory effect on myogenic differentiation[83,91]. Overall, it is evident how various growth factors are intricately involved in these native pathways controlling the development, growth, and regeneration of skeletal muscle. Their interplay with the canonical myogenic regulatory factors is evident in the activation and proliferation of myogenic progenitors, terminal differentiation to myoblasts, and up- or down-regulation of protein synthesis and degradation.

Growth factors for skeletal muscle tissue engineering

Because of the difficulties associated with isolating and purifying satellite cells, it is essential to maximize the myogenic potential of these cells *in vitro*. In addition, isolated satellite cells can only be expanded to a limited extent, because myogenic potential rapidly decreases after isolation[33,92]. This behavior can at least partially be explained by the fact that fibroblasts and other non-myogenic cells in the isolated population double every 18 hours, much more rapidly than the approximately 24 hours for satellite cells[7,38]. Several studies have demonstrated the ability to expand isolated muscle progenitor cells *in vitro* for up to 50 population doublings[36,93]. However, examination of myogenic potential over this expansion period demonstrated a steady decline in Pax7, MyoD, and desmin expression, beginning at over 90% and decreasing to approximately 55% by the third passage[94]. Furthermore, immunocytochemistry for 5-bromo-2'-deoxyuridine-5'-monophosphate (BrdU) showed 60%

positive staining at the time of isolation but steadily decreasing values with each subsequent passage, indicating declining activation and proliferation of isolated satellite cells with increased time *in vitro*. With this understanding of *in vitro* satellite cell behavior, it is essential to maximize proliferation of isolated satellite cells before myogenic potential drops or faster proliferating populations begin to take over the culture. Thus, comprehensive study has determined optimal conditions for promoting proliferation and inducing differentiation of satellite cells.

Tissue engineers have used this understanding of growth factors and their role in myogenesis to direct techniques for the fabrication of skeletal muscle. To date, tissue engineering technologies utilize either scaffold materials ranging from decellularized tissues[95,96] to collagen and fibrin hydrogels[26,27,97] or opt for a scaffold-free approach[28,29,72] to promote the development of an extracellular matrix (ECM) for subsequent muscle tissue. The success of these techniques ultimately depends on the *in vitro* cultivation of isolated primary muscle precursor cells for the development of mature muscle cells within the ECM. The typical techniques for culture of these myogenic cells involves an initial proliferation phase, to allow cell numbers to expand to a sufficiently large population, followed by differentiation and fusion into myotubes and maturation to myofibers[98]. Detailed study of growth factors known to play a role in each of these phases of myogenesis is thus essential to further the understanding of muscle growth *in vitro*. It is generally accepted that media rich in serum promotes initial proliferation of skeletal muscle stem cells to myoblasts while delaying the onset of differentiation, potentially due to large number of hormones and growth factors of varying concentration and potency found in the serum[38]. Dramatic changes in function and speed of contraction were recently observed between engineered muscles cultured in serum from the United States and from the European Union[99].

Similarly, environmental factors in the culture media, such as glucose and antibiotic concentration, have been shown to alter engineered muscle phenotype and function[100]. In this study, ideal conditions for maximizing force production in tissue-engineered skeletal muscle involved high glucose (25mM) and an absence of streptomycin. A drastic reduction in media serum content following the proliferation phase triggers differentiation of the myoblast to the myotube, possibly due to the absence of key mitogenic components. Due to the lot-to-lot variations in growth factors present in the commercially available serum and the consequent variability in satellite cell induction and proliferation, an optimum serum formulation and the identity of these mitogenic components has yet to be fully defined[44]. To date, several growth factors have been implicated as potential serum components with important myogenic effects.

As would be expected based on their *in vivo* influence on skeletal muscle hypertrophy described above, FGF, PDGF, and HGF promote activation and proliferation of myogenic progenitor cells and delay terminal differentiation[91,101,102]. The stimulatory effect of FGF on satellite cell proliferation has been shown to produce a two-fold increase in DNA content, relative to untreated cultures[103]. This enhanced proliferation translated to formation of larger myotubes and increased expression of myogenin and MHC. When added during the differentiation phase of the culture, however, these significant effects were not observed[46,103]. Similarly, the addition of PDGF led to a two-fold increase in DNA synthesis and improved satellite cell proliferation, but did not yield a significant increase in desmin expression and myotube formation[46,104]. In the case of HGF, the time between isolation of satellite cells and the onset of the cell cycle decreased from approximately 42-60 hours to less than 24 hours[102]. These results demonstrate conservation of the signaling pathways involved in native myogenesis in an *in vitro* setting, with HGF activating

quiescent satellite cells to begin progressing down the myogenic lineage. By combining HGF with either FGF or PDGF, tissue engineers may be able to maximize the replicative potential of satellite cells by achieving activation earlier and then increasing subsequent proliferation. Furthermore, HGF and FGF tend to delay terminal differentiation, allowing for extension of the window for satellite cell proliferation. Additionally, IGF plays a key role in all phases of satellite cell myogenesis, from activation and proliferation to induction of the onset of myogenic differentiation[105,106]. In one study, IGF was supplied in the fibrin gel used as a 3D scaffold to support the fabricated muscle tissue[107]. The beneficial effects of IGF addition were seen in the form of MyoD upregulation during initial proliferation, followed by a 50% increase in force production in the final engineered tissue. The functional improvement with IGF addition illustrates its importance in engineering skeletal muscle. In contrast, TGFβ typically has a negative influence on both myogenic phases *in vitro*, slightly suppressing proliferation and severely inhibiting differentiation[46,91,105]. TGFβ, however, can enhance contractility of engineered muscle by promoting collagen type I synthesis in the extracellular matrix, supporting myofiber development and force transmission[108]. As a result of these findings, it is common to supplement media supplied during the initial proliferation phase with HGF and FGF, prior to switching to a media supplemented with IGF or insulin for the induction of differentiation[27,29]. By adding these specific growth factors to influence satellite cell proliferation and differentiation, tissue engineers have successfully created skeletal muscle constructs *in vitro* featuring neonatal functional and structural characteristics[29,72].

Summary

Skeletal muscle tissue engineers seek to fabricate tissue constructs to regenerate damaged muscle. Volumetric muscle loss is one of the primary clinical targets for engineered muscle due to the severity of the associated injury and the limitations to current treatments. As a result, recent research seeks to engineer tissue constructs that mimic native skeletal muscle structure and function to serve as an alternative graft source. Using the natural processes for skeletal muscle development and repair as models, the necessary cells and biochemical cues required to recapitulate myogenesis *in vitro* have been identified and applied for tissue engineering applications. Specifically, the importance of satellite cells in myogenesis makes them the ideal cell source for skeletal muscle tissue engineering, and common methods for obtaining a suitable population are described above. Following isolation of these myogenic cells, methods for maximizing proliferation and differentiation through control of the culture media and growth factors have likewise been developed.

Recently, increasing attention has focused on recreating biophysical cues *in vitro* to promote satellite cell proliferation and differentiation, in concert with controlling media and growth factors. The complex nature of the satellite cell niche *in vivo*[20,21], with signaling not only from chemical factors but also through physical stimuli acting on the ECM and surrounding microenvironment, suggests the need for similar conditions *in vitro*. The substrate onto which isolated satellite cells ultimately attach has thus been engineered to mimic native skeletal muscle with promising results. Instead of using stiff substrates such as polystyrene or glass, culture of isolated satellite cells on more compliant hydrogels promoted myogenic differentiation and allowed formation of advanced sarcomeric structure[80,109]. These hydrogels were engineered to

match the stiffness of healthy skeletal muscle *in vivo,* with Young's Moduli of 12 kPa. Even a slight variation in gel stiffness to values above 20 kPa or below 5 kPa significantly reduced differentiation. From these results, it is clear that the biophysical stimuli transduced through the extracellular microenvironment play a key role in regulating satellite cell behavior *in vitro*.

It naturally follows that researchers have applied additional mechanical stimuli seeking to further recreate the *in vivo* environment, commonly through custom bioreactors. These systems can range from aligned, cylindrical microwells designed to promote alignment and fusion into myotubes[71], to dynamic bioreactors for providing cyclic strain either through fluid flow or mechanical stretch[30,73]. The efficacy of these bioreactors has led especially to improved satellite cell differentiation, but it has also brought attention to the importance of 3D tissue culture. Skeletal muscle tissue engineers are clearly seeking to recreate as much of the *in vivo* satellite cell niche as possible *in vitro*, but these efforts are inherently limited when using a flat, 2D tissue culture surface. The potential benefits of using a 3D culture system include improved satellite cell attachment and viability and myotube alignment[71,110]. It is expected that naturally derived acellularized ECM or collagen hydrogel scaffolds provide the support and 3D architecture necessary for satellite cell growth and development, while also avoiding potential biocompatibility issues[25,80,111]. At the same time, such scaffolds can shield the developing engineered tissue from the desired loading environment if degradation does not occur at the proper rate[69]. To avoid such complications, several labs including ours have developed scaffold-free, 3D culture systems for engineering skeletal muscle tissues and implanting these tissues into small animal models[26,28,72].

Such advances show promise for tissue-engineered skeletal muscle, both in terms of recapitulating myogenesis *in vitro* and restoring lost muscle function *in vivo.* Overall, the improved understanding of isolation methods and culture conditions has aided skeletal muscle tissue engineers in improving myogenesis. Nevertheless, engineered tissues typically exhibit an embryonic phenotype and produce only a fraction of the force generated by native skeletal muscle[26,72]. To address this challenge, the overall objective of this dissertation was to improve *in vitro* force production in tissue-engineered skeletal muscle to decrease its disparity relative to native muscle. It was expected that improving muscle fiber formation and structural development during the tissue engineering process would lead to such increases in force production. In this dissertation, novel methods for purifying isolated satellite cells, enhancing myogenic differentiation through steroid supplementation, and non-invasively evaluating metabolism and structure are described, all of which translated to improved function of tissue-engineered skeletal muscle.

CHAPTER II

Microfluidic Sorting of Isolated Skeletal Muscle Satellite Cells

Introduction

Skeletal muscle has the ability to regenerate itself in response to damage[3], largely due to the presence of potent muscle progenitor cells[112]. As the most abundant tissue in the body[113], skeletal muscle requires this regenerative capacity for maintaining homeostasis and restoring function after injury. The resident skeletal muscle stem cell, the satellite cell, plays an essential role in repairing muscle damage[6,50]. In cases of severe injury, however, the native skeletal muscle repair mechanism is overwhelmed, and external intervention is indicated. A prime example is volumetric muscle loss (VML), defined as surgical or traumatic loss of a large volume of muscle tissue that leads to a functional deficit[4]. With VML, the ability of the damaged muscle to repair such a large defect through the native repair mechanism is insufficient, and fibrotic scar tissue instead accumulates in the defect site[114]. Current treatment options—free functional muscle transfer and composite tissue allotransplantation—involve grafting healthy muscle, innervation, and vasculature into the defect, but limitations such as donor site morbidity and limited tissue availability often prevent complete recovery[111,115,116]. In addition, muscular dystrophies are a family of inherited degenerative disorders characterized by systemic muscle weakness[117-119]. Duchenne muscular dystrophy is particularly distressing, due to its early onset and the lack of an effective treatment[120-122]. To address these clinical challenges, researchers have proposed using

satellite cells in cell therapy[36,123-125] or tissue engineering approaches[26,27,30,126,127]. Although other cell types have been implicated as contributors to skeletal myogenesis[18,57,59], recent research shows that satellite cells act as the primary source of regeneration of adult skeletal muscle[7,50]. Due to this tissue-specific regenerative ability, satellite cells have tremendous therapeutic potential.

Obtaining a suitable population of satellite cells, however, presents a continuing challenge. Satellite cells are relatively few in number, only accounting for 2-7% of the nuclei associated with a muscle fiber[8,18], and current isolation methods have difficulty yielding both the quantity and purity required[5,38,42]. As described in the previous chapter, the prevailing technique is to combine enzymatic isolation techniques with subsequent purification methods, such as pre-plating or fluorescence activated cell sorting (FACS). Pre-plating is limited, however, by the sensitivity of the pre-plate timing and the potential for loss of myogenic cells. On the other hand, FACS requires modification of the cells being analyzed through the addition of exogenous dyes or the electrical perturbations of the sorting process itself[62]. Microfluidic characterization and sorting of fluorescently labeled skeletal muscle cells has been demonstrated as an alternative[58,128] but is currently limited to small throughputs of hundreds of cells or less. By examining the existing techniques, it is clear that an efficient, label-free, high-throughput method for purifying satellite cells following isolation is required.

Inertial microfluidics has the potential to fill this pressing need. The inertial migration of particles in a microfluidic device was first observed by Segré and Silberberg in the 1960s[129] and recently described by Di Carlo[130]. The efficacy of such devices has been demonstrated for separating particles in fluids, and a similar approach was tested in this study to examine

separation of cells in suspension. Thus, the physics behind inertial separation described below refer to forces acting on cells rather than particles. To summarize these forces, cells in straight microfluidic channels experience stresses that act over the channel surface: 1) normal stress that yields drag forces parallel to the flow direction, 2) shear stress that yields lift forces perpendicular to the flow direction, and 3) a wall lift effect in opposition to the shear stress[130-132]. Drag forces accelerate cells in the flow direction along laminar streamlines. In contrast, the lift forces cause cell migration across streamlines. The wall lift force is directed away from the channel walls and decays with increasing distance from the walls. The shear lift force depends on the shear gradient generated by the fluid flow, resulting in forces directed away from the center of the channel. The combination of these lift forces focuses cells to equilibrium positions along the channel cross-section according to the density of particles and the geometry of microfluidic channel. In a curved channel, centrifugal effects induce secondary flow (Dean flow) on the cross-section of the channel. The generated double recirculation (Dean Vortices), along with the aforementioned lift forces, migrate cells transversely. Cell migration is correlated to the cell size and the curvature of the channel, resulting in new profile of equilibrium positions which separates distinct size classes of cells[130]. In our case, a typical skeletal muscle cell isolate contains a mixture of satellite cells ranging from 8-13 μm[34,58] and myofibroblasts ranging from 10-22 μm[133,134], in addition to smaller populations of hematopoietic, neural, and immune cells (ranging from 6 μm for smaller red blood cells up to 30 μm for larger monocytes and macrophages[135]).

A microfluidic device, termed “Labyrinth”, was previously designed for and applied in the separation of circulating tumor cells (15-25 μm) from white blood cells (7-12 μm) using inertial microfluidics-based separation[136]. It is a high throughput (1800-2500 μL/min), continuous, and

biomarker independent microfluidic separation technology. The design of the Labyrinth (Figure 8), inspired by the Labyrinth in Greek mythology, incorporates 11 loops and 56 corners in a total channel length of 637 mm. The loops have small curvature ratios and provide enough channel length for complete focusing of cells, whereas sharp right-angle corners have high curvature ratios to further enhance focusing of smaller cells. Four separate outlets are designed to collect the focused individual streams of cells with differing sizes. Combining these features, the Labyrinth enables the separation of cells in different size classes with high efficiency.

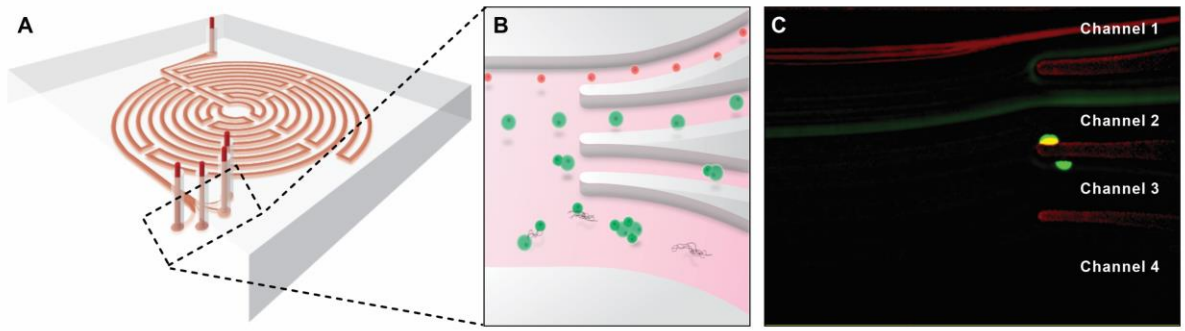

Figure 8. Microfluidic inertial separation in the Labyrinth device. A schematic representation of the Labyrinth is shown in **(A)**. Cells in suspension enter the device at the top of the image and rapidly flow (1800 µL/min) along the circuitous path created by a series of curved channels. Dean forces proportional to cell size and channel curvature act on the cells transversely to the flow direction, separating distinct size classes of particles at the outlets as pictured in **(B)**. Specifically, we intended to separate satellite cells, with a size range of 8-13 µm, from myofibroblasts, with a typical diameter of 10-22 µm. The Labyrinth was designed to focus the smaller satellite cells into Channel 1 (top), larger myofibroblasts into Channel 2 (second from top), and cell aggregates and debris into Channels 3 and 4 (bottom). **(C)** Visualization of a mixed population of Pax7+ satellite cells expressing red tdTomato fluorescence and Achilles tendon fibroblasts labeled with CellTracker Green fluorescent dye during sorting confirmed efficient separation of these two cell types based on their difference in size.

In this study, we demonstrate the power of inertial microfluidic separation for purification of isolated satellite cells. I hypothesized that the size difference between satellite cells and fibroblasts, two primary cell types obtained from chemical dissociation of muscle, would allow for label-free, inertial separation in a microfluidic device and that purified satellite cells could be used to engineer our skeletal muscle units (SMUs). Throughout the engineered tissue fabrication

process described extensively in previous work[29,72,108,127], Labyrinth sorted cells were compared to unsorted controls to assess the efficiency of the microfluidic separation process and to examine potential improvements in myogenic proliferation, differentiation, and overall engineered tissue function as a result.

Methods

Animal Care

All animal care procedures followed *The Guide for Care and Use of Laboratory Animals*[137], according to a protocol approved by the University Committee for the Use and Care of Animals. Validation of the Labyrinth was performed using fluorescently labeled primary mouse cells. Pax7-positive satellite cells expressing red fluorescence were isolated from a transgenic Pax7CreERT2-r26-tdT mouse, provided by collaborators in the lab of Dr. Chris Mendias, Department of Orthopedic Surgery at the University of Michigan. To induce tdTomato fluorescence expression, mice were injected intraperitoneally with tamoxifen (Sigma-Aldrich, St. Louis, MO, cat. no. T5648) in corn oil (Sigma, cat. no. C8267) at a dose of 0.5 mg diluted to 10 mg/mL. Injections were repeated for five consecutive days, and cells were isolated at least ten days after the final injection. Mouse Achilles tendon fibroblasts were isolated from C57BL6 mice supplied by Charles River Laboratories Inc. (Wilmington, MA, USA) and were fluorescently labelled using CellTracker Green CMFDA Dye (Life Technologies, Carlsbad, CA, cat. no. C7025) according to the manufacturer protocol.

SMUs were engineered using soleus muscles and bone marrow from 145-155g female Fischer 344 rats, supplied by Charles River Laboratories. Animals acclimated to colony conditions

for one week prior to any procedure and were fed Purina Rodent Chow 5001 and water ad libitum. Intraperitoneal injections of sodium pentobarbital (50 mg/kg for mice, 65 mg/kg for rats; Merck Animal Health, Madison, NJ, NADA # 119-807) were used to induce a deep plane of anesthesia. Supplemental pentobarbital doses were administered as required to maintain adequate anesthesia depth.

Muscle Dissection and Cell Isolation

From female Fischer 344 rats, both soleus muscles were removed under aseptic conditions and sterilized in 70% ethanol. All hindlimb muscles were dissected when isolating Pax7CreERT2-r26-tdT mouse muscle cells. The muscles were then minced using a razor blade and forceps, placed under ultraviolet light for 15 min in 15 mL of Ham's F12 media (Gibco BRL, Carlsbad, CA, cat. no. 11765-047), and added to a dissociation solution consisting of 32U dispase (1.8 U/mg; Gibco, cat. No. 17105-04) and 2390U type IV collagenase (239 U/mg; Gibco, cat. no. 17104-019) in 20 mL of Ham's F12. The mixture was maintained at 37°C with agitation for 90 minutes and trituration through a 1 mL micropipette every 30 minutes. The resulting suspension was then filtered with a 100 μm mesh filter (Fisher Scientific, Waltham, MA, cat. no. 22363549) prior to centrifugation. The dissociation solution was aspirated off and the cells were resuspended in growth medium.

Microfluidic Device Fabrication

The mold for the polydimethylsiloxane (PDMS) device was fabricated following a standard soft lithography protocol. Using a spin-coater, a negative photoresist layer of SU-8 100 (MicroChem, Westborough, MA, cat. no. SU-8 100) was deposited onto a silicon wafer at 2450

rpm for 1 minute. The wafer was then soft-baked for 10 minutes at 65°C and 70 minutes at 95°C. A mask with the device geometry was aligned to the wafer and exposed to UV light for 20 seconds to cure the photoresist. Post-exposure-baking was applied for 3 minutes at 65°C and 10 minutes at 95°C. Next, the wafer was soaked in developer solution (MicroChem, cat. no SU-8 Developer) for 6 minutes and in isopropyl alcohol (Sigma, cat. no. W292907) for 1 minute to remove the inactivated photoresist. It was finally hard baked for 4 minutes at 150-180°C. The resulting height of the mold on silicon wafer was 100.0 ± 0.5 µm, and the width of the channel was 500 ± 0.5 µm.

The flow chamber for Labyrinth was made from PDMS (Sylgard 184; Dow Chemical Corp., Midland, MI, cat. no. 4019862). 30 mL Sylgard polymer base and 3 mL curing agent were thoroughly mixed and poured onto a silicon mold. The mixture was placed into a desiccator for 2 hours to remove air bubbles from the mixture and then heated at 65°C overnight to harden the polymer. The polymer was next cut into the desired shape, and punched with a needle for tubing insertion. The PDMS device was then bonded to standard sized glass slides via plasma surface activation of oxygen. The bonded device was plumbed with 0.76 mm diameter tubes (Cole-Parmer, Vernon Hills, IL, cat. no. 06419-00).

Microfluidic Inertial Separation

The Labyrinth device was primed with 1% Pluronic acid solution (Sigma, cat. no. P2443) in Dulbecco's Phosphate-Buffered Saline (DPBS; Fisher, cat. no. 14190144) at 100 µL/min for 10 minutes and then incubated for 10 minutes to prevent cell clotting on channel walls. Cell samples in suspension were then pushed through the Labyrinth at a flow rate of 1800 µL/min using a syringe pump (Harvard Apparatus, Holliston, MA, cat. no. 55-2222). After 60 seconds of flow stabilization, the products from each of the four Labyrinth outlets were collected separately.

Preparation of Tissue-engineered Bone and Tendon Anchors

As described in previous studies, bone and tendon constructs were fabricated to act as anchors onto which developing muscle monolayers could attach and fuse[138,139]. Bone marrow from both femurs of Fischer 344 rats was removed under aseptic conditions. Isolated bone marrow cells were plated in 100 mm tissue culture plates (BD Falcon, Franklin Lakes, NJ) in 8mL growth medium for 6 days. Growth medium was resupplied every 2 days and contained 40mL Dulbecco's modified Eagle's medium (DMEM; Gibco, cat. no. 11995- 065) with 10mL fetal bovine serum (FBS; Gibco, cat. no. 10437-028), 6 ng/mL basic fibroblast growth factor (bFGF; Peprotech, Rocky Hill, NJ, cat. no. 100-18B), and 0.5mL antibiotic-anti-mycotic (ABAM; Gibco, cat. no. 15240-062). After achieving approximately 80% confluence, cells were passaged and replated at 310,000 cells per plate. Following four passages, the cells were plated in 100 mm tissue culture plates at a density of 1.3 million cells per plate. They were allowed to grow in 8 mL growth medium for 2 days before being shifted to differentiation medium for 3 days. Differentiation medium consisted of 46 mL DMEM with 3.5 mL horse serum (Gibco, cat. no. 16050-122), 0.13 mg/mL ascorbic acid-2-phosphosate (Sigma, cat. no. A8960), 0.05 mg/mL L-proline (Sigma, cat. no. 81709), 2 ng/mL transforming growth factor beta (TGFβ; Fisher, cat. no. PHG9214), and 0.5 mL ABAM. Cells cultured with the growth and differentiation media described above differentiate to form a tendon monolayer. To drive cells to the bone lineage, 10 nM dexamethasone (DEX; Sigma, cat. no. D4902) was added to both the growth and differentiation media. Following 3 days on differentiation medium, the confluent monolayers delaminated from the tissue culture plate. The monolayers were collected, pinned in cylindrical forms into PDMS-coated dishes and fed differentiation medium, and left for 2 days prior to being cut into 5-mm sections to be used as

engineered bone-tendon anchors for construct implantation. The anchors were then pinned onto the developing muscle monolayers. This process is summarized below in Figure 9.

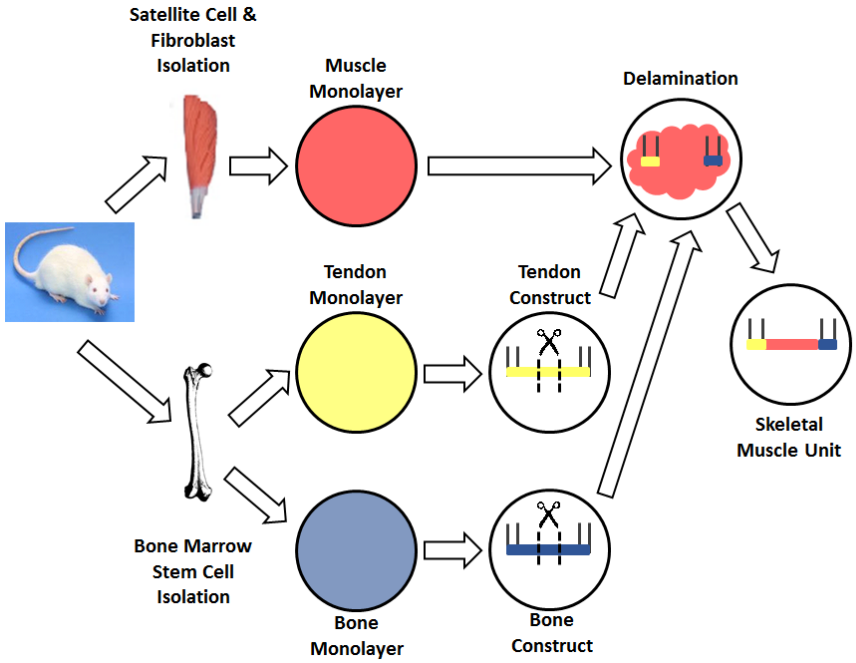

Figure 9. Fabrication of a Skeletal Muscle Unit (SMU). To mimic the structure of native skeletal muscle, a multi-phasic engineered tissue was created. Bone marrow stem cells, isolated from the femur, were directed to form either tendon or bone monolayers by the culture media. After delamination and capture of these monolayers in 3D cylindrical form, sections of these bone-tendon constructs were cut and pinned onto developing muscle monolayers. Muscle monolayers were fabricated from the heterogeneous cell population obtained following digestion of the soleus muscle. Upon delamination, the muscle monolayer fused with the bone-tendon anchors to form a scaffold-free skeletal muscle unit.

SMU Formation

SMUs were engineered in 60 mm polystyrene plates (Fisher, cat no. 353002), and immunocytochemistry (ICC) was performed on 35 mm plates (Fisher, cat. no. 353001) as described previously[72,140]. Briefly, a substrate of PDMS was cured onto each plate, followed by coating with laminin (Natural Mouse Laminin, Gibco, cat. no. 23017-015) at 1mg/cm^2. Isolated muscle satellite cells were seeded in muscle growth medium (MGM) at 600,000 cells per 60 mm

plate or 150,000 cells per 35 mm plate. MGM contained 30mL F-12 Kaighn's Modification Nutrient Mixture (Gibco, cat. no. 21127-022), 12.5mL DMEM, 7.5mL FBS, 2.4 ng/mL bFGF, and 0.5mL ABAM. After initial plating for four days to allow attachment, cells were subsequently fed MGM every two days until becoming fully confluent on Day 7 with a network of elongating myotubes. At this point, 5 mm tissue-engineered bone-tendon anchors were pinned onto the cell monolayers at a spacing of 2.5 cm, and the medium was switched to muscle differentiation medium (MDM). MDM was composed of 35mL M199 (Gibco, cat. no. 11150-059), 11.5mL DMEM, 3mL FBS, 500µL ABAM, 50µL insulin-transferrin selenium-X (Sigma, cat. no. I1884), and 36.2µL 50mM ascorbic acid 2-phosphate. After a week on MDM, re-supplied every other day, the monolayers delaminated from the plates on Day 14, rolling into cylindrical muscle constructs, held at length by the engineered bone anchors (Figure 9).

Immunocytochemical Analysis

At specific time points during SMU fabrication, samples were fixed in 20°C methanol for 10 min and set aside for ICC. Samples were washed for 10 min in 0.1% Triton X-100 (Sigma, cat. no. T8787) in DPBS (PBST) and blocked with PBST containing 3% Bovine Serum Albumin (PBST-S; Sigma, cat. no. A2153) at room temperature. Samples were then incubated overnight at 4°C with primary antibodies diluted in PBST-S. Immunofluorescent staining was performed using the following primary antibodies: mouse monoclonal anti-desmin (1:20 dilution; Developmental Studies Hybridoma Bank, Iowa City, IA, cat. no. D3), mouse monoclonal anti-Pax7 (1:100 dilution; Abcam, Cambridge, MA, cat. no. ab199010), rabbit polyclonal anti-PDGFRα (1:100 dilution; Santa Cruz Biotech, Dallas, TX, cat. no. sc-431), biotin conjugated sheep polyclonal anti-BrdU (1:50 dilution; Abcam, cat. no. ab2284), mouse monoclonal anti-MyoD (1:100 dilution; BD Biosciences,

San Jose, CA, cat. no. 554130), rabbit polyclonal anti-fibroblast-specific protein 1 (FSP1; 1:100 dilution; Abcam cat. no. ab27957), and mouse monoclonal anti-α-actinin (1:200 dilution; Sigma, cat. no. A7752). Plates stained with anti-BrdU had previously been incubated for 24 hours with a BrdU labelling reagent (Life Technologies, cat. no. 00-0103) in the muscle growth medium. Following 3 PBST washes for 5 min each, samples were incubated in 1:500 dilutions of with Alexa Fluor anti-mouse, anti-rabbit, or streptavidin secondary antibodies (Life Technologies) for 3 hours at room temperature. Following 3 washes in PBST for 15 min each, samples were preserved in Prolong Gold with DAPI (Life Technologies, cat. no. P36935) and cover slipped.

Samples were examined and photographed with a Leica Inverted microscope, and images were analyzed using the ImageJ software package (National Institutes of Health, Bethesda, MD)[141]. For ICC analysis, samples from each experimental group were fixed and stained (on Day 0 for Cytospin; Day 4 for BrdU; and Day 11 for α-actinin). Cells fixed on Day 0 were attached to microscope slides via Cytospin at 800 RPM for 8 min. From each sample, ten random areas were imaged, and the number of positively stained nuclei in each image was counted.

Myotube Fusion Index Calculation

From the α-actinin images, the percentage of myogenic nuclei was first calculated by dividing the total number of DAPI-positive nuclei by the number of nuclei associated with an α-actinin-positive cell. The structural protein α-actinin is often used to identify Z-lines in skeletal muscle sarcomeres, but α-actinin is also expressed in the stress fibers of myoblasts prior to fusion[142-144]. To calculate myotube fusion index, α-actinin-positive muscle cells were quantified depending on the number of nuclei contained. Specifically, muscle cells were divided into groups

with one, two, three, and four or more nuclei, and these values were reported as a percentage of the total number of α-actinin-positive nuclei.

Myotube Size and Density Analysis

On Day 14 after initial seeding, light micrographs of monolayers were captured. Ten areas of approximately 1 mm^2 were randomly selected from both the center and periphery of each 60 mm plate and imaged. Every myotube from these images was then measured in ImageJ to determine its diameter and the overall density of the developing myotube network.

SMU Contractile Measurements

SMU force production was measured on Day 16 following roll-up into 3D cylindrical form. The protocol for measuring contractility of engineered muscle constructs has been described previously[31,127,145]. Briefly, the pin on one end of the SMU was attached to a force transducer with a 0-5 mN range and a 0.4 μN resolution (World Precision Instruments, Sarasota, FL, cat. no. SI-KG7A). Platinum wire electrodes were placed along either side of the SMU for field stimulation. The temperature of the construct was maintained at 37° C, using a heated aluminum platform. Twitch contractions were elicited using a single 5 ms pulse at 10, 30, 60 and 90 mA, whereas tetanic force was determined using a 1 s train of 5 ms pulses at 90 mA and 10, 20, 40, 60 and 80 Hz. Data files for each peak twitch force and peak tetanic force trace were recorded and subsequently analyzed using LabVIEW 2013 (National Instruments, Austin, TX).

Statistical Analysis

Values are presented as mean ± standard error. Measurements of significant differences between means were performed using GraphPad Prism 7 software (GraphPad Software, Inc., La

Jolla, CA). Means were compared using either a Student's t-test or one-way ANOVA with Tukey post-hoc comparisons. Differences were considered significant at $p<0.05$.

Results

Initial Validation of Microfluidic Satellite Cell Purification

The sorting efficiency of the Labyrinth microfluidic device was validated using fluorescently labeled primary mouse cells. A combination of Pax7-positive satellite cells expressing red tdTomato fluorescence and Achilles tendon fibroblasts labeled with CellTracker Green fluorescent dye were separated at several different fluid flow rates. Visualization of the fluorescent cells during sorting (Figure 8C) indicated improved separation distances between satellite cells and fibroblasts at lower flow rates (1800 µL/min: 148 µm, 2000 µL/min: 135 µm, 2200 µL/min: 128 µm, 2500 µL/min: 112 µm). Based on these results, a flow rate of 1800 µL/min was used for all subsequent sorting runs. Sorting of the fluorescently labeled cell populations was repeated, and the separated cells were quantified with a hemocytomer (Table 3A). From these results, it is clear the Labyrinth separated the cell populations as intended, significantly enriching the satellite cell population in Channel 1 ($p = 0.015$) and the fibroblast population in Channel 2 ($p > 0.001$) as compared to unsorted controls.

Isolated Cell Populations Immediately Following Microfluidic Sorting

The Labyrinth device demonstrated similar sorting efficiency in separating isolated primary rat cells (Table 3B). Following isolation and sorting, cells attached to microscope slides via Cytospin were immunostained with Pax7 and desmin to characterize myogenic cells and PDGFRα to identify fibroblast progenitors. Analysis of images from the separated cell populations

indicated that a purified population of myogenic cells was evident in Channel 1 of the Labyrinth device. Specifically, compared to the unsorted muscle dissociation, with a myogenic cell purity of 39.9 ± 4.0%, Labyrinth-sorted cells were significantly enriched with myogenic cells, approximately two-fold, to 75.5 ± 1.6% ($p < 0.001$). Because of their larger cell size, the fibroblast cells were separated into Channels 2, 3, and 4 by the Labyrinth device. In comparison to the unsorted dissociation with a fibrogenic cell purity of 45.6 ± 3.1%, channels 2, 3 and 4 demonstrated increased fibroblast purities of 57.4 ± 2.7% ($p = 0.1091$), 60.8 ± 4.9% ($p = 0.023$), and 78.3 ± 4.5% ($p < 0.001$), respectively.

A) Primary Mouse Cells	**Unsorted Control**	**Sorted Channel 1**	**Sorted Channel 2**	**Sorted Channel 3**	**Sorted Channel 4**
Pax7+ Purity (n = 3)	33.3 ± 3.4 %	66.5 ± 6.0 % *	27.2 ± 5.8 %	21.2 ± 11.6 %	0.00 ± 0.00 %
Fibroblast Purity (n = 3)	43.2 ± 2.6 %	11.9 ± 4.8 %	70.6 ± 1.3 % *	17.4 ± 3.0 %	0.2 ± 0.1 %
B) Primary Rat Cells					
Myogenic Purity (n = 6)	39.9 ± 4.0 %	75.5 ± 1.6 % *	27.5 ± 4.2 %	12.0 ± 1.6 %	7.36 ± 1.3 %
Fibrogenic Purity (n = 6)	45.6 ± 3.1 %	21.9 ± 1.9 %	57.4 ± 2.7 %	60.8 ± 4.9 % *	78.3 ± 4.5 % *

Table 3. Purity of separated cell populations following sorting. Purity in mouse cells **(A)** refers to the percentage of fluorescent cells (red for Pax7+ satellite cells, green for fibroblasts) among the total cells counted in each Labyrinth channel. It is worth noting that very few cells were present in Channel 4, and none of these cells were Pax7+. In rat isolates **(B)**, cells were characterized as myogenic if expressing Pax7 or desmin, and fibrogenic based on expression of PDGFRα. The difference in sorted mouse and rat populations, evident in Channels 3 and 4, can be explained by the methods used to label these cells. The mouse cells contained a population of unlabeled fibroblasts from enzymatic digestion of the muscle biopsy. It is expected that these unlabeled fibroblasts represented a sizeable portion of the mouse cells sorted into Channels 3 and 4. In all tables and figures, values are presented as mean ± standard error. ***** indicates significant increases relative to unsorted controls.

Effects of Microfluidic Sorting on Cell Proliferation

To assess the influence of the microfluidic separation process on cell proliferation, Labyrinth sorted cells were seeded and cultured normally. ICC analysis was performed on Day 4 following seeding to identify proliferating cells expressing BrdU, a synthetic nucleoside analog of thymidine. Expression of MyoD and FSP1 was examined simultaneously to identify myogenic cells and matrix-secreting fibroblasts, respectively. From BrdU analysis of plates (n = 10), it was clear that microfluidic sorting did not have an effect on overall cell proliferation (Figure 10).

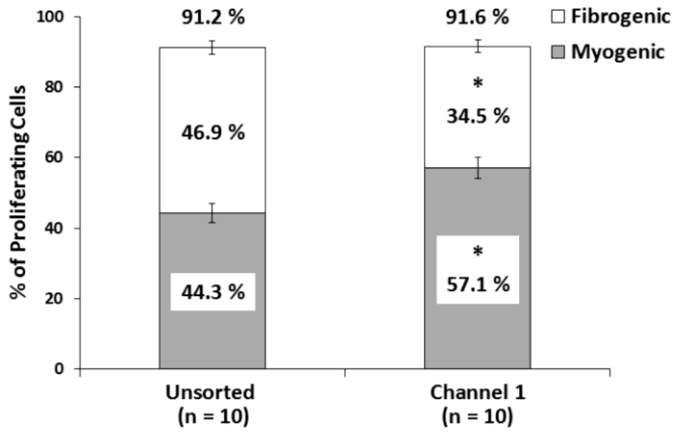

Figure 10. Myogenic and fibrogenic proliferation of sorted cells. Incorporation of BrdU on Day 4 of SMU fabrication was used to identify proliferating cells. No difference in overall proliferation was observed between unsorted controls (91.2 ± 1.2%) and cells sorted into Channel 1 (91.6 ± 1.0%, p = 0.556), suggesting sorting did not adversely affect cell growth. Immunostaining for MyoD and FSP1 indicated myogenic and fibrogenic cells, respectively. Proliferating myogenic cells were significantly enriched (p = 0.004) after sorting into Channel 1 (57.1 ± 3.0%) as compared to unsorted controls (44.3 ± 2.8%). In contrast, FSP1 staining indicated proliferating fibrogenic cells in unsorted controls, 46.9 ± 1.9%, were significantly decreased to 34.5 ± 1.9% by microfluidic sorting (p < 0.001). * Indicates statistical difference from control.

In unsorted controls 91.2 ± 1.2% of cells were proliferating, whereas cells sorted into Channel 1 of the labyrinth exhibited 91.6 ± 1.0% proliferating cells (p = 0.556). Co-staining for MyoD, however, demonstrated a significant increase (p = 0.004) in proliferating myogenic cells

sorted into Channel 1 (57.1 ± 3.0%) as compared to unsorted controls (44.3 ± 2.8%). In contrast, FSP1 co-staining indicated that the percentage of proliferating fibrogenic cells in unsorted controls, 46.9 ± 1.9%, was significantly decreased to 34.5 ± 1.9% by microfluidic sorting ($p < 0.001$). It is worth noting that insufficient myogenic cells for seeding and SMU fabrication were present in Channels 2, 3, and 4, so only unsorted controls and Channel 1 cells were compared for this and subsequent analysis.

Myogenic Differentiation and Myotube Fusion Following Microfluidic Sorting

Myotube fusion index was measured to assess the ability of sorted cells to form a network of myotubes following microfluidic separation. Expression of α-actinin on Day 11 of SMU fabrication was used to identify fused myotubes and sarcomeric structure. Myotubes in both control and Channel 1 plates exhibited dense networks of longitudinally-aligned myofibrils with advanced sarcomeric structure (Figures 11A & B). Quantification of the number of nuclei associated with α-actinin-positive cells yielded a myotube fusion index value. From a t-test, the overall percentage of nuclei associated with cells expressing α-actinin in unsorted control plates ($n = 8$) of 52.0 ± 2.8% was not significantly different ($p = 0.142$) from plates seeded with cells sorted into Channel 1 57.0 ± 2.1% (Figure 11C). However, the number of fused myotubes with four or more nuclei in unsorted control plates, 82.7 ± 3.7%, was significantly increased to 92.3 ± 2.0% in Channel 1 plates ($p < 0.001$, Figure 11D).

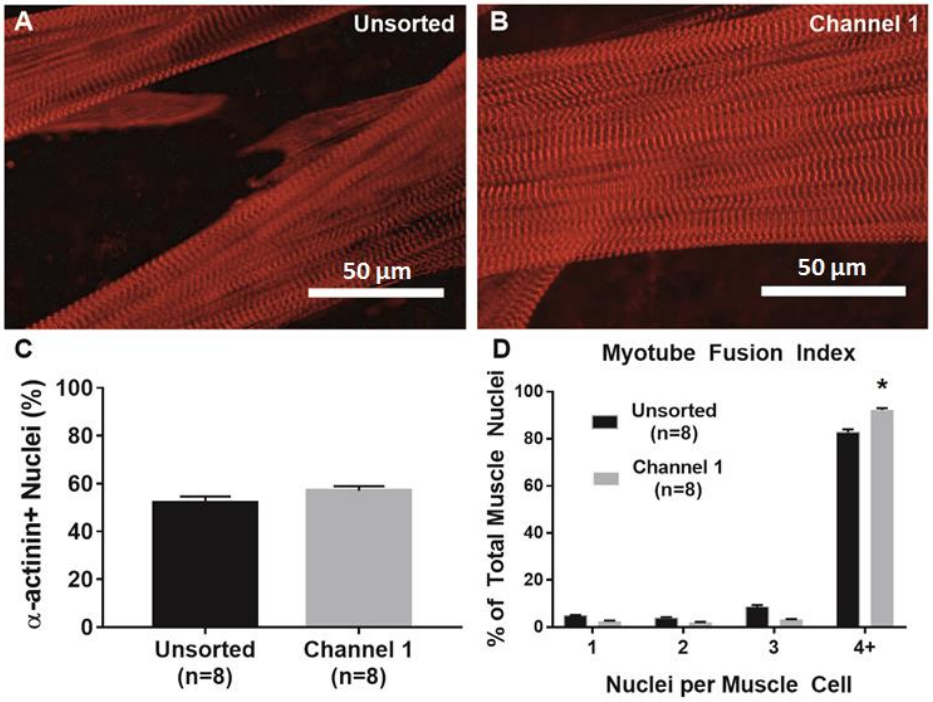

Figure 11. Structural maturation following microfluidic sorting. (A&B) Advanced sarcomeric structure within highly-aligned myofibrils, evident from immunostaining for α-actinin, was observed on Day 11 in both unsorted controls and Channel 1 plates. **(C)** No significant difference was recorded in the total nuclei associated with α-actinin-positive muscle cells ($p = 0.142$). **(D)** Quantification of myotube fusion index, the percentage of muscle cells with either 1, 2, 3, or 4+ nuclei, indicated greater fusion following microfluidic sorting. The percentage of fully fused myotubes with 4+ nuclei significantly increased from 82.7 ± 3.7% in unsorted controls to 92.3 ± 2.0% in Channel 1 ($p < 0.001$). ***** Indicates statistical difference from control.

Further analysis of the myotube network was performed on Day 14 of the fabrication protocol using light microscopy. The average myotube diameter in unsorted controls ($n = 10$) was 16.0 ± 1.3 µm. This value was nearly identical ($p = 0.938$) to the myotube diameter of 16.2 ± 1.4 µm in cells sorted into Channel 1 (Figure 12). In contrast, the density of the myotube networks in unsorted and sorted samples exhibit a stark difference. Specifically, unsorted control plates averaged 18.6 ± 3.3 myotubes/mm^2, whereas cells sorted into Channel 1 formed a significantly denser, more aligned network ($p = 0.004$) averaging 33.9 ± 3.7 tubes/mm^2.

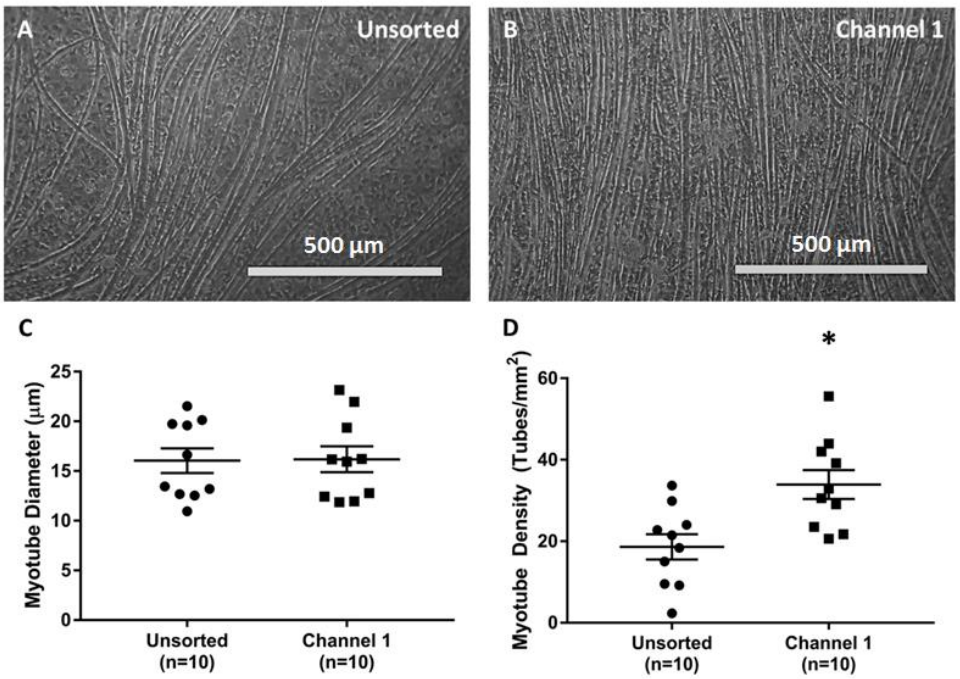

Figure 12. Effects of microfluidic sorting on myotube growth. Shortly before delamination, light microscopy images were captured on Day 14 to assess the size and density of myotubes within the developing muscle monolayer. **(A&B)** Representative images of monolayers from unsorted cells and cell sorted into Channel 1. Scale Bar = 500 µm. **(C)** The average myotube diameter was indistinguishable between the two groups: 16.0 ± 1.3 µm in controls and 16.2 ± 1.4 µm in Channel 1 ($p = 0.938$). **(D)** Channel 1 cells, however, exhibited a significantly denser myotube network ($p = 0.004$), with 33.9 ± 3.7 tubes/mm^2 in comparison to 18.6 ± 3.3 myotubes/mm^2 in unsorted controls. ***** Indicates statistical difference from control.

Force Production in 3D SMUs after Microfluidic Sorting

Finally, overall function of engineered SMUs was assessed by contractile force production on Day 16, following monolayer delamination and capture in 3D form. As shown in Figure 13, the peak isometric tetanic force production in unsorted control SMUs (n = 8) of 71 ± 8 µN was significantly increased ($p = 0.002$) approximately two-fold to 144 ± 17 µN in SMUs fabricated from cells sorted into Channel 1 of the Labyrinth microfluidic device.

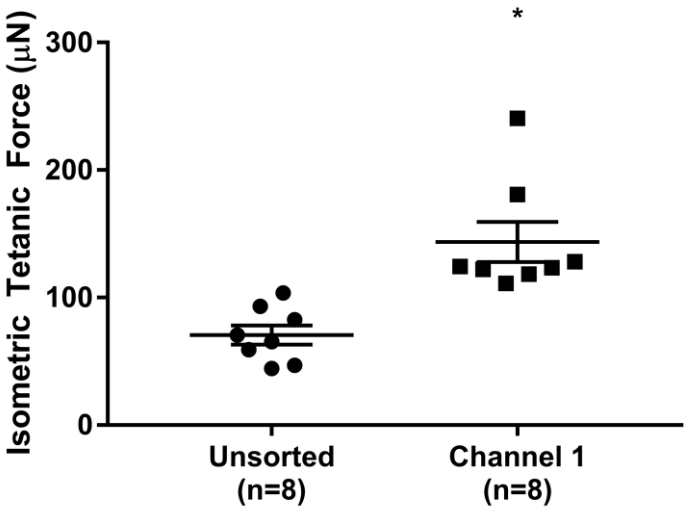

Figure 13. SMU functional development with microfluidic sorting. Functional measurement of isometric tetanic force in 3D SMUs on Day 16 indicated a significant effect of sorting: unsorted control SMU force production of 71 ± 8 μN was significantly increased ($p = 0.002$) approximately two-fold to 144 ± 17 μN in Channel 1 SMUs. ***** Indicates statistical difference from control.

Discussion

Cells separated with microfluidic sorting were analyzed to assess effects on the myogenic purity of the isolated population, along with capability for subsequent proliferation, differentiation, and function. Immediately following microfluidic sorting, two-fold enrichment of the myogenic population was observed in Channel 1 of the Labyrinth device. This enrichment was expected based on the design of the Labyrinth device for focusing smaller particles and cells, including satellite cells and myogenic progenitors, into Channel 1. In contrast, the fibroblast population was enriched in Channels 2, 3, and 4. Again, this result was intended, since the Labyrinth was designed to focus the larger fibroblasts into these channels. A minority population of fibroblasts was present in Channel 1, however, and a similar population of myogenic cells was captured in Channel 2, indicating that microfluidic sorting did not occur with maximal efficiency. It is expected that the overlap in the size distributions of satellite cells (8-13 μm[34,58]) and of

fibroblasts (10-22 μm[133,134]) led to this reduced sorting efficiency. Alternatively, large aggregates of undigested extracellular matrix debris were observed in the microfluidic device during sorting and in outlet Channels 3 and 4 (data not shown). This debris may have impeded fluidic focusing of the different cell populations and reduced the overall sorting efficiency. Nevertheless, the majority of satellite cells and fibroblasts were consistently separated as desired by the Labyrinth device.

After microfluidic sorting, cells separated into Channel 1 were not adversely affected by the high shear forces imposed during flow through the Labyrinth device. These sorted cells exhibited similar overall proliferation to unsorted cells, in addition to improved myogenic proliferation and suppression of non-myogenic proliferation. We know that these sorted cells were more myogenically pure at seeding from our ICC analysis immediately after microfluidic separation, and observation of improved myogenic proliferation confirms this result. Improved myogenesis continued as sorted cells differentiated and fused to form a greater number of skeletal muscle myotubes. Increased myoblast fusion index was observed in cells sorted into Channel 1, resulting in a denser and highly aligned network of myotubes in the differentiation phase of SMU formation. Additionally, structural maturation of the muscle monolayers, indicated by advanced sarcomeric structure within the highly-aligned myofibrils, was observed in both unsorted control and Channel 1 plates. Ultimately, these improvements in myogenic proliferation and differentiation translated to greater force production in SMUs fabricated from Channel 1 cells. In conclusion, microfluidic sorting efficiently separated satellite cells and fibroblasts while improving the capability for myogenic proliferation, differentiation, and function.

Conclusions

Microfluidic sorting, as demonstrated in this study, offers an alternative approach to purification of satellite cells enzymatically digested from a muscle biopsy. The most comparable approach, pre-plating to remove rapidly adhering non-myogenic cells, can achieve greater than 80% myogenic purity[40]. The primary drawbacks to pre-plating, however, are the length of time required (5 days) and the potential for decreased cell yields. Recently, purification of isolated satellite cells through FACS has gained popularity due to its ability to rapidly sort Pax7+ satellite cells with greater than 90% purity[60,146]. With FACS, labeling with exogenous dyes is required, and incubation with these antibodies decreases throughput. Microfluidic sorting has the potential to fill a niche distinct from these established methods. Although the myogenic purity of cells separated with the Labyrinth devices was slightly lower at 75%, the sorting process was label-free and required approximately 5 minutes. For tissue engineers, this high-throughput and label-free purification process presents an exciting alternative.

CHAPTER III

Dexamethasone Supplementation to Enhance Myogenic Differentiation in Engineered SMUs

The text and figures in this chapter were originally published with the following citation: Syverud BC, VanDusen KW, and Larkin LM. "Effects of dexamethasone on satellite cells and tissue engineered skeletal muscle units." Tissue Eng Pt A 22(5-6): 480 (2016). Excerpts from this article have been included with permission from the publisher, Mary Ann Liebert, Inc.

Introduction

Potential applications for engineered skeletal muscle include implantation as a graft material for repair of traumatic damage[30,69], recapitulation of native development and regeneration for detailed physiological study or pharmaceutical testing[27], and use as biomechanical actuators[70,71]. In each case, recreating the complex function and structure of skeletal muscle *in vivo* is a challenging, but essential, consideration. Engineered tissues to date, however, have been characterized by a neonatal phenotype in terms of force production and structural maturity[26,29]. Following sufficient recovery time, engineered skeletal muscles implanted into an *in vivo* regenerative environment have advanced towards the adult phenotype[24,72], and several studies have attempted to utilize key chemical and mechanical stimuli to improve the maturity of these engineered muscles *in vitro*[65,73].

Tissue engineers have used the influence of such growth factors on myogenesis to direct techniques for engineering skeletal muscle. Current tissue engineering techniques utilize scaffold materials, ranging from acellularized tissues[95,96] to collagen and fibrin hydrogels[26,27,97], or opt for a scaffold-free approach[28,29,72] to support development of extracellular matrix (ECM) for subsequent muscle tissue. The ultimate success of these approaches depends on the *in vitro* culture of isolated primary muscle precursor cells. A common technique in cultivation of these myogenic cells begins with an initial proliferation phase, allowing cells to expand sufficiently, followed by induction of differentiation and fusion into myotubes[98]. Use of media with high serum content is generally accepted to promote the initial proliferation phase while delaying the onset of differentiation, potentially due to the presence of a variety of growth factors[38]. Drastic reduction in media serum content subsequently triggers satellite cell differentiation, possibly due to the removal of essential mitogenic components. Because of variations in the activity and concentration of growth factors between lots of commercially available serum, as well as the consequent variability in satellite cell induction and proliferation, an optimum serum formulation and the identity of these mitogenic components has yet to be fully defined[44]. By understanding the essential growth factors and supplementing media with the appropriate doses, tissue engineers can maximize the myogenic potential of satellite cells when engineering skeletal muscle.

The synthetic glucocorticoid dexamethasone (DEX) has previously been studied due to its profound effects on muscle *in vivo* and on satellite cell cultures *in vitro*, but its application in skeletal muscle tissue engineering has yet to be evaluated. In a clinical setting, DEX is typically used for its anti-inflammatory or immunosuppressant activity to treat several rheumatologic and

skin diseases, because it is 25 times more potent than endogenous cortisol[147]. In skeletal muscle specifically, exogenously delivered DEX has a variety of effects depending on the timing and dosage of the administration. DEX induces atrophy in adult human skeletal muscle when supplied orally in 4 mg doses, approximately 10 times greater than endogenous cortisol levels[148,149]. This atrophic effect has been linked to up-regulation of the myostatin promoter and inhibition of IGF-1 expression[148,150]. In contrast, the administration of 5 to 25nM DEX has improved myogenesis *in vitro* by enhancing differentiation and myotube fusion of myogenic murine cells, potentially through its induction of dysferlin, a calcium-binding transmembrane protein thought to play a key role in both myogenesis and membrane repair[151]. Similar studies have demonstrated that DEX can inhibit protein synthesis and myoblast proliferation *in vitro* [152], however, reinforcing the need for careful timing of addition to culture.

Recent research from our lab has focused on optimizing and testing Skeletal Muscle Units (SMUs), cylindrical tissue constructs featuring muscle fabricated from monolayers of primary fibroblasts and contractile myotubes[9]. The papers referenced above regarding DEX activity *in vitro* describe its effects on the immortal C2C12 mouse myoblast cell line in two-dimensional culture, rather than the primary cell population and functional three-dimensional constructs used in our SMU experiments. We hypothesized that exposing the heterogeneous pool of satellite cells and fibroblasts used for SMU fabrication to different doses of DEX at several time points may yield an optimal combination for improving myogenesis and ultimately maximizing *in vitro* development of our engineered skeletal muscle. Thus, the purpose of this study was to examine the potential of the steroid dexamethasone as a growth factor for skeletal muscle tissue engineering.

Methods

Animal care

Tissue engineering studies were conducted using soleus muscles and bone marrow from 145-155g female Fischer 344 rats, obtained from Charles River Laboratories Inc. (Wilmington, MA, USA) and Harlan Laboratories (Haslett, MI, USA). All animals were acclimated to colony conditions for one week prior to any procedure. Animals were fed Purina Rodent Chow 5001 and water *ad libitum.* All surgical procedures were performed in an aseptic environment, with animals in a deep plane of anesthesia induced by intraperitoneal injections of sodium pentobarbital (65 mg/kg). Supplemental doses of pentobarbital were administered as required to maintain an adequate depth of anesthesia. All animal care and animal surgery procedures were in accordance with *The Guide for Care and Use of Laboratory Animals*[137], and the protocol was approved by the University Committee for the Use and Care of Animals.

SMU formation and Dexamethasone addition

SMUs were fabricated in individual coated 60 mm polystyrene plates (BD Falcon, Franklin Lakes, NJ, USA), and ICC was performed on 35 mm plates as described previously[29,72,127]. Briefly, a substrate of Sylgard (type 184 silicon elastomer; Dow Chemical Corp., Midland, MI) was initially cured onto each plate, followed by coating with laminin (Natural Mouse Laminin, cat. No. 23017-015; Gibco BRL, Carlsbad, CA) at 1mg/cm^2. The cell isolation mixture was plated in muscle growth medium (MGM) at a density of 600,000 cells per 60 mm plate and 150,000 cells per 35 mm plate. MGM contained 30mL F-12 Kaighn's Modification Nutrient Mixture (cat. No. 21127-022; Gibco BRL), 12.5mL Dulbecco's modified Eagle's medium (DMEM; cat. No. 11995- 065; Gibco BRL), 7.5mL fetal bovine serum (FBS; cat. No. 10437-028; Gibco BRL), 2.4 ng/mL basic fibroblast growth

factor (bFGF; cat. No. 100-18B; Peprotech, Rocky Hill, NJ), and 0.5mL antibiotic-anti-mycotic (ABAM; cat. No. 15240- 062; Gibco BRL).

After the initial plating, cells were left undisturbed for four days and subsequently fed MGM every two days until becoming fully confluent with elongating myotubes forming a network across the base of the plate. Next, 5 mm tissue-engineered bone-tendon anchors were pinned onto the cell monolayers 2.5 cm apart, and the medium was switched to muscle differentiation medium (MDM). MDM was composed of 35mL M199 (cat. No. 11150-059; Gibco BRL), 11.5mL DMEM, 3mL FBS, 50µL insulin-transferrin selenium-X (cat. No. I1884; Sigma-Aldrich, St. Louis, MO), 0.5mL ABAM, and 36.2µL 50mM ascorbic acid 2-phosphate. After approximately a week on MDM, re-supplied every other day, the monolayers delaminated from the plates, rolling into cylindrical muscle constructs, held at length by the engineered bone anchors. During this SMU formation process, described in Figure 14, DEX was added to the medium beginning at three different time points: initial plating (Day 0), six days after initial plating (Day 6), and two days after the switch to MDM (Day 9). These three time points were chosen to evaluate the efficacy of DEX in controlling isolated cell proliferation, differentiation, and maturation of the delaminating monolayer and subsequent 3D SMU, respectively. After the first addition, supplemental doses of DEX were added with each medium change. Three experimental doses were supplied (5nM, 10nM, and 25nM), with untreated plates as controls.

SMU contractile measurements

Contractile properties of SMUs (n=6) from each experimental group were measured following roll-up into cylindrical form. The protocol for measuring contractility of engineered muscle constructs has been described in the previous chapter[145,153]. To reiterate, the pin on one

end of the SMU was raised from the Sylgard and attached to a force transducer. Platinum wire electrodes were placed along either side of the SMU for field stimulation. The temperature of the construct was maintained at 37° C, using a heated aluminum platform. Passive force was measured as the average baseline force produced prior to the onset of stimulation. Twitch contractions were elicited using a single 5 ms pulse at 10, 30, 60 and 90 mA, whereas tetanic force was determined using a 1 s train of 5 ms pulses at 90 mA and 10, 20, 40, 60 and 80 Hz. Data files for each peak twitch force and peak tetanic force trace were recorded and subsequently analyzed using LabVIEW 2013.

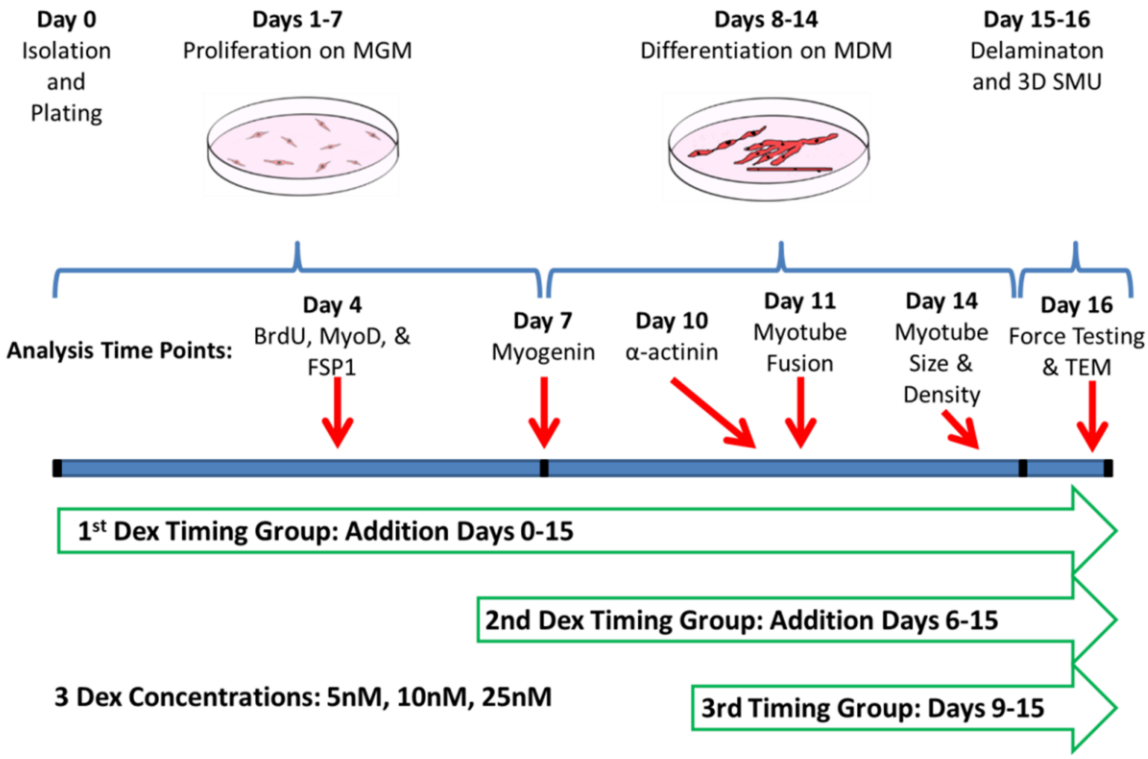

Figure 14. Experimental timeline with dexamethasone timings and dosages. Addition of dexamethasone was initiated at three time points: on Day 0 to study effects on proliferation, on Day 6 to study effects on late proliferation and differentiation, and on Day 9 to study effects on structural maturation. During this SMU fabrication process, subsets of the developing plates were analyzed for expression of BrdU, MyoD, Fibroblast-specific protein 1 (FSP1), myogenin, and α-actinin as listed above. Additionally, myotube fusion and myotube size and density were measured in the developing muscle monolayers. Finally, the 3D SMUs were assessed for force production in response to electrical stimulation and for strucutral development with TEM. MGM stands for Muscle Growth Medium, MDM for Muscle Differentiation Medium.

Immunocytochemical Analysis

During SMU fabrication, a subset of the plates from each experimental group was fixed in 20°C methanol for 10 min and set aside for immunocytochemistry (ICC). The plates were submerged for 15 min in 0.1% Triton X-100 (Sigma, St. Louis, MO, USA, cat. no. T8787) in DPBS (PBST) and blocked with PBST containing 3% Bovine Serum Albumin (PBST-S; Sigma, cat. no. A2153) at room temperature. The sections were then incubated overnight at 4^0C with the primary antibodies diluted in PBST-S. Immunofluorescent staining with specific antibodies was performed to detect the presence of BrdU (biotin conjugated sheep polyclonal antibody; Abcam, Cambridge, MA, USA, cat. no. ab2284), MyoD (mouse monoclonal antibody 1:100 dilution; BD Biosciences, San Jose, CA, USA, cat. no. 554130), FSP1 (rabbit polyclonal antibody 1:100 dilution; Abcam, cat. no. ab27957), myogenin (rabbit polyclonal antibody 1:50 dilution; Santa Cruz Biotechnology, Dallas, TX, USA, cat. no. sc-576), desmin (mouse monoclonal antibody 1:20 dilution; Developmental Studies Hybridoma Bank, Iowa City, IA, USA, cat. no. D3), and α-actinin (mouse monoclonal antibody 1:200 dilution; Sigma, cat. no. A7752). Plates stained with antibodies for BrdU had previously been incubated for 24 hours with a BrdU labelling reagent (Life Technologies, cat. no. 00-0103) in the culture media. Following three washes in PBST, samples were incubated in 1:500 dilutions of with Alexa Fluor anti-mouse, anti-rabbit, or streptavidin secondary antibodies (Life Technologies) for three hours at room temperature. Following three washes in PBST, samples were preserved in Prolong Gold with DAPI (Life Technologies, cat. no. P36935) and cover slipped.

Samples were examined and photographed with a Leica Inverted microscope, and images were analyzed using the ImageJ software package. For ICC analysis, plates (n=5) from each

experimental group were fixed and stained (on Day 4 for BrdU, MyoD, and FSP1; Day 7 for myogenin; and Day 11 for desmin). From each plate, ten areas were randomly selected and imaged, and the number of positively stained nuclei in each image was counted. To calculate myotube fusion index from the desmin images, the number of nuclei associated with a desmin-positive myotube was divided by the total number of nuclei.

Myotube Size and Density Analysis

On day 14 after initial plating of satellite cells, light micrographs of the developing monolayers in each experimental group were captured and analyzed. Specifically, five areas from each 60 mm plate (n=8) were randomly selected and imaged. Every myotube from these images was then measured in ImageJ to determine its size and the overall density of the myotube network.

Transmission Electron Microscopy Analysis

Following measures of mechanical function, SMUs were fixed overnight at room temperature in 0.1M phosphate buffer (Fisher Scientific, Pittsburgh, PA, USA, cat. no. S369-500) containing 2.5% glutaraldehyde (Electron Microscopy Sciences, Hatfield, PA, USA, cat no. 16210), post fixed at 4°C for one hour in 0.1M phosphate buffer containing 1% osmium tetroxide (Electron Microscopy Sciences, cat no. 19150), and polymerized in Embed 812 resin (Electron Microscopy Sciences, cat. no. 14900) at 60°C for 24 hours. Ultra-thin 70nm sections were then cut and stained with uranyl acetate (Electron Microscopy Sciences, cat. no. 22400) and lead citrate (Electron Microscopy Sciences, cat. nos. 17900 and 21140) and imaged using a JEOL JEM-1400Plus transmission electron microscope (TEM).

Statistical Analysis

Values are presented as mean ± SE. Measurements of significant differences between means were performed using GraphPad software. Means were compared using either one-way or two-way ANOVA tests with Tukey post-hoc comparisons. Differences were considered significant at $p<0.05$.

Results

Effects of Dexamethasone on Proliferation of Satellite Cells

To assess the influence of DEX on the induction and proliferation of isolated myogenic satellite cells, DEX was added at the time of plating (Day 0). ICC analysis of cells expressing BrdU, a synthetic nucleoside analog of thymine, was used on Day 4 to identify proliferating cells[154], and expression of MyoD and Fibroblast-specific protein 1 (FSP1) was examined simultaneously to identify myogenic cells and matrix-secreting fibroblasts, respectively (Figure 15). From the analysis of BrdU and MyoD co-staining, a dose dependent response to DEX treatment was evident, with the density of proliferating myogenic nuclei increasing with increasing DEX concentration. Following addition of 10nM and 25nM DEX, a statistically significant increase in MyoD+ cell proliferation relative to No DEX controls was observed ($p = 0.012$ and 0.003, respectively). Addition of 5nM DEX exhibited no difference from controls and resulted in significantly fewer proliferating MyoD+ cells than the 10nM and 25nM DEX doses ($p = 0.037$ and 0.009, respectively). Similarly, ICC analysis for both BrdU and FSP1 showed that the administration of DEX on Day 0 led to a decrease in the number of proliferating FSP1+ cells. This decrease in FSP1+ cells was significant following 10nM and 25nM DEX addition, relative to untreated controls

(p = 0.002 and 0.004, respectively). Administration of 5nM DEX indicated no difference in FSP1+ cells from No DEX controls. In comparison to the 10nM and 25nM concentrations, however, 5nM DEX yielded significantly decreased proliferation of FSP1+ cells (p = 0.004 and 0.005, respectively). Thus, the results for MyoD and FSP1 expression in proliferating cells demonstrate that the influence of 10nM and 25nM DEX on early growth of heterogeneous muscle isolates was two-fold: improved proliferation of cells in the myogenic lineage and decreased proliferation of non-myogenic fibroblasts.

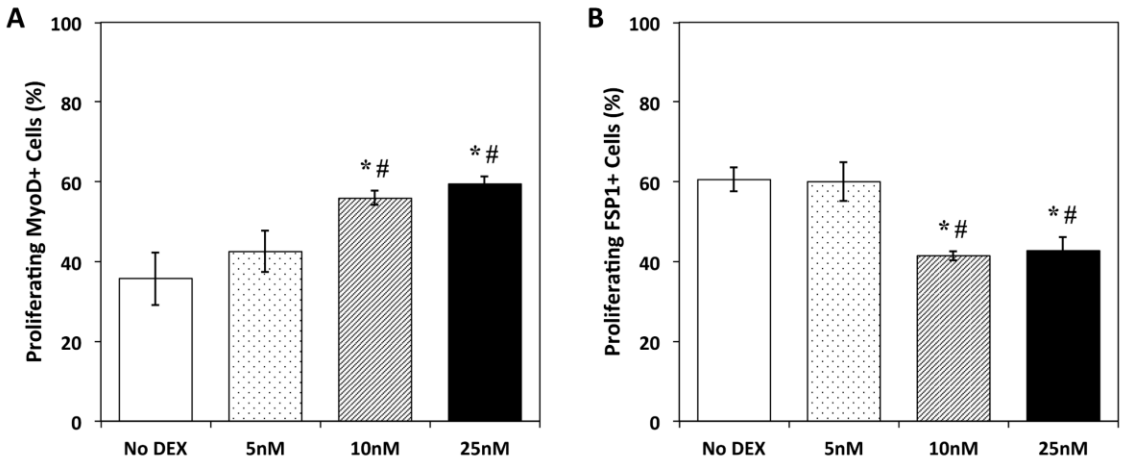

Figure 15. Myogenic and fibroblast cell proliferation following dexamethasone addition. (A) With DEX addition on the day of initial seeding (D0), the percentage of proliferating cells expressing MyoD followed an increasing trend with increasing DEX concentration, as indicated by BrdU and MyoD co-staining on Day 4. A statistically significant increase in proliferation (p = 0.012 for 10nM, p = 0.003 for 25nM) was observed when comparing the higher concentrations of DEX (10nM and 25nM) to untreated controls (No DEX). **(B)** ICC analysis for BrdU and FSP1 on Day 4 showed a decrease in the percentage of proliferating cells expressing FSP1+ following DEX addition. In response to administration of 10nM and 25nM DEX, the number of proliferating cells expressing FSP1 significantly decreased relative to No DEX controls (p = 0.002 and 0.004, respectively). Error bars indicate mean ± standard error. ***** Indicates statistical difference from control, # from 5nM DEX.

Dexamethasone Induction of Muscle Cell Differentiation and Myotube Fusion

ICC analysis of myogenin expression was used as an indicator of myoblast differentiation into myotubes on Day 7 of the experiment[155]. A dose-dependent increase in myogenin-positive

cell density was observed in response to DEX treatment, independent of the timing of its addition (Figure 16A). Groups receiving 5nM DEX showed no difference from No DEX controls, whereas 10nM addition significantly increased the number cells expressing myogenin ($p = 0.001$), and 25nM DEX led to even greater increases ($p < 0.001$). Ultimately, treatment with 25nM DEX beginning on Day 6 yielded the highest density of myogenin+ cells, approximately 2.8 times greater than untreated controls.

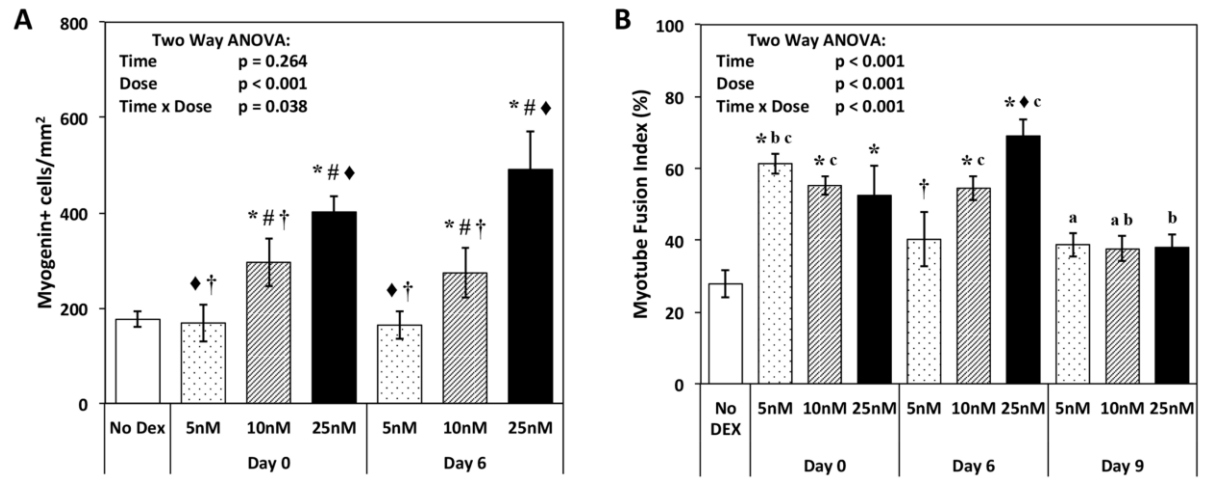

Figure 16. DEX effects on myogenic differentiation. (A) ICC analysis for myogenin expression on Day 7 indicated differentiation of myoblasts into myotubes. From two-way ANOVA, a dose-dependent increase in myogenin-positive cell density was observed in response to DEX treatment ($p < 0.001$), independent of the timing of addition. **(B)** Myotube fusion index, calculated from desmin and DAPI staining on Day 11, quantified the number of nuclei associated with a myotube as a percentage of total nuclei. Two-way ANOVA indicated a significant effect of both DEX dose and timing ($p < 0.001$ for both). When averaged across the three timing groups, all three DEX concentrations yielded significantly increased myotube fusion relative to No DEX controls ($p = 0.002$ for 5nM, $p > 0.001$ for 10nM and 25nM). Similarly, fusion index increased significantly with DEX addition on Day 0 and Day 6 ($p = 0.015$ and 0.008, respectively). Error bars indicate mean ± standard error. ***** Indicates statistical difference from No DEX controls, # from 5nM in the same DEX timing group, ♦ from 10nM in the same timing group, **†** from 25nM in the same timing group, (a) from Day 0 at the same DEX dose, (b) from Day 6 at the same DEX dose, and (c) from Day 9 at the same DEX dose.

Myotube fusion index was measured to assess the ability of myoblasts to terminally differentiate and form a network of myotubes in the presence of DEX. Expression of desmin, a protein specific to muscle cells and a key subunit in intermediate filaments[38,156], identified fused myotubes, and subsequent analysis of the percentage of nuclei associated with a myotube

yielded a myotube fusion index value. Two-way ANOVA indicated that both the dose and timing of DEX addition significantly affected myotube fusion (Figure 16B). Compared to untreated controls, all three experimental concentrations significantly increased myotube fusion ($p = 0.002$ for 5nM, $p > 0.001$ for 10nM and 25nM). The effect of time indicates that the early addition of DEX at cell seeding (Day 0) or towards the end of the proliferative stage (Day 6) significantly increased myotube fusion ($p = 0.015$ and 0.008, respectively), whereas plates treated with DEX during the differentiation stage (Day 9) exhibited no difference from controls. Although no difference in myotube fusion was observed between the 5nM, 10nM, and 25nM concentrations when averaged across the three timing groups, focus on the Day 6 time point alone revealed a dose-dependent trend, with fusion index increasing with each DEX concentration. This trend included a statistically significant difference between the Day 6 5nM and 25nM DEX concentrations ($p = 0.007$). Across all experimental groups, addition of 25nM DEX on Day 6 yielded the highest myotube fusion index at 69%, a 250% increase over the No DEX controls. The combined results for myogenin expression and myotube fusion demonstrate that DEX addition increased myogenic differentiation and myotube fusion, with the addition of the highest experimental dose, 25nM, on Day 6 producing the greatest increases.

Further analysis of myotube size and number was performed on Day 14, immediately prior to monolayer delamination. The dose and timing of DEX addition were observed to have significant effects on myotube diameter (Figure 17E). In response to the experimental DEX concentrations, a significant dose-dependent increase in myotube diameter was observed, resulting in myotubes 1.2, 1.3, and 1.4 times larger than No DEX controls following addition of 5nM, 10nM, and 25nM DEX, respectively ($p = 0.001$ for 5nM, $p < 0.001$ for 10nM and 25nM).

Additionally, in plates receiving DEX at the two early time points, Day 0 and Day 6, myotube diameters increased significantly relative to untreated controls ($p < 0.001$ for both days). Plates subsequently treated with DEX on Day 9 showed no difference in myotube diameter from controls. Day 6 addition of 10nM and 25nM DEX produced the largest myotubes, with average diameters of 14.8 and 16.1 µm, respectively. Myotube diameters for both doses were significantly greater than control myotubes, with an average diameter of 9.8 µm ($p < 0.001$ for both doses).

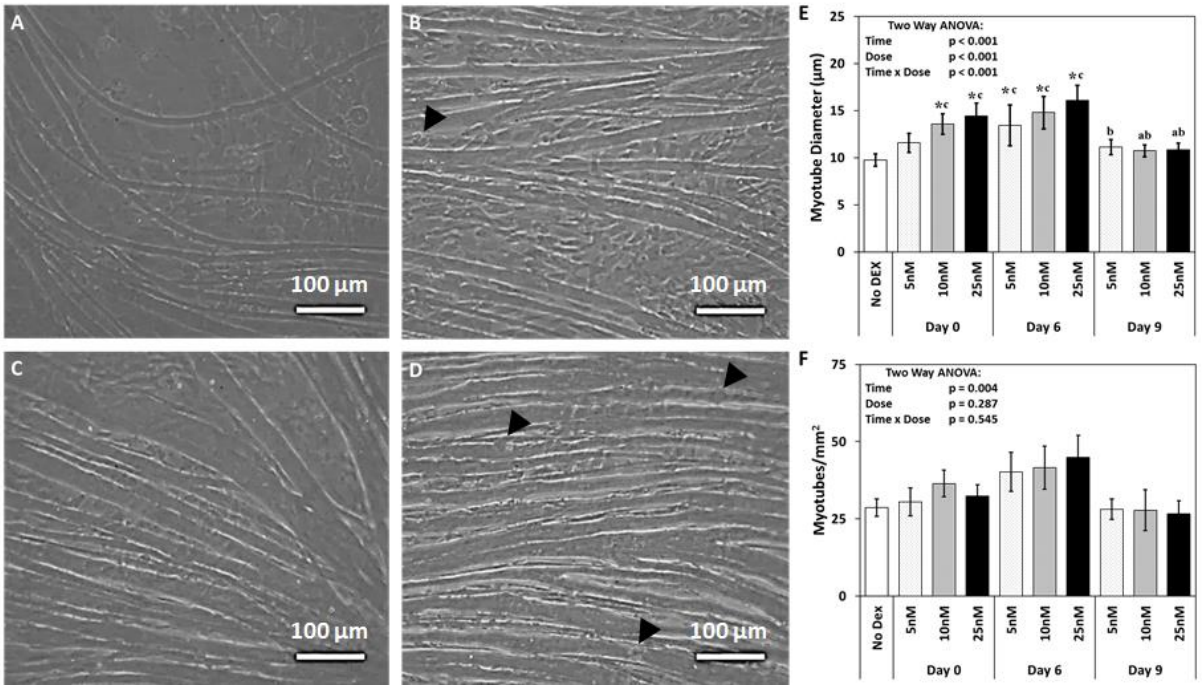

Figure 17. DEX effects on myotube growth. Monolayers were observed just prior to delamination on Day 14. Representative images are shown above for **(A)** No DEX, **(B)** Day 6 5nM, **(C)** Day 6 10nM, and **(D)** Day 6 25nM. Images from the Day 6 timing group were chosen because this time point demonstrated the significant effects of DEX addition detailed below. The black arrowheads in **(B)** & **(D)** indicate blebbing of myotubes. All images were analyzed for **(E)** myotube diameter and **(F)** myotube density. The effects of DEX dose and timing on myotube size were both evident from two-way ANOVA ($p < 0.001$ for both). Post-hoc analysis demonstrated significant increases in myotube diamter in response to all three DEX concentrations ($p = 0.001$ for 5nM, $p < 0.001$ for 10nM and 25nM). Similarly, Day 0 and Day 6 DEX addition led to significantly increased myotube diameters relative to untreated controls ($p < 0.001$ for both days). When examining myotube density, the timing of DEX addition had a significant effect ($p = 0.004$). Specifically, the number of myotubes increased significantly with DEX addition on Day 6 in comparison to No DEX controls ($p = 0.008$) , but Day 0 and Day 9 addition resulted in no significant difference. Error bars indicate mean ± standard error. * Indicates statistical difference from No DEX controls, (a) from Day 0 at the same DEX dose, (b) from Day 6 at the same dose, and (c) from Day 9 at the same dose.

The effects of the timing of DEX addition on the overall density of the myotube network were also evident. Administration of DEX on Day 6 improved myotube density significantly ($p = 0.008$), while addition of DEX on Day 0 and Day 9 exhibited no significant differences from untreated controls. Similarly, no significant differences were observed when examining the influence of the three DEX doses on myotube density. Together, the myotube size and density data indicate that the addition of DEX on Day 6 leads to a more robust network of larger myotubes, which may be preferable for engineering skeletal muscle.

Structural and Functional Maturation of 3D SMUs with Dexamethasone Addition

The influence of DEX on the overall structure and function of engineered SMUs was also observed during delamination and in the final 3-D form. Immunocytochemical analysis of α-actinin (Figures 18A & B) demonstrated improved maturation of myotubes in the delaminating monolayer following addition of all three DEX concentrations. Plates receiving DEX on Day 0 and Day 6 exhibited advanced sarcomeric structure within highly aligned myofibrils in the confluent monolayers. This development of sarcomeric structure was not observed in control muscle cultures or plates receiving DEX during the differentiation stage on Day 9. Similarly, administration of DEX led to improved structural maturation in the fully formed 3D SMUs. Electron micrographs of a SMU receiving 10nM DEX on Day 6 exhibited a denser network of aligned collagen fibers at the junctions of each myofiber than the No DEX SMU (Figures 18C & D). Furthermore, following 10nM DEX administration on Day 6, the resulting SMU demonstrated development of aligned myofilaments and maturing Z-lines, similar to the organization of parallel sarcomeres in adult skeletal muscle (Figures 18E & F). Aligned myofilaments were evident in untreated control SMUs, but few developing sarcomeric structures were observed.

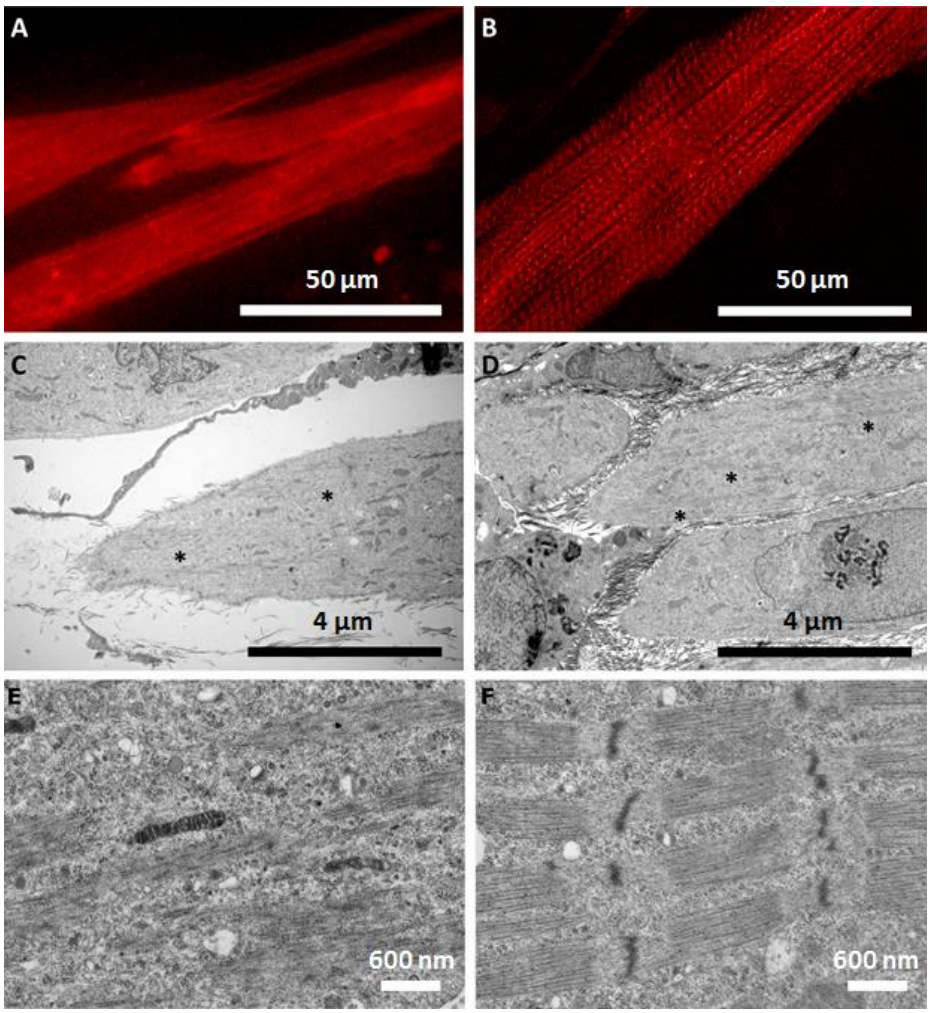

Figure 18. SMU structural maturation with DEX addition. Representative images of muscle monolayers **(A)** without DEX and **(B)** following DEX addition (Day 0 10nM). These images show α-actinin in muscle monolayers 10 days post-seeding. Formation of advanced sarcomeric structure and aligned myofibrils was evident in plates receiving DEX on either Day 0 or Day 6 in all three experimental concentrations. Transmission electron micrographs of longitudinal sections of SMUs following formation of a 3-D construct, **(C & E)** without DEX administration and **(D & F)** following Day 6 addition of 10nM DEX, corroborate the positive effects of DEX on structural maturation during SMU fabrication. Both No DEX and D6 10nM DEX images show developing ECM at myofiber junctions, but greatly increased density and alignment of collagen fibers is evident following DEX addition. Similarly, both SMUs contain myofibers with highly aligned myofilaments, indicated by asterisks in **(C & D)**. However, the formation of organized Z-lines indicative of developing sarcomeric structure was observed to a much greater extent in SMUs receiving DEX administration, evident in **(E & F)**.

This improved structural maturation translated to increased function, as assessed by contractile force production in the 3-D SMUs. The maximum isometric tetanic forces produced by

engineered SMUs are displayed in Figure 19A, and two-way ANOVA indicated both DEX timing and dose significantly affected SMU function.

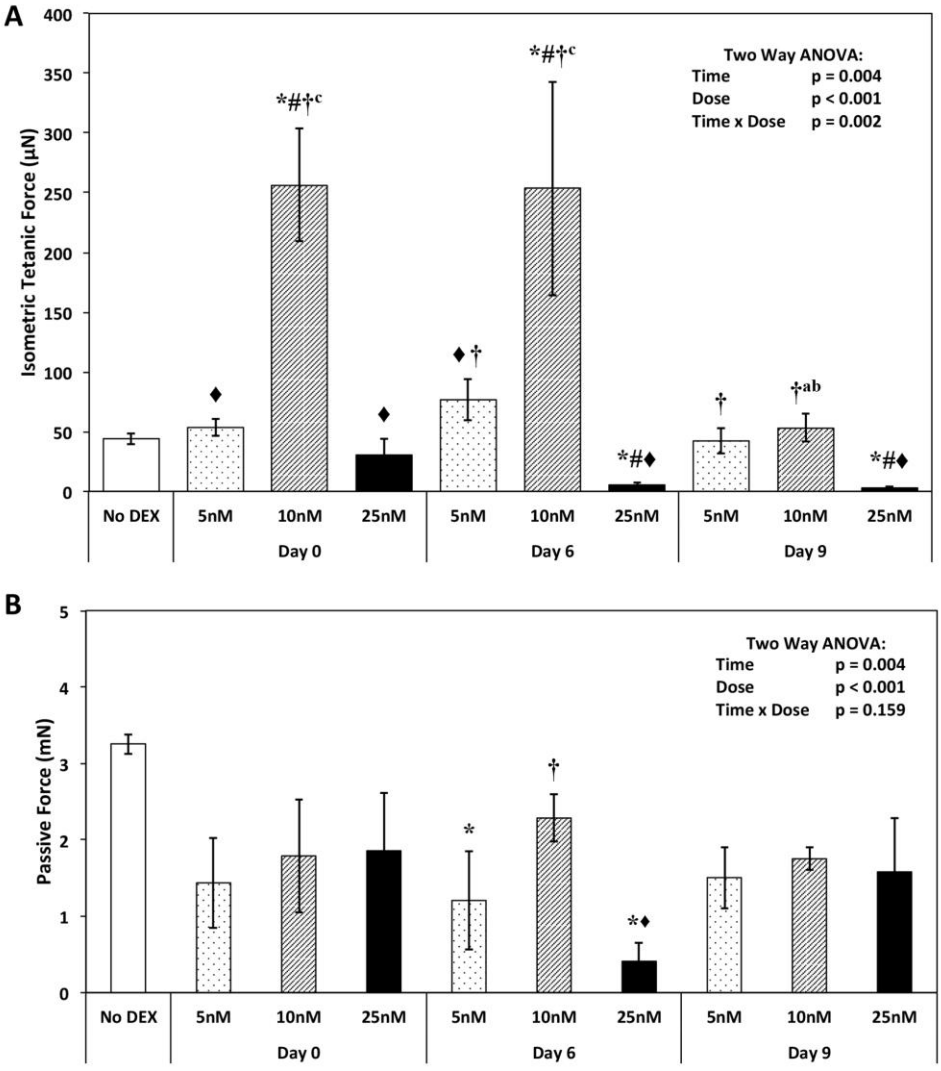

Figure 19. SMU functional maturation with DEX addition. (A) Isometric tetanic force production in 3D SMUs indicated a significant effect of both DEX dose and timing ($p < 0.001$ for dose, $p = 0.004$ for timing). Addition of 10nM DEX was optimal for SMU fabrication, producing a significant, five-fold increase relative to untreated controls ($p = 0.004$). Additionally, Day 0 and Day 6 administration of DEX both led to a significant, two-fold increase in force production ($p = 0.016$ for Day 0, $p = 0.018$ for Day 6), whereas Day 9 DEX addition yielded a 20% decrease compared to No DEX controls. **(B)** Examination of passive force generation also showed a significant effect of DEX timing and dose ($p = 0.004$ for timing, $p < 0.001$ for dose). Further analysis indicated that DEX treatment led to significant decreases compared to No DEX controls regardless of DEX timing or concentration ($p < 0.001$ for Days 0 and 6, $p = 0.006$ for Day 9, $p < 0.001$ for 5nM, $p = 0.003$ for 10nM, $p = 0.002$ for 25nM). Error bars indicate mean ± standard error. ***** Indicates statistical difference from No DEX controls, # from 5nM in the same DEX timing group, ♦ from 10nM in the same DEX timing group, **†** from 25nM in the same DEX timing group, (a) from Day 0 at the same DEX dose, (b) from Day 6 at the same dose, and (c) from Day 9 at the same dose.

When averaging the values across all experimental concentrations to study timing effects, administration of DEX on Day 0 and Day 6 both led to a significant, two-fold increase in force production ($p = 0.016$ for Day 0, $p = 0.018$ for Day 6). Addition of DEX on Day 9 led to a 20% decrease in force production compared to No DEX controls. Surprisingly, however, when examining the effects of DEX dosage, only addition of 10nM DEX produced a significant improvement in function, represented by a five-fold increase in isometric force production relative to No DEX controls ($p = 0.004$). SMUs receiving 5nM DEX showed no increase relative to control SMUs, whereas addition of 25nM DEX significantly decreased force production ($p = 0.024$). Overall, optimal force production was observed in SMUs receiving 10nM DEX on Day 0 and Day 6, with average isometric tetanic forces of 257 and 254 μN, respectively.

Additionally, administration of DEX may have affected the development and maintenance of passive tension in the maturing muscle monolayers, and eventually in the SMUs fabricated from the monolayers. This passive tension effect was quantitatively observed in the timing of delamination of the developing monolayers. Rather than rolling up on Day 14 as is typical in our SMU fabrication protocol, plates treated with DEX remained in monolayer form approximately 20% longer, regardless of the dosage administered. Plates receiving DEX rolled up, on average, on day 17, and manual manipulation was occasionally necessary to assist this process. Following delamination, passive tension development in the newly formed SMUs was measured during assessment of contractile force production 24 hours post roll-up. Two-way ANOVA indicated a significant effect of both DEX timing and dose on passive tension (Figure 19B). Further analysis showed that addition of DEX addition significantly decreased passive tension in fabricated SMUs

($p < 0.001$ for Days 0 and 6, $p = 0.006$ for Day 9, $p < 0.001$ for 5nM, $p = 0.003$ for 10nM, and $p = 0.002$ for 25nM), regardless of the timing or dose of DEX administration.

Discussion

The overall effects of DEX during the SMU fabrication process can be divided into distinct proliferation, differentiation, and maturation phases. The addition of DEX prior to myocyte differentiation led to improved myogenic proliferation and suppression of non-myogenic proliferation, indicated by increased MyoD+ cell density and decreased FSP1+ cell density. In addition, administration of 10nM and 25nM DEX at the beginning of proliferation (Day 0) or one day prior to the transition from proliferation to differentiation (Day 6) yielded increased myoblast fusion, resulting in a dense network of larger myotubes in the subsequent differentiation phase. Similarly, addition of DEX during the proliferative stage on either Day 0 or Day 6 resulted in the greatest structural maturation of the delaminating monolayers and the resulting fully formed 3D SMUs, characterized by the presence of advanced sarcomeric structure within highly aligned myofibrils. Ultimately, administration of 10nM DEX during proliferation on either Day 0 or Day 6 yielded optimal force production in fabricated SMUs.

Although administration of 25nM DEX improved myogenic proliferation and differentiation, force production in these SMUs actually decreased compared to No DEX controls. Several factors potentially explain the ultimate decrease in the contractile function associated with addition of 25nM DEX. As described above, supplementation with DEX led to decreased non-myogenic proliferation and increased myogenesis, concomitant with decreased passive tension. Extracellular matrix is essential to SMU fabrication, both for generation of the passive tension

promoting delamination and for structural support of the contractile components of the SMU. DEX addition may have promoted myogenic differentiation and down-regulated functional extracellular matrix formation. Although TEM images indicated increased collagen deposition and alignment following DEX treatment (Figures 18C & D), this collagen content did not translate to a more robust extracellular matrix, as evident from the decrease in passive tension values. Since plates receiving 25nM DEX exhibited the largest myotubes in the highest density, additional ECM would be required to support these robust muscle networks, and it is possible that the ECM present in the 25nM plates was insufficient to transmit force along the SMUs. Another potential explanation was the formation of blebs on the periphery of several myotubes accompanying myoblast fusion. This blebbing, seen in the light microscopy images in Figure 17, typically began shortly after the switch from M-GM to M-DM on Day 7 and became more pronounced during differentiation. Upon gross examination, these blebs were increasingly prevalent at the 25nM DEX dosage. Blebbing has been identified as a potential biomarker of cell injury that can occur in myotubes in response to toxic agents or hypotonic osmotic shock[157]. Based on the current understanding of the action of DEX *in vivo*[148,150], namely acting as a potential agent for the induction of skeletal muscle atrophy, it may be possible to draw a connection between DEX addition and myotube membrane damage and blebbing. Further analysis is necessary to determine whether membrane blebbing, an inhibition of ECM formation, or some additional unexpected cause, resulted in the decrease in force production accompanying 25nM DEX addition.

Conclusions

This experiment demonstrates that addition of DEX to isolated muscle satellite cells in culture can improve functional and structural characteristics of our tissue-engineered skeletal muscle when administered at optimal doses and timings. Addition of DEX prior to induction of differentiation improved myogenic proliferation of muscle satellite cells, which subsequently led to increased myogenic differentiation and myotube fusion. The benefits of the administration of DEX during proliferation were further evident during the SMU maturation phase, as characterized by formation of advanced sarcomeric structure and increased contractile function observed in the fully formed 3-D SMU. The most promising improvements in SMU function were achieved with the addition of 10nM DEX on either Day 0 or Day 6. In addition to increased myogenic differentiation and myotube fusion, SMUs exposed to this concentration exhibited advanced structural development of sarcomeric structure and a five-fold increase in force production. Thus, the utilization of dexamethasone in our existing tissue-engineering model presents a blueprint for advancing tissue engineering of skeletal muscle.

CHAPTER IV

Quantitative, Label-Free Evaluation of Tissue-Engineered Skeletal Muscle through Multiphoton Microscopy

Introduction

The growing deficit in suitable tissues for patients awaiting organ transplants demonstrates the clinical need for engineered tissues as alternative graft sources[158,159]. Although government funding for tissue engineering and regenerative medicine reached $2 billion in 2009, only a fraction of potential tissue-engineered products has obtained clinical approval[160,161]. A major obstacle is a lack of non-invasive methods for *in vitro* validation of construct robustness prior to implantation. A reliable, rapid method to assess construct viability is needed that avoids destroying or compromising the cell-based device[162,163] and yields parameters employable as release criteria. Unfortunately, current methods to evaluate engineered tissue viability and structural integrity prior to implantation have significant drawbacks, including being invasive, destructive, or non-sterile[164-166].

To meet the need for a rigorous, quantitative methodology for evaluating engineered tissues in a non-destructive manner, multiphoton microscopy is a promising novel technology. In comparison to the gold standards of histology and immunohistochemistry (IHC), multiphoton microscopy presents several beneficial aspects[163,167]. Whereas the combination of histology and

IHC can provide spatial information about cells and matrix proteins in a quantitative manner that has been accepted by regulatory scientists, multiphoton microscopy adds the ability to acquire the same information in real-time without irrevocably damaging the engineered tissue. Multiphoton microscopy is a form of non-linear microscopy utilizing laser scanning in an extremely thin focal plane. It differs from conventional techniques, such as light microscopy or confocal microscopy, by localizing sample excitation to the focal plane alone as multiple photons of approximately equal energy are focused onto approximately the same molecular component[166,168]. As a result, multiphoton microscopy is beneficial as a means of imaging in thicker tissues, producing minimal photodamage or photobleaching, and avoiding the use of labelling reagents. Using such a technology, imaging up to 500 µm into a sample with spatial resolution on the order of 1 µm becomes possible[166].

Optical molecular imaging (OMI) techniques utilizing multiphoton microscopy have been demonstrated in native skeletal muscle[166,169,170] and in select engineered tissues[167,168,171], but they have not been applied to engineered musculoskeletal tissues. In particular, the following OMI approaches have been identified: 1) excitation of endogenous nicotinamide adenine dinucleotide (NADH) and flavin adenine dinucleotide (FAD) fluorescence to evaluate metabolic activity, and 2) second harmonic generation (SHG) imaging of myosin in skeletal muscle sarcomeres and of collagen in the extracellular matrix to assess structural composition. We sought to demonstrate the applicability of these OMI approaches to non-invasively evaluate the structure and metabolic activity in our tissue-engineered skeletal muscle.

For studying metabolic activity, multiphoton excitation fluorescence targeting NADH and FAD was monitored. These two mitochondrial coenzymes are necessary for cell metabolism and

oxygen consumption and can act as endogenous cellular fluorophores. The reduced and oxidized states of these coenzymes naturally fluoresce in response to multiphoton excitation[166,167,172,173]. Captured images of intracellular concentrations of NADH and FAD in engineered tissues can be used to characterize size, morphology, and cellular organization[174-176]. In addition, NADH and FAD signals can be used to calculate a redox ratio (RR) metric, calculated as [FAD] / [NADH] + [FAD][167], as an indication of metabolic activity. Intensity ratios like the RR metric measure metabolic variations with increased sensitivity by reducing intensity-based artifacts, including signal variations due to optical loss, which may be difficult to quantify or control in tissues. Previous work with engineered oral mucosa fabricated from primary human cells demonstrated the ability of this OMI method to detect significantly different RR values in metabolically stressed constructs as compared to controls[167]. Similar nonlinear OMI and quantitative analytic methods were applied in the current study to non-invasively assess the viability of engineered skeletal muscle constructs. In both our previous and current studies, label-free OMI of local tissue structure and biochemistry characterized morphologic and functional differences between controls and metabolically stressed constructs. Unlike traditional histological and functional tissue analyses, label-free OMI has the advantage of being non-invasive.

To study structural composition at a molecular level, second harmonic generation (SHG) is a useful tool. SHG is a multiphoton microscopy technique collecting light from non-linear scattering processes, differing slightly from multiphoton fluorescence. SHG depends on the interaction of multiphoton excitation with highly polarizable, non-centrosymmetric structures[166,170]. Myosin in skeletal muscle sarcomeres and collagen in ECM are two of the few biomolecular structures capable of generating a SHG signal[166,168,170,177]. Myosin is a filamentous

protein with a coiled rod region and a cross-head region responsible for interaction with actin filaments[169]. The SHG signal arises from the coiled rod region, specifically, due to the non-centrosymmetric structure of this domain. Several researchers have used myosin SHG to examine native skeletal muscle, extracting measures of sarcomeric spacing correlated to contractile function[169,178-180]. In one such study, muscle biopsies from healthy patients and those with Pompe disease were analyzed by myosin SHG[178]. Pompe disease is characterized by enlarged, glycogen-filled lysosomes and autophagic debris in muscle fibers, resulting in widespread sarcomere disruption. After acquiring myosin SHG images, subsequent processing of sarcomeric spacing and alignment data was used to generate a score indicating the condition of the muscle. These values were then used to distinguish between healthy and diseased patients, providing a potential tool for assessing muscle health. Similarly, collagen SHG has been used to image the triple helical fibrillar collagen structure in a range of tissues[177]. The SHG signal is sensitive to the fiber structural organization and especially to changes due to disorders such as fibrosis and connective tissue disorders. In engineered tissues specifically, it has been utilized to assess structural organization of engineered heart valves, detecting the difference in collagen deposition by cells cultured under normal and supraphysiological conditions[181,182].

While these studies demonstrate the efficacy of the OMI techniques proposed, to date most have collected data from fixed samples, not living tissues. Furthermore, the majority of published data examines native tissues, not engineered tissues[166,167,169,178,179]. Thus, there exists a lack of knowledge about label-free, nonlinear OMI in engineered tissue. In this study, I combine these two complementary OMI methods to obtain redox ratio values indicative of metabolic activity and SHG of structural organization as measures of the overall integrity of our tissue-

engineered SMUs. Thus, our goal was to use known protocols to alter the structural integrity and metabolic activity within our engineered tissues and to determine if these perturbations could be monitored using OMI. Additionally, we sought to demonstrate applicability of the reliable method previously demonstrated in our work[167] for non-destructive and quantitative evaluation and characterization to engineered skeletal muscle tissue. Such optical measures could serve as reliable release criteria for cell-based tissue-engineered constructs prior to human implantation, thereby addressing a critical regulatory need in regenerative medicine.

Methods

Animal Care

All animal care procedures followed *The Guide for Care and Use of Laboratory Animals*[137], according to a protocol approved by the University Committee for the Use and Care of Animals. As described in Chapter II, SMUs were engineered from female Fischer 344 rats.

Muscle Dissection and Cell Isolation

To yield a single cell suspension, muscles were processed using the protocol described in Chapters II and III. Both soleus muscles were removed, minced using a razor blade, and digested in a dissociation solution containing dispase and type IV collagenase. The resulting suspension was then filtered, centrifuged, and the cells were resuspended in growth medium for seeding.

SMU Formation

SMUs were engineered as described in Figure 9 and in previous work from our laboratory[72,140]. In this study, 3 variations of this established SMU fabrication protocol were used.

The first group (Control) contained SMUs fed every 48 hours as per our published protocol[72], prior to studying the addition of dexamethasone. The second group (Metabolic Stress) had its metabolic activity altered through feeding every 72 hours. The third group (Steroid Supplement) of SMUs were fed every 48 hours and supplemented with dexamethasone to generate improved myogenesis and structural advancement[140]. Isolated cells were divided evenly between experimental groups, allowing all three to begin with cells that were essentially equivalent. To accommodate the constraints of the microscope, custom 60mm polystyrene dishes were used for SMU fabrication. After curing PDMS onto each plate, the substrate was removed and punched with a 46 mm punch (McMaster-Carr, Elmhurst, IL, cat no. 3418A46). This central portion of this layer of PDMS was then replaced in the polystyrene dish, coated with laminin at 1mg/cm^2, and used for seeding. After initial plating, cells were left unaltered for four days to allow attachment and were subsequently fed muscle growth medium (MGM) as per the feeding schedule for each experimental group until becoming fully confluent on Day 7 with a network of elongating myotubes. At this point, 5 mm tissue-engineered bone-tendon anchors were pinned onto the cell monolayers at a spacing of 2.5 cm, and the media was switched to muscle differentiation medium (MDM). After a week on MDM, the monolayers delaminated from the plates on Day 14, rolling into cylindrical muscle constructs, held at length by the engineered bone anchors.

Evaluation of SMU Contractile Properties

To evaluate force production[29,72,140], one end of the SMU was attached to a force transducer with a 0-5 mN range and a 0.4 μN resolution, and platinum wire electrodes were placed along either side of the SMU for field stimulation. Passive tension was measured prior to stimulation. Peak tetanic force was determined after subtracting the passive tension baseline in

response to a 1 s train of 5 ms pulses at 90 mA and 60 Hz, and data files for force traces were recorded and analyzed using LabVIEW 2013.

Non-linear Optical Molecular Imaging

OMI was performed on a Leica TCS SP5 microscope equipped with an ultrafast-pulsed Ti:sapphire laser (Spectra-Physics, Mountain View, CA, cat. no. "Mai-Tai"). The excitation laser source and emitted light were coupled through an inverted microscope with a 25X water immersion objective lens (0.95 NA, 2.5 mm working distance) to image developing muscle monolayers and 3D SMUs. Prior to measurement on the inverted microscope, the PDMS substrate and monolayers were flipped over onto custom measurement dishes with the polystyrene bottom removed and replaced with a coverslip. All images were collected in a controlled environment at 37 °C with 5% CO^2 to mimic normal tissue culture conditions. Before each measurement, the excitation power at the specimen surface plane at both excitation wavelengths with a 10X objective was calibrated at 20 mW for cell monolayers and 30 mW for 3D SMUs to limit photobleaching and nonreversible changes in the sample[166,183]. All imaging was thus performed at incident power levels below 30 mW, since such excitation has proven non-damaging after thousands of scans[183]. Furthermore, the ability of the engineered tissue to assume 3D form and produce contractile force comparable to historical values[72,140] suggests that OMI analysis did not adversely affect tissue health or function.

These monolayers were analyzed on Day 11 of the fabrication protocol. Because this procedure is sterile and non-invasive, the same monolayers were evaluated again on Day 16 following 3D formation and contractile properties measurement. 3D SMUs were transferred onto

similar measurement dishes with a coverslip bottom and the addition of stainless steel pins to constrain the engineered tissue.

For imaging of NADH and FAD molecules, two-photon excitation at 715 nm and 900 nm was used, respectively. Backscattered fluorescence for NADH and FAD were filtered through a band pass (440-490 nm for NADH and 500-550 nm for FAD) prior to collection with non-descanned photomultiplier tubes (PMT) to increase collection efficiency. High-resolution images (1024 x 1024 pixels) were collected at a 200 Hz line-scanning rate, with a line average of eight to reduce noise. This line average value indicates each line of pixels is scanned eight times, with the resulting intensities combined and displayed as an average. The PMT gain was maintained at its maximum to keep measurements consistent between images and samples.

For second harmonic generation imaging, 860 nm excitation was used to generate a myosin SHG signal[169,170]. To isolate this SHG signal, a 425-435 nm filter was placed in front of the PMT. For the collagen SHG signal, 900 nm excitation and a 395-405 nm filter was used[169,170]. Since SHG is a scattering process, its intensity is highly dependent on direction. In relatively thicker samples, such as the 3D SMU, back-scattered myosin and collagen SHG signals dominate, and a PMT on the same side of the sample as the excitation was employed. For the thinner monolayers, forward-scattered SHG signals were captured with a PMT on the opposite side of the sample form the excitation. As with metabolic activity imaging, high-resolution images (1024 x 1024 pixels) were collected at a 200 Hz line-scanning rate with a line average of eight to reduce noise. The PMT gain was set at maximum for every measurement.

From each sample, 6 images were captured by sequentially scanning for myosin SHG, collagen SHG, FAD, and NADH. These sample sizes were chosen based on previous work using OMI to detect differences in control and stressed engineered oral mucosa[167].

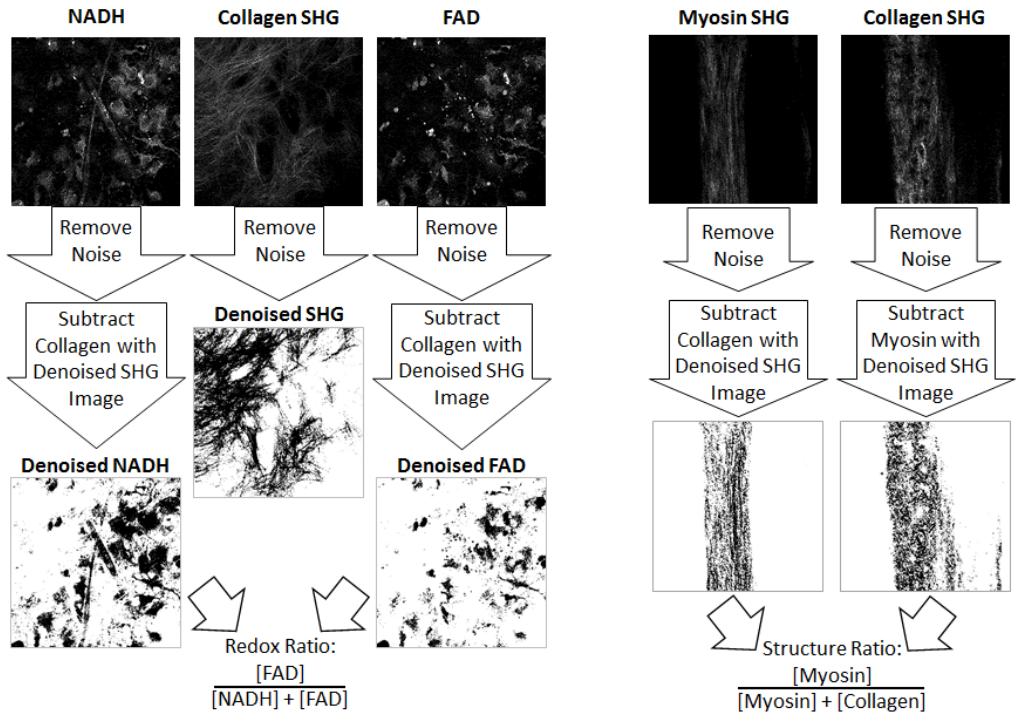

Figure 20. OMI processing schematic. Raw images were analyzed in ImageJ. Pre-processing involved noise reduction with a 3 x 3 median filter and subtraction of background fluorescence signals. For the metabolic indicators, NADH and FAD, the collagen SHG signal was subtracted from each to remove collagen regions. For the structural indicators, myosin and collagen, each SHG signal was subtracted from the other to remove overlapping regions.

Redox Ratio Calculation

For analysis of metabolic activity, the raw fluorescence images of NADH and FAD were inputs into ImageJ software (Figure 20). The collagen SHG signal was also incorporated into this analysis. These three images were then processed with a 3 x 3 median filter to increase image contrast. A threshold value, set as the average fluorescence intensity signal from the whole image, created a binary mask to reduce background fluorescence signals. This binary mask

filtered each raw NADH and FAD fluorescence image. In the collagen SHG image, pixels having intensity greater than the average SHG signals from the whole image were subsequently subtracted from the corresponding NADH and FAD fluorescence images. Following removal of background noise and collagen signals, the processed NADH and FAD images were then used to derive a redox ratio (RR) at each image pixel as [FAD] / ([NADH] + [FAD]). Ultimately, the average RR across the entire image was used to quantify local intracellular metabolic activity, providing a quantitative parameter with minimized background artifacts[184-187].

Structure Ratio Calculation

Myosin and collagen SHG signals were analyzed to obtain a structure ratio metric indicative of engineered tissue structural composition (Figure 20). Each pair of images were first processed with a 3 x 3 median filter in ImageJ to increase image contrast. A binary mask, based on a threshold at the average image intensity, was used to reduce background. Next, pixels having intensity greater than the average collagen SHG signal from the whole image were subsequently subtracted from the corresponding myosin SHG imaging, and vice versa. After removing noise and overlapping SHG signals, an average structure ratio was calculated for each image as [Myosin] / ([Myosin] + [Collagen]).

Immunocytochemical and Immunohistochemical Analysis

To validate the NADH signal, MitoTracker® (Fisher, cat. no. M-7512), an exogenous fluorescence dye that only fluoresces within mitochondria, was used to stain developing muscle monolayers. A 50 nM MitoTracker® solution was added to MDM on Day 11 of SMU fabrication and incubated for 30 minutes. Fresh medium was then resupplied, and samples were imaged for

colocalized fluorescence from both MitoTracker® and NADH. Additionally, media containing a metabolic inhibitor, 4 mM KCN (Sigma, cat. no. 60178), or an uncoupler, 0.5 mM FCCP (Sigma, cat. no. C2920), were employed to vary cellular metabolism during imaging. Variations in both NADH and FAD signals were monitored for 10 min, and KCN or FCCP was administered immediately after acquiring the first image.

To confirm the accuracy of myosin and collagen SHG signals, following force testing and OMI evaluation, 3D SMUs were fixed in 20°C methanol for 10 min and set aside for IHC. Samples were washed for 10 min in 0.1% Triton X-100 (Sigma, cat. no. T8787) in DPBS (PBST) and blocked with PBST containing 3% Bovine Serum Albumin (PBST-S; Sigma, cat. no. A2153) at room temperature. Samples were then incubated overnight at 4°C with primary antibodies diluted in PBST-S. Immunofluorescent staining was performed using the following primary antibodies: mouse anti-myosin heavy chain (1:100 dilution; DSHB, cat. no. MF20) and rabbit anti-collagen I (1:200 dilution; Biorbyt, San Francisco, CA, cat. no. orb312178). Following 3 PBST washes for 5 min each, samples were incubated in a 1:500 dilution of Alexa Fluor secondary antibodies (Life Technologies) for 3 hours at room temperature. Following 3 washes in PBST for 15 min each, samples were preserved in Prolong Gold with DAPI (Life Technologies, cat. no. P36935) and cover slipped. Samples were then examined for colocalization of the antibody fluorescence and SHG signals.

Statistical Analysis

All values are presented as mean ± standard error. Measurements of significant differences between means were performed using GraphPad software. Means were compared using either a Student's t-test or one-way ANOVA with Tukey post-hoc comparisons. Correlation

between experimentally measured OMI metrics and contractile force values was assessed based on the Pearson correlation coefficient, r. Differences were considered significant at $p<0.05$.

Results

Metabolic Activity in Muscle Monolayers and 3D SMUs

The multiphoton fluorescence signal for NADH was validated using cells labelled with MitoTracker®. Colocalization of the NADH and MitoTracker® signals confirmed the presence of NADH in cell mitochondria as expected (Figure 21). Treatment with the metabolic inhibitor, KCN, and the metabolic uncoupler, FCCP, also produced the expected variations in NADH and FAD (Figure 21). Specifically, KCN inhibits complex IV of the electron transport chain, increasing NADH and decreasing FAD concentrations. Following KCN addition, the normalized NADH intensity for treated cells increased approximately 3-fold over the 10 minutes of observation, while the FAD intensity decreased by half. On the other hand, FCCP uncouples electron transport and drives the metabolic pathway to oxidation, decreasing NADH and increasing FAD concentrations. In living cells, an initial increase in FAD intensity was observed 2 minutes after FCCP treatment, before values returned to baseline levels. The normalized NADH intensity decreased approximately 4-fold in response to addition of FCCP.

After confirming the sensitivity of the NADH and FAD signals to variations in metabolic activity, images from the control and metabolically stressed tissues were analyzed to obtain RR values. As mentioned previously, the redox ratio, defined as [FAD]/([NADH] + [FAD])[167], is a quantitative metric to compare relative metabolic rates of measured samples. Because a lower RR indicates a higher cellular metabolic rate, with relatively lower FAD fluorescence and higher

NADH fluorescence, values in this study are presented as the inverse RR. As a result, higher inverse RR values indicate greater metabolic activity.

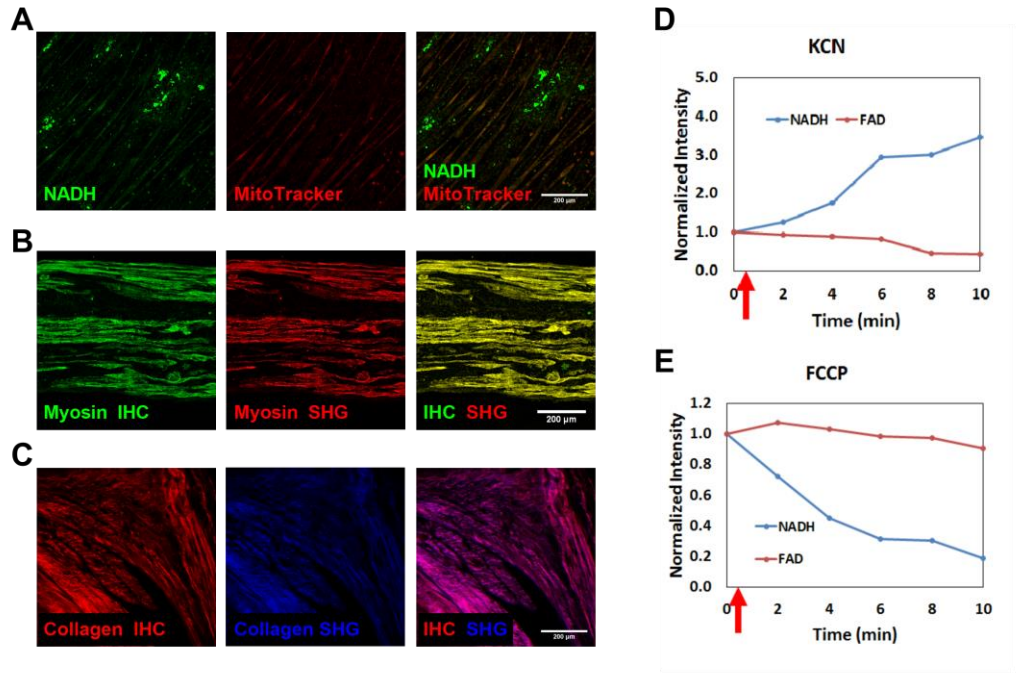

Figure 21. OMI signal validation. (A) Colocalization of the NADH and MitoTracker® signals confirmed the source of the OMI NADH signal. Sections of 3D SMUs visualized using both IHC and OMI for **(B)** myosin SHG and **(C)** collagen SHG validated the source of the myosin and collagen SHG signals. Treatment with **(D)** the metabolic inhibitor, KCN, and **(E)** the metabolic uncoupler, FCCP, produced the expected variations in NADH and FAD. Following KCN addition (indicated by the red arrow), OMI observed increasing NADH and decreasing FAD concentrations. FCCP led to decreasing NADH concentrations and FAD concentrations that increased initially before returning to baseline levels.

This inverse RR metric was used to assess cell metabolism in engineered skeletal muscle monolayers and in 3D SMUs. Representative raw fluorescence images from which RR metrics were extracted are shown in Figure 22. In monolayer form, control plates (n = 9) exhibited significantly greater (p = 0.02) inverse RR values (0.66 ± 0.04) than metabolically stressed cells (0.55 ± 0.03). Similarly, after formation of a 3D SMU, images of control tissues (n = 9) yielded average inverse RR values of 0.46 ± 0.02, which were significantly greater than 0.40 ± 0.02 in the

metabolic stress group (p = 0.04). When comparing all values for metabolic activity by imaging time point, a significant decrease (p < 0.01) in inverse RR value was observed in 3D SMUs (0.46 ± 0.02) relative to the cells in monolayer (0.62 ± 0.08).

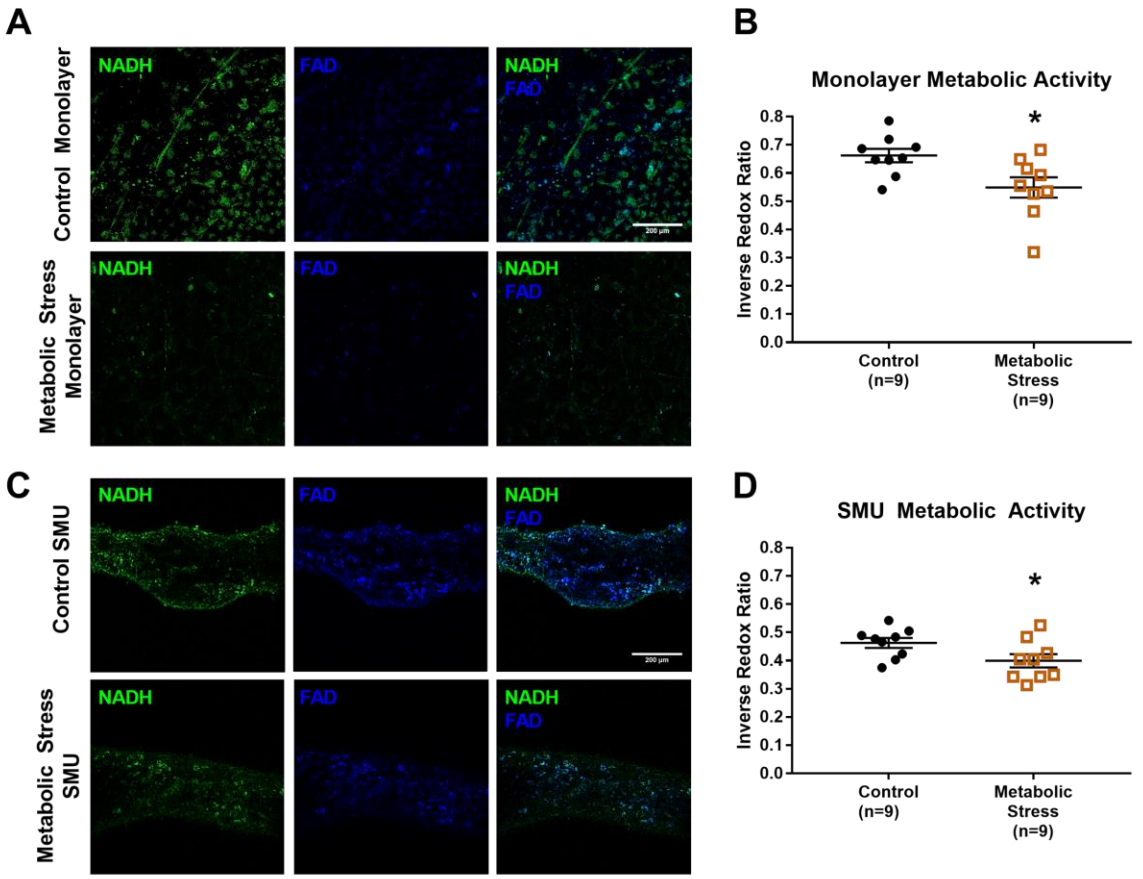

Figure 22. Endogenous NADH and FAD fluorescence as indicators of metabolic activity. NADH and FAD are mitochondrial coenzymes that function in cell metabolism and oxygen consumption. NADH fluorescence was excited at 715 nm, and emitted light was filtered in a band from 400-475 nm. FAD fluorescence was excited at 900 nm and was captured from 500-600 nm. Representative images of these signals are shown above for engineered tissues **(A)** in monolayer form and **(C)** in SMU form. For each engineered tissue, n=6 images were recorded. Following processing of captured images as described in Figure 20, a redox ratio metric was calculated as [FAD] / ([NADH] + [FAD]). The calculated redox ratios are summarized graphically for monolayers in **(B)** and for 3D SMUs in **(D)**. For engineered tissues in monolayer form, metabolic stress significantly increased (p = 0.02) the redox ratio to 0.45 ± 0.06, as compared to the average control redox ratio of 0.34 ± 0.02. After formation of a 3D SMU, redox ratios in both groups increased. Again, the average redox ratio in the metabolic stress group, 0.60 ± 0.04, was significantly greater (p = 0.04) than that of the control group, 0.54 ± 0.02. Differences are considered significant at p < 0.05. Values are presented as Mean ± Standard Error, and * indicates significant difference from control.

Structural Organization in Monolayers and 3D SMUs

As with the metabolic fluorescence signals, engineered tissues were simultaneously analyzed with both OMI and with IHC to validate the source of the myosin and collagen SHG signals. Following cryosectioning and staining with fluorescent antibodies for either myosin heavy chain or collagen type I, samples of 3D SMUs were imaged and examined for colocalization of the SHG signal with the antibody fluorescence (Figure 21).

Furthermore, the myosin SHG signal in fixed samples of native and engineered skeletal muscle was examined for the presence of advanced sarcomeric organization. Without any exogenous labelling reagent, both native and engineered myofibers exhibited a dense network of parallel sarcomeres (Figures 23A & B). The average sarcomere length measured in these images (2.5 ± 0.4 µm in native, 2.6 ± 0.2 µm) matched the historical range from 2.4 to 2.9 µm. Additionally, in living engineered SMUs, sarcomeric organization was evident during collection of the myosin SHG signal (Figure 23C).

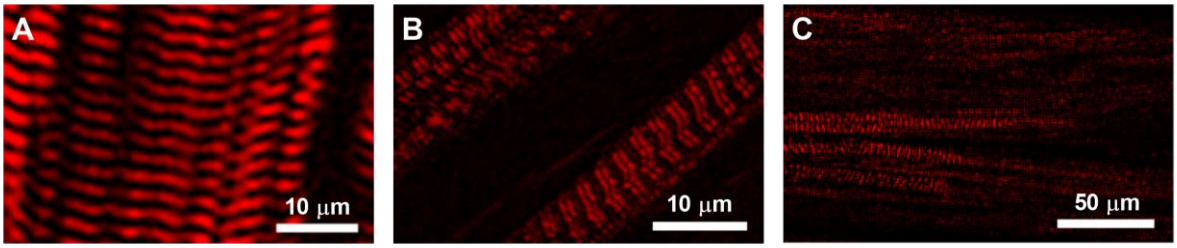

Figure 23. Myosin SHG in native and engineered skeletal muscle. Light scattered from myosin filaments was captured from fixed samples of **(A)** a native muscle section and **(B)** an engineered SMU. From such images (n = 12), the average sarcomere length measured in native muscle was 2.5 ± 0.4 µm. This value was statistically equivalent (p = 0.005) to the average sarcomere length of 2.6 ± 0.2 µm measured in engineered skeletal muscle. The average sarcomere length in rat skeletal muscle varies from 2.4 to 2.9 µm, and the values measured in engineered muscle fall within this range. **(C)** In living engineering SMUs, sarcomeric structure was evident from the myosin SHG signal. This OMI technique has not been demonstrated previously in living engineered tissue.

After confirming the accuracy of the myosin and collagen SHG signals, images from the control and steroid supplemented tissues were analyzed to obtain structure ratio (SR) values

modelled after the RR metric in the previous section. The structure ratio was defined as [Myosin] / ([Myosin] + [Collagen]) to create a quantitative metric for comparing the relative structural composition of these two key proteins. Representative raw images of the myosin and collagen SHG signals are shown in Figure 24. From these images, SR values were calculated and used to compare experimental groups.

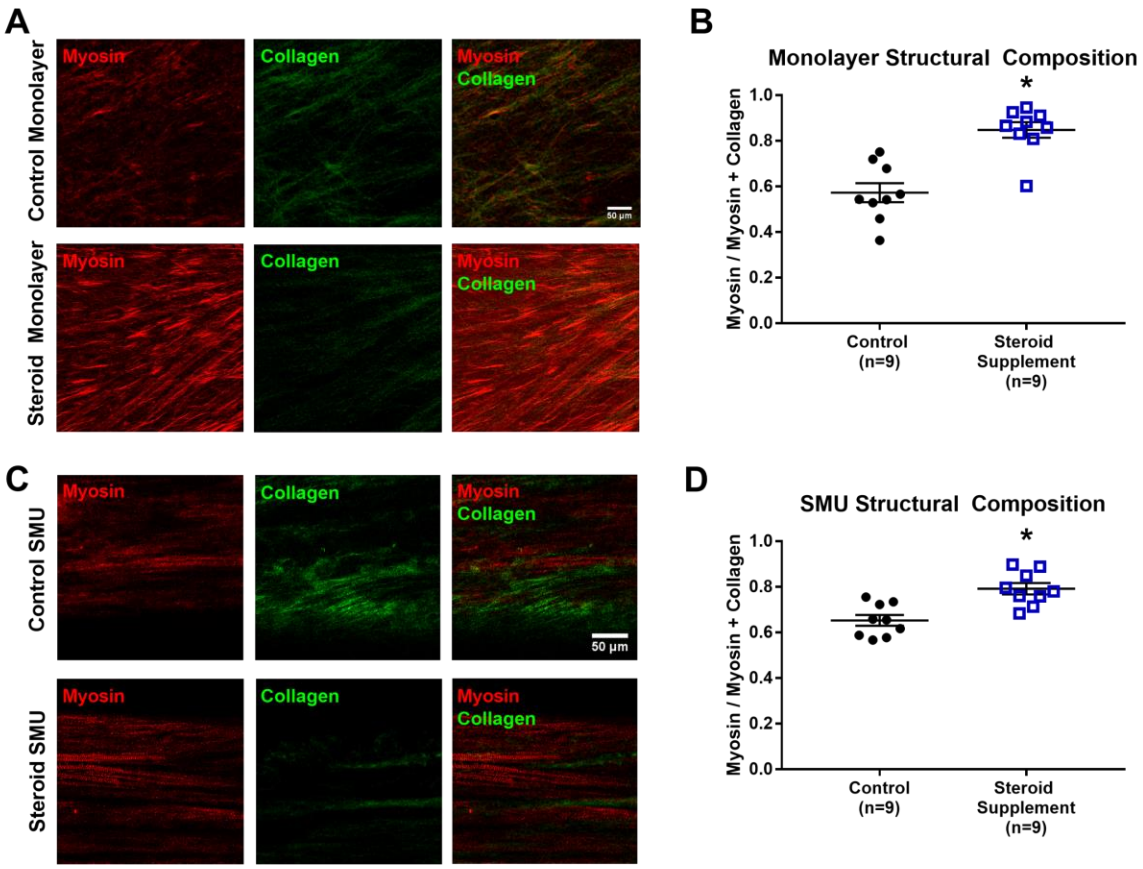

Figure 24. Myosin and collagen SHG as indicators of structural organization. SHG signals from myosin and collagen were collected in response to excitation at 860 nm and 920 nm, respectively. Due to the nature of SHG, scattered light was captured at half the excitation wavelength, 425-435 nm for myosin and 455-465 nm for collagen. Representative images of the two are pictured in **(A)** for engineered tissues in monolayer form and in **(C)** as 3D SMUs. n = 6 images were recorded for each sample. Following image processing summarized in Figure 20, a structure ratio was calculated as the myosin density relative to the combined myosin and collagen density. These ratios for monolayers are summarized in **(B)** and for 3D SMUs in **(D)**. In monolayer form, steroid supplementation significantly increased ($p < 0.01$) the structure ratio to 0.85 ± 0.03, as compared to control at 0.57 ± 0.04. Similarly, the average ratio with steroid supplement, 0.79 ± 0.03, was significantly greater ($p < 0.01$) than that of the control SMUs, 0.65 ± 0.02. Differences are considered significant at $p < 0.05$. * indicates significant difference from control.

Steroid supplemented monolayers (n = 9) yielded significantly greater ($p < 0.01$) SR values (0.85 ± 0.03) than control plates (0.57 ± 0.04). In 3D SMU form, steroid supplemented tissues (n = 9) exhibited average inverse SR values of 0.79 ± 0.02, which were significantly greater ($p < 0.01$) than the average of 0.65 ± 0.03 in controls. When comparing structural composition values by imaging time point, no significant difference ($p = 0.70$) in SR value was observed between monolayers (0.65 ± 0.03) and 3D SMUs (0.67 ± 0.02).

Contractile Properties of 3D SMUs

Overall function of engineered SMUs was assessed by measuring passive tension and contractile force production on Day 15, following monolayer delamination and capture in 3D form. As shown in Figure 25, no significant differences in passive force generation were observed among the three groups. Control SMUs (n = 9) exhibited average passive tensions of 2370 ± 785 μN, slightly higher ($p = 0.208$) than the average tension of 1260 ± 333 μN in steroid supplemented SMUs, and slightly lower ($p = 0.554$) than the average tension of 2970 ± 591 μN in metabolically stressed SMUs. The peak isometric tetanic force generated in response to electrical stimulation was also similar in control SMUs (67 ± 22 μN) and metabolically stressed SMUs (45 ± 12 μN, $p = 0.391$). SMUs in the steroid supplement group exhibited active forces of 287 ± 82 μN, significantly greater than control forces ($p = 0.028$).

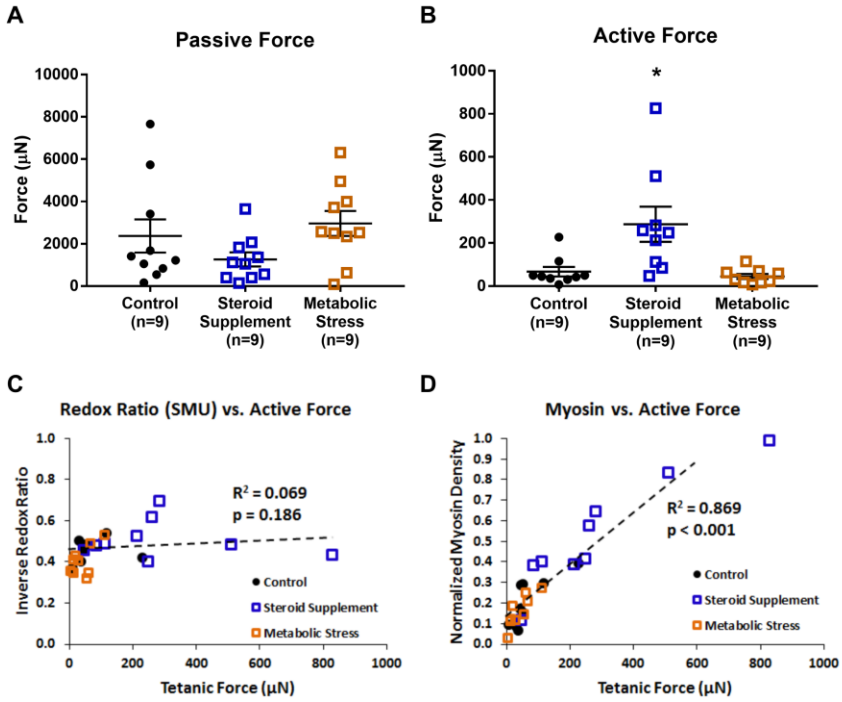

Figure 25. Comparison of SMU contractile properties and OMI measures. The ability of 3D SMUs to generate force was used to measure tissue function. **(A)** Passive force was measured as resting tension generated by the engineered tissue, and **(B)** active force was measured in response to tetanic electrical stimulation after subtracting resting tension. Steroid supplementation significantly increased active force generation, 287 ± 82 µN, as compared to control, 67 ± 22 µN ($p = 0.028$). When comparing functional and OMI measures, **(C)** correlation was not evident between metabolic activity and force, and **(D)** a clear correlation was present between overall myosin density and active force generation. Differences are considered significant at $p < 0.05$. Values are presented as Mean ± Standard Error, and * indicates significant difference from control.

Correlation between OMI Metrics and Functional Measures

To evaluate the potential of the OMI metrics for evaluation of engineered skeletal muscle tissue, redox ratio and structure ratio values from samples were compared to the current gold standard for functional evaluation, contractile force production. A weak, non-significant correlation (Pearson $r = 0.26$, $p = 0.19$) was observed between inverse RR and force production in 3D SMUs (Figure 25). On the other hand, a significant correlation ($p < 0.01$) was measured

between structure ratio and force production, with a Pearson correlation coefficient of 0.62. Furthermore, comparing OMI measures of myosin density alone to force production values demonstrated the strongest correlation ($r = 0.93$, $p < 0.01$).

Discussion

This work demonstrates the potential for using label-free optical molecular imaging to characterize and evaluate tissue-engineered skeletal muscle constructs. In both monolayers and 3D SMUs, the novel OMI measures successfully evaluated metabolic activity and structural organization. Previous work with tissue-engineered SMUs has determined that generation of contractile force greater than 100 μN serves as suitable threshold with which to judge constructs viable for implantation[29,72,127,145]. As a result, the optical approaches described in this work were first validated in tissue-engineered skeletal muscle and subsequently compared to functional evaluation of peak tetanic force production.

The potential of label-free OMI for evaluation of tissue viability has been demonstrated in biopsies from native skeletal muscle[169,178,180] and in engineered oral mucosa[167], and the ability to use such methods for a diverse range of engineered tissues holds great promise for advancing the field as a whole. In this study, cell metabolic activity, primarily contained within fluorescence signals from metabolic coenzymes NADH and FAD, was obtained by optically imaging thin cellular layers. Because OMI was performed in a non-invasive manner without the need for preservation or exogenous labelling reagents, metabolic activities were evaluated at multiple time points without adversely affecting the tissue engineering process. Using the redox ratio metric extracted from these signals, we successfully differentiated control and metabolically stressed engineered

tissues. A non-significant correlation relating increased metabolic activity to increased force production was observed, suggesting OMI measures of metabolism alone may not be sufficient to evaluate SMU suitability for implantation. Overall, decreased metabolic activity was detected through the RR metric in both metabolically stressed monolayers and 3D SMUs.

Additionally, OMI captured essential information describing structural composition through myosin and collagen SHG signals. The myosin SHG signal, in particular, shows great promise for the evaluation of organized sarcomeric structure in tissue-engineered skeletal muscle. In this study, I captured high-resolution images of myosin SHG in fixed native and engineered tissues and extracted sarcomere lengths indicative of tissue structural maturity. Furthermore, we demonstrated novel applicability of myosin SHG by imaging sarcomeric structure in living engineered tissue. Utilizing the ratio of myosin to collagen SHG signals, I was able to quantify structural development in our engineering tissues. The efficacy of the structure ratio metric was then demonstrated by distinguishing between dexamethasone-supplemented and control samples. Using OMI we were able to show that the addition of dexamethasone increased the relative myosin content, quantified by the structure ratio metric, in both developing muscle monolayers and 3D SMUs relative to control tissues. Furthermore, a relation between the structural OMI measures and force production was evident. As would be expected based on skeletal muscle contractile mechanics, increased myosin density observed through OMI was significantly correlated to increased force production. Ultimately, this positive correlation suggests OMI measures of SMU structure could potentially serve as an accurate predictor of successful implantation and tissue regeneration.

Conclusions

In this work, we demonstrated the potential of non-invasive optical techniques to provide manufacturing release criteria that correlate to functional measures of engineered skeletal muscle. The optical methods described here were previously used for quality control of tissue-engineered oral mucosa[167], and this use in an engineered skeletal muscle in this work suggests applicability for a variety of other tissues. Because nonlinear OMI has the ability to optically penetrate several hundred microns into tissues, this approach should be suitable for other engineered cell-based devices. Additionally, this approach could be employed to evaluate the integration and maturation of implanted tissues *in vivo* during the regeneration process, whether through a microendoscope and or an imaging window[169,172]. This work illustrates how OMI techniques could benefit the fabrication of tissue-engineered products by enabling non-destructive analysis of engineered tissues in real-time. Using this approach, reliable tools for providing quantitative measures of engineered tissue viability can enable selection of the healthiest engineered tissues for implantation, thereby improving therapeutic outcomes and enhancing patient care.

CHAPTER V

Conclusions

This work sought to develop methods for improving contractile force production in tissue-engineered skeletal muscle. Although engineered skeletal muscle tissues hold great potential as a graft source for repairing muscle damage, a significant barrier to clinical translation is the ability to fabricate tissue with an adult phenotype *in vitro*[160,161]. Rapid maturation towards the adult phenotype does occur with implantation *in vivo*[72], and it is hypothesized that improving the structure and function of engineered SMUs prior to implantation would unlock the maximum regenerative potential of these engineered tissues.

The first aim of this dissertation demonstrated how microfluidic separation utilizing a Labyrinth device was able to purify satellite cells from the heterogeneous population of isolated cells. From initial optimization experiments, sorting at a flow rate of 1800 µL/min yielded the greatest separation of fluorescently labelled mouse cells. Rat cells isolated according to the established SMU fabrication protocol and sorted by the Labyrinth subsequently demonstrated significant enrichment of the myogenic population, increased myogenic proliferation and differentiation, and improved SMU function. Thus, microfluidic sorting was shown to efficiently separate satellite cells from fibroblasts while ultimately improving the force production in 3D SMUs engineered from the purified population.

In the second aim, several experimental doses of dexamethasone and timing of administration were studied to maximize the beneficial effects of this glucocorticosteroid on myogenic differentiation[140]. In developing muscle monolayers, treatment with 10 and 25nM Dex significantly increased myogenic proliferation, early and late differentiation, and structural maturation. Ultimately, addition of 10nM DEX beginning on Day 0 or Day 6 led to a five-fold increase in force production in 3D SMUs. From these results, it was clear that dexamethasone supplementation could be employed to enhance structure and function of engineered skeletal muscle tissues.

The third aim developed optical molecular imaging (OMI) methods to non-invasively evaluate engineered SMUs, potentially removing the need for invasive, non-sterile functional measures prior to use for repair of volumetric muscle loss. In this study, redox ratios indicative of tissue metabolic activity extracted from NADH and FAD fluorescence successfully distinguished control and metabolically-stressed SMUs. Similarly, the OMI ratio metric comparing myosin and collagen SHG differentiated control SMUs from those supplemented with dexamethasone. Among these OMI measures, myosin density correlated to SMU force production, suggesting this technique can predict SMU force production and could potentially replace this functional measure. Overall, this study demonstrated the potential of OMI for evaluating metabolism and structure in engineered SMUs without the need for addition of exogenous labelling reagents or destructive sample preparation.

As intended in the initial experimental designs, the three studies demonstrated means for either increasing force production or removing evaluation methods that potentially damage and decrease force production in tissue-engineered skeletal muscle *in vitro*. The applicability of

these novel methods is evident from incorporation of microfluidic sorting with the Labyrinth and addition of 10nM dexamethasone into our current SMU fabrication protocol. With additional development and refinement, it is expected that the OMI techniques developed in this work will be incorporated as well. With consistent improvements in force production *in vitro* through the methods established in this dissertation, tissue-engineered skeletal muscle is closer to utility as a graft for repairing VML. This work is thus essential for advancing our tissue engineering model towards clinical translation. It is hoped that these and similar techniques can be applied to advance the tissue engineering and regenerative medicine field as a whole.

To continue advancing our engineered skeletal muscle, several future directions will play an essential role. In addition to the methods for promoting advanced *in vitro* myogenesis described in this dissertation, researchers have applied mechanical stimuli seeking to further recreate the *in vivo* environment. These systems can range from aligned, cylindrical microwells or micropatterned substrates designed to promote alignment and fusion into myotubes[71,188,189] to dynamic bioreactors for providing cyclic strain through either fluid flow or mechanical stretch[30,73]. Maximizing *in vitro* advancement of engineered tissues by utilizing both these mechanical stimuli and the techniques developed in my research have the potential to decrease even further the gap between our SMUs and native skeletal muscle.

The ultimate success of these engineered SMUs will depend on their ability to regenerate damaged muscle. Thus, future studies will fabricate engineered skeletal muscle characterized by increased myogenesis and improved *in vitro* force production for implantation into a model of volumetric muscle loss[72]. It is expected that *in vitro* phenotypic advancement will translate to

improved *in vivo* regeneration, and these implantation studies will reveal the degree to which this hypothesis is applicable.

Finally, scaling up of the engineered skeletal muscle from a rat model to a large animal model will be essential for achieving clinical relevance. Although the need for improved vascularization of these larger engineered tissues will prevent a significant challenge, previous work in our laboratory in scaling up tissue-engineered bone and ligament constructs will provide a model for this future research[139,190]. Additionally, recent studies have demonstrated potential methods for promoting vascularization of engineered skeletal muscle to maintain *in vitro* viability and metabolic activity and to promote anastomosis with native vasculature *in vivo* following implantation[26,154]. An additional challenge to the scaling up of our engineered SMUs is the limited proliferative capacity of muscle satellite cells. Isolated satellite cells can only be expanded to a limited extent, because myogenic potential rapidly decreases after a period of two weeks *in vitro*[33,80,92]. Developing methods to maintain the stem cell capacity for self-renewal in satellite cells will be essential as we seek to expand these cells for engineering skeletal muscle tissues suitable for repair of large-scale VML defects. With these goals and challenges in mind, it is exciting to imagine the potential for tissue-engineered skeletal muscle in the years to come.

BIBLIOGRAPHY

1. Marieb, E.N., and Hutchinson, M. Human Anatomy & Physiology. San Francisco: Benjamin Cummings, 2001.

2. Widmaier, E.P., Raff, H., Strang, K.T., and Vander, A.J. Vander's Human Physiology: The Mechanisms of Body Function. New York: McGraw-Hill, 2014.

3. Järvinen, T.A.H., Järvinen, T.L.N., Kääriäinen, M., Kalimo, H., and Järvinen, M. Muscle injuries: biology and treatment. The American Journal of Sports Medicine **33**, 745, 2005.

4. Grogan, B.F., and Hsu, J.R. Volumetric muscle loss. The Journal of the American Academy of Orthopaedic Surgeons **19 Suppl 1**, S35, 2011.

5. Syverud, B.C., Lee, J.D., VanDusen, K.W., and Larkin, L.M. Isolation and purification of satellite cells for skeletal muscle tissue engineering. Journal of Regenerative Medicine **3**, 117, 2014.

6. Tedesco, F.S., Dellavalle, A., Diaz-Manera, J., Messina, G., and Cossu, G. Repairing skeletal muscle: regenerative potential of skeletal muscle stem cells. The Journal of clinical investigation **120**, 11, 2010.

7. Fishman, J.M., Tyraskis, A., Maghsoudlou, P., Urbani, L., Totonelli, G., Birchall, M.A., and De Coppi, P. Skeletal Muscle Tissue Engineering: Which Cell to Use? Tissue engineering. Part B-Reviews **19**, 503, 2013.

8. Mauro, A. Satellite Cell of Skeletal Muscle Fibers. The Journal of Biophysical and Biochemical Cytology **9**, 493, 1961.

9. Lepper, C., Partridge, T.A., and Fan, C. An absolute requirement for Pax7-positive satellite cells in acute injury-induced skeletal muscle regeneration. Development (Cambridge, England) **138**, 3639, 2011.

10. McCarthy, J.J., Mula, J., Miyazaki, M., Erfani, R., Garrison, K., Farooqui, A.B., Srikuea, R., Lawson, B.A., Grimes, B., Keller, C., Van Zant, G., Campbell, K.S., Esser, K.A., Dupont-Versteegden, E.E., and Peterson, C.A. Effective fiber hypertrophy in satellite cell-depleted skeletal muscle. Development (Cambridge, England) **138**, 3657, 2011.

11. Murphy, M.M., Lawson, J.A., Mathew, S.J., Hutcheson, D.A., and Kardon, G. Satellite cells, connective tissue fibroblasts and their interactions are crucial for muscle regeneration. Journal of cell science **124**, e1, 2011.

12. Sambasivan, R., Yao, R., Kissenpfennig, A., Van Wittenberghe, L., Paldi, A., Gayraud-Morel, B., Guenou, H., Malissen, B., Tajbakhsh, S., and Galy, A. Pax7-expressing satellite cells are indispensable for adult skeletal muscle regeneration. Development (Cambridge, England) **138**, 3647, 2011.

13. Judson, R.N., Zhang, R., and Rossi, F.M.A. Tissue-resident mesenchymal stem/progenitor cells in skeletal muscle: collaborators or saboteurs? FEBS Journal **280**, 4100, 2013.

14. Zammit, P.S., Relaix, F., Nagata, Y., Ruiz, A.P., Collins, C.A., Partridge, T.A., and Beauchamp, J.R. Pax7 and myogenic progression in skeletal muscle satellite cells. Journal of cell science **119**, 1824, 2006.

15. Relaix, F., Rocancourt, D., Mansouri, A., and Buckingham, M. A Pax3/Pax7-dependent population of skeletal muscle progenitor cells. Nature **435**, 948, 2005.

16. Relaix, F., Montarras, D., Zaffran, S., Gayraud-Morel, B., Rocancourt, D., Tajbakhsh, S., Mansouri, A., Cumano, A., and Buckingham, M. Pax3 and Pax7 have distinct and overlapping functions in adult muscle progenitor cells. The Journal of cell biology **172**, 91, 2006.

17. Tanaka, K.K., Hall, J.K., Troy, A.A., Cornelison, D.D.W., Majka, S.M., and Olwin, B.B. Syndecan-4-Expressing Muscle Progenitor Cells in the SP Engraft as Satellite Cells during Muscle Regeneration. Cell Stem Cell **4**, 217, 2009.

18. Péault, B., Rudnicki, M., Torrente, Y., Cossu, G., Tremblay, J.P., Partridge, T., Gussoni, E., Kunkel, L.M., and Huard, J. Stem and progenitor cells in skeletal muscle development, maintenance, and therapy. Molecular therapy : the journal of the American Society of Gene Therapy **15**, 867, 2007.

19. Dhawan, J., and Rando, T.A. Stem cells in postnatal myogenesis: molecular mechanisms of satellite cell quiescence, activation and replenishment. Trends in cell biology **15**, 666, 2005.

20. Yin, H., Price, F., and Rudnicki, M.A. Satellite cells and the muscle stem cell niche. Physiological Reviews **93**, 23, 2013.

21. Pannérec, A., Parlakian, A., Gomes, E.R., Sassoon, D.A., Mitchell, K.J., Marazzi, G., Besson, V., and Cadot, B. Identification and characterization of a non-satellite cell muscle resident progenitor during postnatal development. Nature cell biology **12**, 257, 2010.

22. Wagers, A. The Stem Cell Niche in Regenerative Medicine. Cell Stem Cell **10**, 362, 2012.

23. Vandenburgh, H.H., Karlisch, P., and Farr, L. Maintenance of highly contractile tissue-cultured avian skeletal myotubes in collagen gel. In vitro cellular & developmental biology : journal of the Tissue Culture Association **24**, 166, 1988.

24. Corona, B.T., Ward, C.L., Baker, H.B., Walters, T.J., and Christ, G.J. Implantation of in vitro tissue engineered muscle repair constructs and bladder acellular matrices partially restore in vivo skeletal muscle function in a rat model of volumetric muscle loss injury. Tissue engineering. Part A **20**, 705, 2014.

25. Valentin, J.E., Turner, N.J., Gilbert, T.W., and Badylak, S.F. Functional skeletal muscle formation with a biologic scaffold. Biomaterials **31**, 7475, 2010.

26. Juhas, M., Engelmayr, G.C., Fontanella, A.N., Palmer, G.M., and Bursac, N. Biomimetic engineered muscle with capacity for vascular integration and functional maturation in vivo. Proceedings of the National Academy of Sciences of the United States of America **111**, 5508, 2014.

27. Lee, P.H.U., and Vandenburgh, H.H. Skeletal Muscle Atrophy in Bioengineered Skeletal Muscle: A New Model System. Tissue engineering. Part A **19**, 2147, 2013.

28. Carosio, S., Barberi, L., Rizzuto, E., Nicoletti, C., Del Prete, Z., and Musarò, A. Generation of eX vivo-vascularized Muscle Engineered Tissue (X-MET). Scientific reports **3**, 1420, 2013.

29. Williams, M.L., Kostrominova, T.Y., Arruda, E.M., and Larkin, L.M. Effect of implantation on engineered skeletal muscle constructs. Journal of tissue engineering and regenerative medicine **7**, 434, 2013.

30. Bach, A.D., Stern-Straeter, J., Beier, J.P., Bannasch, H., and Stark, G.B. Engineering of muscle tissue. Clinics in plastic surgery **30**, 589, 2003.

31. Kosnik, P.E., Faulkner, J.A., and Dennis, R.G. Functional development of engineered skeletal muscle from adult and neonatal rats. Tissue engineering **7**, 573, 2001.

32. Bischoff, R. Proliferation of muscle satellite cells on intact myofibers in culture. Developmental biology **115**, 129, 1986.

33. Rosenblatt, J.D., Lunt, A.I., Parry, D.J., and Partridge, T.A. Culturing satellite cells from living single muscle fiber explants. In vitro cellular & developmental biology.Animal **31**, 773, 1995.

34. Conboy, M.J., and Conboy, I.M. Preparation of adult muscle fiber-associated stem/precursor cells. Methods in molecular biology (Clifton, N.J.) **621**, 149, 2010.

35. Blau, H.M., and Webster, C. Isolation and Characterization of Human Muscle Cells. Proceedings of the National Academy of Sciences of the United States of America **78**, 5623, 1981.

36. Rando, T.A., and Blau, H.M. Primary mouse myoblast purification, characterization, and transplantation for cell-mediated gene therapy. The Journal of cell biology **125**, 1275, 1994.

37. Bischoff, R. Enzymatic liberation of myogenic cells from adult rat muscle. The Anatomical Record **180**, 645, 1974.

38. Allen, R.E., Temm-Grove, C.J., Sheehan, S.M., and Rice, G. Skeletal muscle satellite cell cultures. Methods in cell biology **52**, 155, 1997.

39. Lees, S.J., Rathbone, C.R., and Booth, F.W. Age-associated decrease in muscle precursor cell differentiation. AJP - Cell Physiology **290**, C609, 2005.

40. Tebbets, J., Péault, B., Crisan, M., Lu, A., Zheng, B., Huard, J., Cummins, J., Gharaibeh, B., and Feduska, J. Isolation of a slowly adhering cell fraction containing stem cells from murine skeletal muscle by the preplate technique. Nature Protocols **3**, 1501, 2008.

41. Yablonka-Reuveni, Z., and Day, K. "Skeletal Muscle Stem Cells in the Spotlight: The Satellite Cell" in *Regenerating the Heart*. , 173, 2011.

42. Danoviz, M.E., and Yablonka-Reuveni, Z. Skeletal muscle satellite cells: background and methods for isolation and analysis in a primary culture system. Methods in molecular biology (Clifton, N.J.) **798**, 21, 2012.

43. Lee, E., Choi, J., Hyun, J., Cho, K., Hwang, I., Lee, H., Chang, J., and Choi, I. Steroid Effects on Cell Proliferation, Differentiation and Steroid Receptor Gene Expression in Adult Bovine Satellite Cells. Asian Australas J Anim Sci **20**, 501, 2007.

44. Doumit, M.E., and Merkel, R.A. Conditions for isolation and culture of porcine myogenic satellite cells. Tissue and Cell **24**, 253, 1992.

45. McFarland, D.C., Doumit, M.E., and Minshall, R.D. The turkey myogenic satellite cell: Optimization of in vitro proliferation and differentiation. Tissue and Cell **20**, 899, 1988.

46. Maley, M.A.L., Davies, M.J., and Grounds, M.D. Extracellular Matrix, Growth Factors, Genetics: Their Influence on Cell Proliferation and Myotube Formation in Primary Cultures of Adult Mouse Skeletal Muscle. Experimental cell research **219**, 169, 1995.

47. Dodson, M.V., Mathison, B.A., and Mathison, B.D. Effects of medium and substratum on ovine satellite cell attachment, proliferation and differentiation in vitro. Cell differentiation and development : the official journal of the International Society of Developmental Biologists **29**, 59, 1990.

48. Boonen, K., Rosaria-Chak, K., Baaijens, F., van der Schaft, D., and Post, M. Essential environmental cues from the satellite cell niche: optimizing proliferation and differentiation. American Journal of Physiology - Cell Physiology **296**, C1338, 2009.

49. Wilschut, K.J., Haagsman, H.P., and Roelen, B.A.J. Extracellular matrix components direct porcine muscle stem cell behavior. Experimental cell research **316**, 341, 2010.

50. Shadrach, J.L., and Wagers, A.J. Stem cells for skeletal muscle repair. Philosophical transactions of the Royal Society of London.Series B, Biological sciences **366**, 2297, 2011.

51. Mathew, S.J., Hansen, J.M., Merrell, A.J., Murphy, M.M., Lawson, J.A., Hutcheson, D.A., Hansen, M.S., Angus-Hill, M., and Kardon, G. Connective tissue fibroblasts and Tcf4 regulate myogenesis. Development **138**, 371, 2011.

52. Richler, C., and Yaffe, D. The in vitro cultivation and differentiation capacities of myogenic cell lines. Developmental biology **23**, 1, 1970.

53. Qu, Z., Balkir, L., van Deutekom, J.C., Robbins, P.D., Pruchnic, R., and Huard, J. Development of approaches to improve cell survival in myoblast transfer therapy. The Journal of cell biology **142**, 1257, 1998.

54. Park, Y.G., Moon, J.H., and Kim, J. A comparative study of magnetic-activated cell sorting, cytotoxicity and preplating for the purification of human myoblasts. Yonsei medical journal **47**, 179, 2006.

55. Blanco-Bose, W.E., Yao, C., Kramer, R.H., and Blau, H.M. Purification of Mouse Primary Myoblasts Based on α7 Integrin Expression. Experimental cell research **265**, 212, 2001.

56. Pasut, A., Oleynik, P., and Rudnicki, M.A. Isolation of muscle stem cells by fluorescence activated cell sorting cytometry. Methods in molecular biology (Clifton, N.J.) **798**, 53, 2012.

57. Sherwood, R.I., Christensen, J.L., Conboy, I.M., Conboy, M.J., Rando, T.A., Weissman, I.L., and Wagers, A.J. Isolation of adult mouse myogenic progenitors: functional heterogeneity of cells within and engrafting skeletal muscle. Cell **119**, 543, 2004.

58. Chapman, M.R., Balakrishnan, K.R., Li, J., Conboy, M.J., Huang, H., Mohanty, S.K., Jabart, E., Hack, J., Conboy, I.M., and Sohn, L.L. Sorting single satellite cells from individual myofibers reveals heterogeneity in cell-surface markers and myogenic capacity. Integrative Biology , 692, 2013.

59. Asakura, A., Seale, P., Girgis-Gabardo, A., and Rudnicki, M.A. Myogenic specification of side population cells in skeletal muscle. The Journal of cell biology **159**, 123, 2002.

60. Bosnakovski, D., Xu, Z., Li, W., Thet, S., Cleaver, O., Perlingeiro, R.C.R., and Kyba, M. Prospective isolation of skeletal muscle stem cells with a Pax7 reporter. Stem cells (Dayton, Ohio) **26**, 3194, 2008.

61. Jankowski, R.J., Haluszczak, C., Trucco, M., and Huard, J. Flow cytometric characterization of myogenic cell populations obtained via the preplate technique: potential for rapid isolation of muscle-derived stem cells. Human Gene Therapy **12**, 619, 2001.

62. Beliakova-Bethell, N., Massanella, M., White, C., Lada, S.M., Du, P., Vaida, F., Blanco, J., Spina, C.A., and Woelk, C.H. The effect of cell subset isolation method on gene expression in leukocytes. Cytometry.Part A : the journal of the International Society for Analytical Cytology **85**, 94, 2014.

63. Fong, C.Y., Peh, G.S.L., Gauthaman, K., and Bongso, A. Separation of SSEA-4 and TRA-1-60 labelled undifferentiated human embryonic stem cells from a heterogeneous cell population using magnetic-activated cell sorting (MACS) and fluorescence-activated cell sorting (FACS). Stem cell reviews **5**, 72, 2009.

64. Maxwell, W.M., and Johnson, L.A. Chlortetracycline analysis of boar spermatozoa after incubation, flow cytometric sorting, cooling, or cryopreservation. Molecular reproduction and development **46**, 408, 1997.

65. Martin, N.R.W., Passey, S.L., Player, D.J., Khodabukus, A., Ferguson, R.A., Sharples, A.P., Mudera, V., Baar, K., and Lewis, M.P. Factors affecting the structure and maturation of human tissue engineered skeletal muscle. Biomaterials **34**, 5759, 2013.

66. Servida, F., Soligo, D., Caneva, L., Bertolini, F., de Harven, E., Campiglio, S., Corsini, C., and Deliliers, G.L. Functional and morphological characterization of immunomagnetically selected CD34+ hematopoietic progenitor cells. Stem cells (Dayton, Ohio) **14**, 430, 1996.

67. O'Connor, M.S., Carlson, M.E., and Conboy, I.M. Differentiation rather than aging of muscle stem cells abolishes their telomerase activity. Biotechnology progress **25**, 1130, 2009.

68. Syverud, B.C., VanDusen, K.W., and Larkin, L.M. Growth Factors for Skeletal Muscle Tissue Engineering. Cells Tissues Organs **202**, 169, 2016.

69. Koning, M., Harmsen, M.C., van Luyn, M.J.A., and Werker, P.M.N. Current opportunities and challenges in skeletal muscle tissue engineering. Journal of tissue engineering and regenerative medicine **3**, 407, 2009.

70. Sakar, M.S., Neal, D., Boudou, T., Borochin, M.A., Li, Y., Weiss, R., Kamm, R.D., Chen, C.S., and Asada, H.H. Formation and optogenetic control of engineered 3D skeletal muscle bioactuators. Lab on a chip **12**, 4976, 2012.

71. Neal, D., Sakar, M.S., Ong, L.S., and Asada, H.H. Formation of elongated fascicle-inspired 3D tissues consisting of high-density, aligned cells using sacrificial outer molding. Lab on a chip **14**, 1907, 2014.

72. VanDusen, K.W., Syverud, B.C., Williams, M.L., Lee, J.D., and Larkin, L.M. Engineered Skeletal Muscle Units for Repair of Volumetric Muscle Loss in the Tibialis Anterior Muscle of a Rat. Tissue Engineering Part A **20**, 2920, 2014.

73. Dennis, R., Smith, B., Philp, A., Donnelly, K., and and Baar, K. Bioreactors for Guiding Muscle Tissue Growth and Development. Adv Biochem Engin/Biotechnol **112**, 39, 2009.

74. Bentzinger, C.F., Wang, Y.X., and Rudnicki, M.A. Building muscle: molecular regulation of myogenesis. Cold Spring Harbor perspectives in biology **4**, 2012.

75. Biressi, S., Molinaro, M., and Cossu, G. Cellular heterogeneity during vertebrate skeletal muscle development. Developmental biology **308**, 281, 2007.

76. Buckingham, M., and Mayeuf, A. Chapter 52 - Skeletal Muscle Development. In: Olson, J.A.H.N., ed. Muscle. Boston/Waltham: Academic Press, 2012, pp. 749-762.

77. Grefte, S., Kuijpers-Jagtman, A.M., Torensma, R., and Hoff, J.W.V.d. Skeletal muscle development and regeneration. Stem Cells and Development **16**, 857, 2007.

78. Schiaffino, S., and Mammucari, C. Regulation of skeletal muscle growth by the IGF1-Akt/PKB pathway: insights from genetic models. Skeletal muscle **1**, 4, 2011.

79. Dhawan, J., and Rando, T.A. Stem cells in postnatal myogenesis: molecular mechanisms of satellite cell quiescence, activation and replenishment. Trends in cell biology **15**, 666, 2005.

80. Cosgrove, B.D., Sacco, A., Gilbert, P.M., and Blau, H.M. A home away from home: Challenges and opportunities in engineering in vitro muscle satellite cell niches. Differentiation **78**, 185, 2009.

81. Zhang, P., Liang, X., Shan, T., Jiang, Q., Deng, C., Zheng, R., and Kuang, S. mTOR is necessary for proper satellite cell activity and skeletal muscle regeneration. Biochemical and biophysical research communications **463**, 102, 2015.

82. Murphy, M.M., Lawson, J.A., Mathew, S.J., Hutcheson, D.A., and Kardon, G. Satellite cells, connective tissue fibroblasts and their interactions are crucial for muscle regeneration. Development **138**, 3625, 2011.

83. Zanou, N., and Gailly, P. Skeletal muscle hypertrophy and regeneration: interplay between the myogenic regulatory factors (MRFs) and insulin-like growth factors (IGFs) pathways. Cellular and molecular life sciences : CMLS **70**, 4117, 2013.

84. Glass, D.J. Signalling pathways that mediate skeletal muscle hypertrophy and atrophy. Nature cell biology **5**, 87, 2003.

85. Glass, D.J. Skeletal muscle hypertrophy and atrophy signaling pathways. International Journal of Biochemistry and Cell Biology **37**, 1974, 2005.

86. Jackman, R.W., and Kandarian, S.C. The molecular basis of skeletal muscle atrophy. American Journal of Physiology - Cell Physiology **287**, 834, 2004.

87. Sandri, M. Signaling in muscle atrophy and hypertrophy. Physiology **23**, 160, 2008.

88. Gumucio, J.P., and Mendias, C.L. Atrogin-1, MuRF-1, and sarcopenia. Endocrine **43**, 12, 2013.

89. Wagers, A.J., and Conboy, I.M. Cellular and Molecular Signatures of Muscle Regeneration: Current Concepts and Controversies in Adult Myogenesis. Cell **122**, 659, 2005.

90. Huard, J., Li, Y., and Fu, F.H. Muscle Injuries and Repair: Current Trends in Research. The Journal of Bone & Joint Surgery **84**, 822, 2002.

91. Husmann, I., Soulet, L., Gautron, J., Martelly, I., and Barritault, D. Growth factors in skeletal muscle regeneration. Cytokine & growth factor reviews **7**, 249, 1996.

92. Renault, V., Thornell, L., Butler-Browne, G., and Mouly, V. Human skeletal muscle satellite cells: aging, oxidative stress and the mitotic clock. Experimental gerontology **37**, 1229, 2002.

93. Gaster, M., Beck-Nielsen, H., and Schrøder, H.D. Proliferation conditions for human satellite cells. The fractional content of satellite cells. APMIS : Acta Pathologica, Microbiologica, et Immunologica Scandinavica **109**, 726, 2001.

94. S. Machida, E. E. Spangenburg, and F. W. Booth. Primary rat muscle progenitor cells have decreased proliferation and myotube formation during passages. Cell proliferation **37**, 267, 2004.

95. Sicari, B.M., Rubin, J.P., Dearth, C.L., Wolf, M.T., Ambrosio, F., Boninger, M., Turner, N.J., Weber, D.J., Simpson, T.W., Wyse, A., Brown, E.H.P., Dziki, J.L., Fisher, L.E., Brown, S., and Badylak, S.F. An acellular biologic scaffold promotes skeletal muscle formation in mice and humans with volumetric muscle loss. Science Translational Medicine **6**, 1, 2014.

96. Wu, X., Corona, B.T., Chen, X., and Walters, T.J. A Standardized Rat Model of Volumetric Muscle Loss Injury for the Development of Tissue Engineering Therapies. BioResearch Open Access **1**, 280, 2012.

97. Lam, M.T., Huang, Y., Birla, R.K., and Takayama, S. Microfeature guided skeletal muscle tissue engineering for highly organized 3-dimensional free-standing constructs. Biomaterials **30**, 1150, 2009.

98. Clegg, C.H., Linkhart, T.A., Olwin, B.B., and Hauschka, S.D. Growth Factor Control of Skeletal Muscle Differentiation: Commitment to Terminal Differentiation Occurs in G1Phase and Is Repressed by Fibroblast Growth Factor. The Journal of cell biology **105**, 949, 1987.

99. Khodabukus, A., and Baar, K. The Effect of Serum Origin on Tissue Engineered Skeletal Muscle Function. Journal of cellular biochemistry **115**, 2198, 2014.

100. Khodabukus, A., and Baar, K. Glucose Concentration and Streptomycin Alter In Vitro Muscle Function and Metabolism. Journal of cellular physiology **230**, 1226, 2015.

101. Kuang, S., Gillespie, M.A., and Rudnicki, M.A. Niche Regulation of Muscle Satellite Cell Self-Renewal and Differentiation. Cell Stem Cell **2**, 22, 2008.

102. Allen, R.E., Sheehan, S.M., Taylor, R.G., Kendall, T.L., and Rice, G.M. Hepatocyte growth factor activates quiescent skeletal muscle satellite cells in vitro. Journal of cellular physiology **165**, 307, 1995.

103. Düsterhöft, S., and Pette, D. Evidence that acidic fibroblast growth factor promotes maturation of rat satellite-cell-derived myotubes in vitro. Differentiation **65**, 161, 1999.

104. Yablonka-Reuveni, Z., Balestreri, T.M., and Bowen-Pope, D.F. Regulation of Proliferation and Differentiation of Myoblasts Derived from Adult Mouse Skeletal Muscle by Specific Isoforms of PDGF. The Journal of cell biology **111**, 1623, 1990.

105. Allen, R.E., and Boxhorn, L.K. Regulation of skeletal muscle satellite cell proliferation and differentiation by transforming growth factor-beta, insulin-like growth factor I, and fibroblast growth factor. Journal of cellular physiology **138**, 311, 1989.

106. Chakravarthy, M.V., Abraha, T.W., Schwartz, R.J., Fiorotto, M.L., and Booth, F.W. Insulin-like growth factor-I extends in vitro replicative life span of skeletal muscle satellite cells by enhancing G1/S cell cycle progression via the activation of phosphatidylinositol 3'-kinase/Akt signaling pathway. The Journal of biological chemistry **275**, 35942, 2000.

107. Huang, Y., Dennis, R.G., Larkin, L.M., and Baar, K. Rapid formation of functional muscle in vitro using fibrin gels. Journal of applied physiology **98**, 706, 2004.

108. Weist, M.R., Wellington, M.S., Bermudez, J.E., Kostrominova, T.Y., Mendias, C.L., Arruda, E.M., and Larkin, L.M. TGFβ1 enhances contractility in engineered skeletal muscle. Journal of Tissue Engineering and Regenerative Medicine **7**, 562, 2013.

109. Engler, A.J., Griffin, M.A., Sen, S., Bönnemann, C.G., Sweeney, H.L., and Discher, D.E. Myotubes differentiate optimally on substrates with tissue-like stiffness: pathological implications for soft or stiff microenvironments. The Journal of cell biology **166**, 877, 2004.

110. Cimetta, E., Flaibani, M., Mella, M., Serena, E., Boldrin, L., De Coppi, P., and Elvassore, N. Enhancement of viability of muscle precursor cells on 3D scaffold in a perfusion bioreactor. The International journal of artificial organs **30**, 415, 2007.

111. Mertens, J.P., Sugg, K.B., Lee, J.D., and Larkin, L.M. Engineering muscle constructs for the creation of functional engineered musculoskeletal tissue. Regenerative medicine **9**, 89, 2014.

112. Turner, N., and Badylak, S. Regeneration of skeletal muscle. Cell and Tissue Research **347**, 759, 2012.

113. Johnny Huard, Yong Li, and Freddie H Fu. Muscle injuries and repair: Current trends in research. Journal of Bone and Joint Surgery **84**, 822, 2002.

114. Menetrey, J., Kasemkijwattana, C., Fu, F.H., Moreland, M.S., and Huard, J. Suturing Versus Immobilization of a Muscle Laceration. The American Journal of Sports Medicine **27**, 222, 1999.

115. Greene, T.L., and Beatty, M.E. Soft Tissue Coverage for Lower-Extremity Trauma: Current Practice and Techniques. Journal of orthopaedic trauma **2**, 173, 1988.

116. Lin, C., Lin, Y., Yeh, J., and Chen, C. Free functioning muscle transfer for lower extremity posttraumatic composite structure and functional defect. Plastic and Reconstructive Surgery **119**, 2118, 2007.

117. Emery, A.E. The muscular dystrophies. The Lancet **359**, 687, 2002.

118. Mercuri, E., and Muntoni, F. Muscular dystrophies. Lancet (London, England) **381**, 845, 2013.

119. Wicklund, M.P. The Muscular Dystrophies. CONTINUUM: Lifelong Learning in Neurology **19**, 1535, 2013.

120. Bushby, K. Diagnosis and management of Duchenne muscular dystrophy, part 1: diagnosis, and pharmacological and psychosocial management. Lancet Neurol **9**, 77, 2010.

121. Cossu, G., and Sampaolesi, M. New therapies for Duchenne muscular dystrophy: challenges, prospects and clinical trials. Trends in molecular medicine **13**, 520, 2007.

122. Deconinck, N. Pathophysiology of duchenne muscular dystrophy: current hypotheses. Pediatr Neurol **36**, 1, 2007.

123. Badylak, S.F., Taylor, D., and Uygun, K. Whole-Organ Tissue Engineering: Decellularization and Recellularization of Three-Dimensional Matrix Scaffolds. Annual Review of Biomedical Engineering **13**, 27, 2011.

124. Beattie, A., Gilbert, T., Guyot, J., Yates, A., and Badylak, S. Chemoattraction of Progenitor Cells by Remodeling Extracellular Matrix Scaffolds. Tissue Engineering, Part A: Tissue Engineering **15**, 1119, 2009.

125. Li, Q., Bai, Y., Xu, Y., and Yu, H. Autografting satellite cells to repair damaged muscle induced by repeated compression: an animal model. Foot & ankle international **31**, 706, 2010.

126. Corona, B.T., Machingal, M.A., Criswell, T., Vadhavkar, M., Dannahower, A.C., Bergman, C., Zhao, W., and Christ, G.J. Further development of a tissue engineered muscle repair construct in vitro for enhanced functional recovery following implantation in vivo in a murine model of volumetric muscle loss injury. Tissue engineering.Part A **18**, 1213, 2012.

127. Larkin, L.M., Calve, S., Kostrominova, T.Y., and Arruda, E.M. Structure and functional evaluation of tendon-skeletal muscle constructs engineered in vitro. Tissue engineering **12**, 3149, 2006.

128. Carbonaro, A., Mohanty, S.K., Huang, H., Godley, L.A., and Sohn, L.L. Cell characterization using a protein-functionalized pore. Lab on a chip **8**, 1478, 2008.

129. Segre, G., and Silberberg, A. Radial Particle Displacements in Poiseuille Flow of Suspensions. Nature **189**, 209, 1961.

130. Di Carlo, D. Inertial microfluidics. Lab on a chip **9**, 3038, 2009.

131. Lee, D.J., Brenner, H., Youn, J.R., and Song, Y.S. Multiplex particle focusing via hydrodynamic force in viscoelastic fluids. Scientific reports **3**, 3258, 2013.

132. Gossett, D.R., Weaver, W.M., Mach, A.J., Hur, S.C., Tse, H.T.K., Lee, W., Amini, H., and Di Carlo, D. Label-free cell separation and sorting in microfluidic systems. Analytical and bioanalytical chemistry **397**, 3249, 2010.

133. Akhoondi, M., Oldenhof, H., Stoll, C., Sieme, H., and Wolkers, W.F. Membrane hydraulic permeability changes during cooling of mammalian cells. BBA - Biomembranes **1808**, 642, 2011.

134. Jester, J.V., Brown, D., Pappa, A., and Vasiliou, V. Myofibroblast differentiation modulates keratocyte crystallin protein expression, concentration, and cellular light scattering. Investigative ophthalmology & visual science **53**, 770, 2012.

135. Handin, R.I., Lux, S.E., and Stossel, T.P. Blood: Principles and Practice of Hematology. Philadelphia: Lippincott Williams & Wilkins, 2003.

136. Lin, E., and Nagrath, S. Labyrinth CTC Paper. Nature Methods **Submitted**, 2016.

137. Committee for the Update of the Guide for the Care and Use of Laboratory Animals. Guide for the Care and use of Laboratory Animals: Eighth Edition. : National Academies Press, 2010.

138. Syed-Picard, F., Larkin, L., Shaw, C., and Arruda, E. Three-Dimensional Engineered Bone from Bone Marrow Stromal Cells and Their Autogenous Extracellular Matrix. Tissue Engineering, Part A: Tissue Engineering **15**, 187, 2009.

139. Ma, J., Smietana, M.J., Kostrominova, T.Y., Wojtys, E.M., Larkin, L.M., and Arruda, E.M. Three-Dimensional Engineered Bone–Ligament–Bone Constructs for Anterior Cruciate Ligament Replacement. Tissue Engineering Part A **18**, 13, 2012.

140. Syverud, B.C., VanDusen, K.W., and Larkin, L.M. Effects of Dexamethasone on Satellite Cells and Tissue Engineered Skeletal Muscle Units. Tissue Engineering Part A **22**, 480, 2016 Mar.

141. Caroline A Schneider, Wayne S Rasband, and Kevin W Eliceiri. NIH Image to ImageJ: 25 years of image analysis. Nature Methods **9**, 671, 2012.

142. Costa, M. Cytoskeleton and Adhesion in Myogenesis. ISRN Developmental Biology **2014**, 1, 2014.

143. Mills, M., Yang, N., Weinberger, R., Vander Woude, D., Beggs, A., Easteal, S., and North, K. Differential expression of the actin-binding proteins, alpha -actinin-2 and -3, in different species: implications for the evolution of functional redundancy. Human molecular genetics **10**, 1335, 2001.

144. van der Ven, P.F., Schaart, G., Jap, P.H., Sengers, R.C., Stadhouders, A.M., and Ramaekers, F.C. Differentiation of human skeletal muscle cells in culture: maturation as indicated by titin and desmin striation. Cell and tissue research **270**, 189, 1992.

145. Dennis, R.G., and Kosnik II, P.E. Excitability and Isometric Contractile Properties of Mammalian Skeletal Muscle Constructs Engineered in vitro. In Vitro Cellular & Developmental Biology.Animal **36**, 327, 2000.

146. Montarras, D., Morgan, J., Collins, C., Relaix, F., Zaffran, S., Cumano, A., Partridge, T., and Buckingham, M. Direct Isolation of Satellite Cells for Skeletal Muscle Regeneration. Science **309**, 2064, 2005.

147. Zimmerman, H.J. Hepatotoxicity: The Adverse Effects of Drugs and Other Chemicals on the Liver. Philadelphia, PA, USA: Lippincott, Williams & Wilkins, 1999.

148. Inder, W.J., Jang, C., Obeyesekere, V.R., and Alford, F.P. Dexamethasone administration inhibits skeletal muscle expression of the androgen receptor and IGF-1 implications for steroid-induced myopathy. Clinical Endocrinology **73**, 126, 2010.

149. Dracott, B.N., and Smith, C.E. Hydrocortisone and the antibody response in mice. II. Correlations between serum and antibody and PFC in thymus, spleen, marrow and lymph nodes. Immunology **38**, 437, 1979.

150. Qin, J., Du, R., Yang, Y., Zhang, H., Li, Q., Liu, L., Guan, H., Hou, J., and An, X. Dexamethasone-induced skeletal muscle atrophy was associated with upregulation of myostatin promoter activity. Research in veterinary science **94**, 84, 2013.

151. Belanto, J.J., Diaz-Perez, S.V., Magyar, C.E., Maxwell, M.M., Yilmaz, Y., Topp, K., Boso, G., Jamieson, C.H., Jamieson, C.A.M., and Cacalano, N.A. Dexamethasone induces dysferlin in myoblasts and enhances their myogenic differentiation. Neuromuscular Disorders **20**, 111, 2010.

152. Desler, M.M., Jones, S.J., Smith, C.W., and Woods, T.L. Effects of dexamethasone and anabolic agents on proliferation and protein synthesis and degradation in C2C12 myogenic cells. Journal of animal science **74**, 1265, 1996.

153. Larkin, L.M., Kuzon, J.,W M., Supiano, M.A., Galecki, A., and Halter, J.B. Effect of age and neurovascular grafting on the mechanical function of medial gastrocnemius muscles of Fischer 344 rats. The journals of gerontology.Series A, Biological sciences and medical sciences **53**, B252, 1998.

154. Blitterswijk, C.V., Rouwkema, J., Mulligan, R.C., Langer, R., Garfein, E.S., D'Amore, P.A., Marini, R., Kohane, D.S., Macdonald, M., Darland, D.C., and Levenberg, S. Engineering vascularized skeletal muscle tissue. Nature biotechnology **23**, 879, 2005.

155. McFarland, D.C., Pesall, J.E., Coy, C.S., and Velleman, S.G. Effects of 17ß-estradiol on turkey myogenic satellite cell proliferation, differentiation, and expression of glypican-1, MyoD and myogenin. Comparative biochemistry and physiology.Part A, Molecular & integrative physiology **164**, 565, 2013.

156. Jacquemin, V., Furling, D., Bigot, A., Butler-Browne, G.S., and Mouly, V. IGF-1 induces human myotube hypertrophy by increasing cell recruitment. Experimental cell research **299**, 148, 2004.

157. Wang, B., Yang, Z., Brisson, B.K., Feng, H., Zhang, Z., Welch, E.M., Peltz, S.W., Barton, E.R., Brown Jr., R.H., and Sweeney, H.L. Membrane blebbing as an assessment of functional rescue of dysferlin-deficient human myotubes via nonsense suppression. Journal of applied physiology **109**, 901, 2010.

158. Heidary Rouchi, A., and Mahdavi-Mazdeh, M. Regenerative Medicine in Organ and Tissue Transplantation: Shortly and Practically Achievable? International journal of organ transplantation medicine **6**, 93, 2015.

159. Orlando, G., Soker, S., Stratta, R.J., and Atala, A. Will regenerative medicine replace transplantation? Cold Spring Harbor perspectives in medicine **3**, a015693, 2013.

160. Butler, D. Translational research: Crossing the valley of death. Nature **453**, 840, 2008.

161. Lee, M., Arcidiacono, J., Bilek, A., Wille, J., Hamill, C., Wonnacott, K., Wells, M., and Oh, S. Considerations for Tissue-Engineered and Regenerative Medicine Product Development Prior to Clinical Trials in the United States. Tissue Engineering, Part B: Reviews **16**, 41, 2010.

162. Izumi, K., Song, J., and Feinberg, S.E. Development of a Tissue-Engineered Human Oral Mucosa: From the Bench to the Bed Side. Cells Tissues Organs **176**, 134, 2004.

163. Omstead, D., Baird, L., Christenson, L., Du Moulin, G., Tubo, R., Maxted, D., Davis, J., and Gentile, F. Voluntary Guidance for the Development of Tissue-Engineered Products. Tissue engineering **4**, 239, 1998.

164. Malavika Chandra, Karthik Vishwanath, Greg D. Fichter, Elly Liao, Scott J. Hollister, and Mary-Ann Mycek. Quantitative molecular sensing in biological tissues: an approach to non-invasive optical characterization. Optics Express **14**, 6157, 2006.

165. Chandra, M., Wilson, R.H., Lo, W., Vishwanath, K., Izumi, K., Feinberg, S.E., and Mycek, M. Sensing metabolic activity in tissue engineered constructs. Proceedings of SPIE **6628**, 2007.

166. Georgakoudi, I., Rice, W., Hronik-Tupaj, M., and Kaplan, D. Optical Spectroscopy and Imaging for the Noninvasive Evaluation of Engineered Tissues. Tissue Engineering, Part B: Reviews **14**, 321, 2008.

167. Chen, L., Lloyd, W.R., Kuo, S., Kim, H.M., Marcelo, C.L., Feinberg, S.E., and Mycek, M. The potential of label-free nonlinear optical molecular microscopy to non-invasively characterize the viability of engineered human tissue constructs. Biomaterials **35**, 6667, 2014.

168. Zipfel, W.R., Williams, R.M., and Webb, W.W. Nonlinear magic: multiphoton microscopy in the biosciences. Nature biotechnology **21**, 1369, 2003.

169. Barretto, R.P.J., Schnitzer, M.J., Llewellyn, M.E., and Delp, S.L. Minimally invasive high-speed imaging of sarcomere contractile dynamics in mice and humans. Nature **454**, 784, 2008.

170. Plotnikov, S.V., Millard, A.C., Campagnola, P.J., and Mohler, W.A. Characterization of the Myosin-Based Source for Second-Harmonic Generation from Muscle Sarcomeres. Biophysical journal **90**, 693, 2006.

171. Yan, W., Fotadar, U., George, S., Yost, M., Price, R., and Terracio, L. Tissue Engineering of Skeletal Muscle. Microscopy and Microanalysis **11**, 1254, 2005.

172. Weigert, R., Porat-Shliom, N., and Amornphimoltham, P. Imaging cell biology in live animals: ready for prime time. The Journal of cell biology **201**, 969, 2013.

173. Pitts, J.D., Sloboda, R.D., Dragnev, K.H., Dmitrovsky, E., and Mycek, M.A. Autofluorescence characteristics of immortalized and carcinogen-transformed human bronchial epithelial cells. Journal of Biomedical Optics **6**, 31, 2001.

174. Heikal, A.A. Intracellular coenzymes as natural biomarkers for metabolic activities and mitochondrial anomalies. Biomarkers in medicine **4**, 241, 2010.

175. Huang, S., Heikal, A.A., and Webb, W.W. Two-Photon Fluorescence Spectroscopy and Microscopy of NAD(P)H and Flavoprotein. Biophysical journal **82**, 2811, 2002.

176. B Chance, B Schoener, R Oshino, F Itshak, and Y Nakase. Oxidation-reduction ratio studies of mitochondria in freeze-trapped samples. NADH and flavoprotein fluorescence signals. Journal of Biological Chemistry **254**, 4764, 1979.

177. Chen, X., Nadiarynkh, O., Plotnikov, S., and Campagnola, P.J. Second harmonic generation microscopy for quantitative analysis of collagen fibrillar structure. Nature protocols **7**, 654, 2012.

178. Liu, W., Raben, N., and Ralston, E. Quantitative evaluation of skeletal muscle defects in second harmonic generation images. Journal of Biomedical Optics **18**, 26005, 2013.

179. Kyle J. Edmunds, and Paolo Gargiulo. Imaging approaches in functional assessment of implantable myogenic biomaterials and engineered muscle tissue. European Journal of Translational Myology **25**, 63, 2015.

180. Plotnikov, S.V., Kenny, A.M., Walsh, S.J., Zubrowski, B., Joseph, C., Scranton, V.L., Kuchel, G.A., Dauser, D., Xu, M., Pilbeam, C.C., Adams, D.J., Dougherty, R.P., Campagnola, P.J., and Mohler, W.A. Measurement of muscle disease by quantitative second-harmonic generation imaging. Journal of Biomedical Optics **13**, 044018, 2008.

181. König, K., Schenke-Layland, K., Riemann, I., and Stock, U.A. Multiphoton autofluorescence imaging of intratissue elastic fibers. Biomaterials **26**, 495, 2005.

182. Schenke-Layland, K., Riemann, I., Stock, U.A., and Ko¨nig, K. Imaging of cardiovascular structures using near-infrared femtosecond multiphoton laser scanning microscopy. Journal of Biomedical Optics **10**, 024017, 2005.

183. Galli, R., Uckermann, O., Andresen, E.F., Geiger, K.D., Koch, E., Schackert, G., Steiner, G., and Kirsch, M. Intrinsic indicator of photodamage during label-free multiphoton microscopy of cells and tissues. PloS one **9**, e110295, 2014.

184. Drezek, R., Sokolov, K., Utzinger, U., Boiko, I., Malpica, A., Follen, M., and Richards-Kortum, R. Understanding the contributions of NADH and collagen to cervical tissue fluorescence spectra: modeling, measurements, and implications. Journal of Biomedical Optics **6**, 385, 2001.

185. Quinn, K.P., Bellas, E., Fourligas, N., Lee, K., Kaplan, D.L., and Georgakoudi, I. Characterization of metabolic changes associated with the functional development of 3D engineered tissues by non-invasive, dynamic measurement of individual cell redox ratios. Biomaterials **33**, 5341, 2012.

186. Rice, W.L., Kaplan, D.L., and Georgakoudi, I. Two-photon microscopy for non-invasive, quantitative monitoring of stem cell differentiation. PloS one **5**, e10075, 2010.

187. Zhang, Z., Blessington, D., Li, H., Busch, T.M., Glickson, J., Luo, Q., Chance, B., and Zheng, G. Redox ratio of mitochondria as an indicator for the response of photodynamic therapy. Journal of Biomedical Optics **9**, 772, 2004.

188. Lam, M.T., Huang, Y., Birla, R.K., and Takayama, S. Microfeature guided skeletal muscle tissue engineering for highly organized 3-dimensional free-standing constructs. Biomaterials **30**, 1150, 2009.

189. Raghavan, S., Lam, M., Foster, L., Gilmont, R., Somara, S., Takayama, S., and Bitar, K. Bioengineered Three-Dimensional Physiological Model of Colonic Longitudinal Smooth Muscle In Vitro. Tissue Engineering, Part C: Methods **16**, 999, 2010.

190. Mahalingam, V.D., Behbahani-Nejad, N., Ronan, E.A., Olsen, T.J., Smietana, M.J., Wojtys, E.M., Wellik, D.M., Arruda, E.M., and Larkin, L.M. Fresh Versus Frozen Engineered Bone–Ligament–Bone Grafts for Sheep Anterior Cruciate Ligament Repair. Tissue Engineering Part C: Methods **21**, 548, 2015.